Master of Science Thesis

Investigation of Alignment Methods and Its Effect on Mechanical Performance of Discontinuous Tow-based Composites

An experimental design study

Huub H. Urselmann

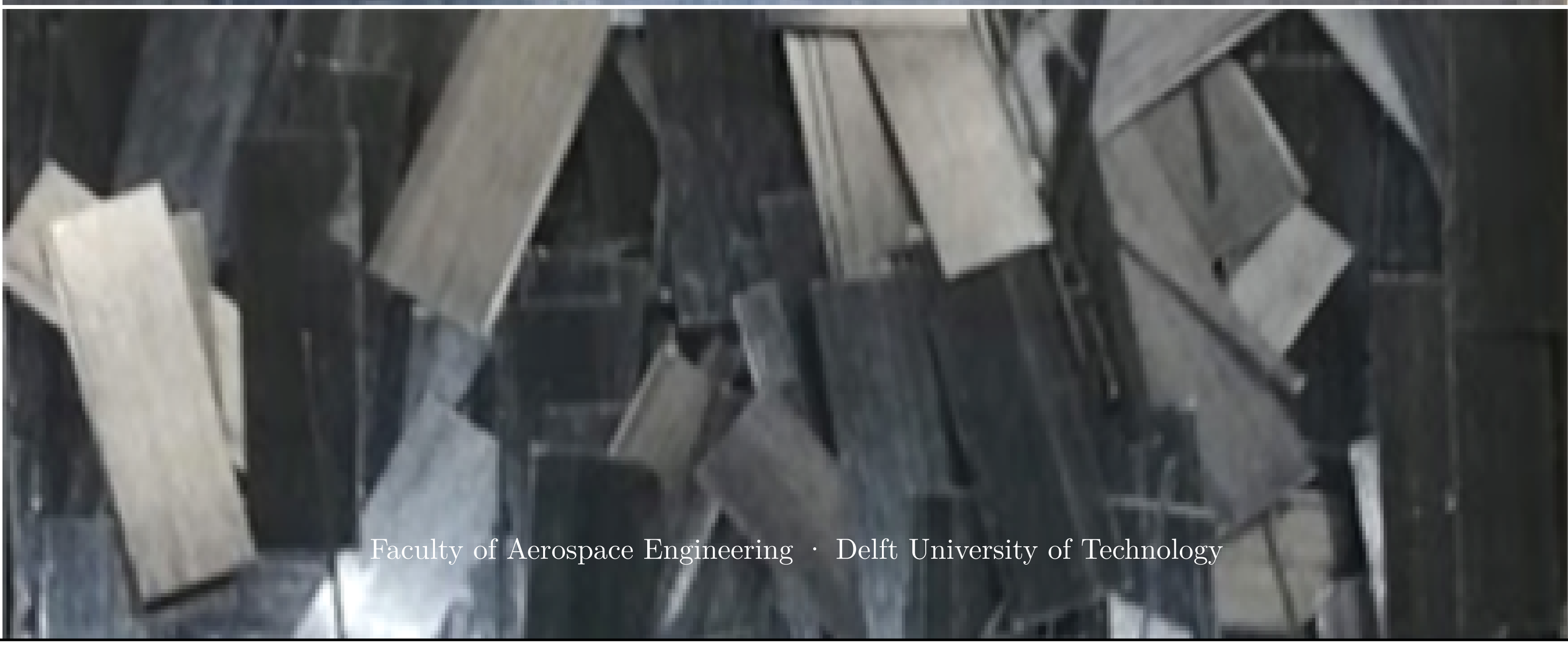

Faculty of Aerospace Engineering · Delft University of Technology

TU Delft Delft University of Technology

Investigation of Alignment Methods and Its Effect on Mechanical Performance of Discontinuous Tow-based Composites

An experimental design study

Master of Science Thesis

For obtaining the degree of Master of Science in Aerospace Engineering
at Delft University of Technology

Huub H. Urselmann

June 30th, 2021

Faculty of Aerospace Engineering · Delft University of Technology

Delft University of Technology
Faculty of Aerospace Engineering
Department of Aerospace Structures and Materials

GRADUATION COMMITTEE

Dated: June 30th, 2021

Chair holder: Prof. Clemens Dransfeld

Committee members: Prof. Clemens Dransfeld

Dr. Laura Rossi

Dr. Saullo Giovani Pereira Castro

Abstract

Composites are used in applications where the combination of low density and high stiffness is wanted, as can be frequently found in the aerospace industry. Within the composites family, discontinuous fiber composites (DFC) started to gain interest in the aerospace and automotive industry, due to their potential for high production rates. In order to make these materials more appealing for real structure applications, their mechanical properties have to be improved and predicted with higher accuracy. This can be achieved by modifying the fiber orientation inside the material so properties such as stiffness and strength can be tailored for the application.

The present thesis has focused on the development of different alignment methods and investigation of the effect of the alignment of discontinuous composite tapes on the material properties. The characterization of the alignment methods is performed by quantifying the level of alignment in the manufacturing process with a digital image processing tool. Based on these results, one alignment method is proposed for the manufacturing of specimens for mechanical testing. Besides this, an outlook is given for the implementation of this method into an automated process. Multiple test samples with different tape orientation distributions have been manufactured and tested in order to quantify the effect of tape alignment on the strength and modulus under tensile and shear loading.

It is found that aligned DFC have an average tensile strength and stiffness of respectively 96% and 145% above the average values of randomly orientated DFC. This research has proved the potential of aligned DFC by showing their enhanced mechanical performance and time-efficient manufacturing cycle. It is intended that the obtained results can help make the use of DFC more appealing for academia, but also for industrial applications in the near future.

Keywords: *Discontinuous Fiber Composites, Thermoplastic Composites, Tow alignment, Digital Image Recognition, Mechanical Properties*

List of Abbreviations

Abbreviation	Meaning
AMT	Aerospace Manufacturing Technologies
CAD	Computer Aided Design
CF	Carbon Fiber
CFC	Continuous Fiber Composites
CFD	Computational Flow Dynamics
CLT	Classical Laminate Theory
DFC	Discontinuous Fiber Composite
DIC	Digital Image Correlation
FDM	Fused Deposition Modeling
FEM	Finite Element Method
GFRP	Glass Fiber Reinforced Plastic
LED	Light Emitting Diode
PEEK	Polyetheretherketone
PoC	Proof of Concept
RGB	Red Green Blue
RTM	Resin Transfer Moulding
TS	Thermoset
TP	Thermoplastic
UD	Unidirectional
USS	Ultimate Shear Strength
UTS	Ultimate Tensile Strength
VIP	Vacuum Infusion Processing
V_f	Fiber volume fraction
V_m	Matrix volume fraction

Samenvatting

De lucht- en ruimtevaartindustrie maakt veel gebruik van composieten vanwege hun hoge specifieke stijfheid en sterkte. Hierbij zijn composieten met ononderbroken vezels al geruime tijd de standaard. Het gebruik van composieten met onderbroken vezels wordt weinig toegepast door hun mindere mechanische eigenschappen.

Doordat dit materiaal (onderbroken vezels) geproduceerd kan worden uit gebruikte composiet onderdelen, wordt dit gezien als oplossing voor de vermindering van de groeiende hoeveelheid composiet afval. Dit kan gedaan worden door bestaande onderdelen te downcycelen. Een van de redenen dat dit materiaal niet veel gebruikt wordt is tevens de complexiteit van het materiaal. Van dit materiaal zijn de mechanische eigenschappen moeilijk te modeleren. Om dit materiaal meer te kunnen toepassen moet er daarom meer kennis zijn van de materiaaleigenschappen. Deze kennis kan worden toegepast om de eigenschappen beter te voorspellen en te kunnen verbeteren.

Een methode om de mechanische eigenschappen te verbeteren is door de vezels in het materiaal uit te lijnen met de richting van de belasting. Hierdoor wordt het materiaal sterker en stijver in deze richting ten opzichte van een materiaal waarvoor de oriëntatie willekeurig is. Deze thesis focust zich op het ontwerpen van methodes voor het uitlijnen van de vezels in de gewenste richting. Hierbij zijn meerdere concepten voor het uitlijnen van de vezels ontwikkeld gevolgd door de uitwerking in vier proof-of-concepts. Op basis van meerdere criteria is een uiteindelijk ontwerp geselecteerd.

Aanvullend is voor het meten van de vezeluitlijning een meetsysteem ontworpen dat op basis van afbeeldingen de oriëntatie van vezels kan vaststellen. Tevens zijn de kosten voor ontwikkeling en gebruik van de proof-of-concepts in beeld gebracht.

Voor het produceren van proefstukken is het geselecteerde ontwerp doorontwikkeld voor de toepassing. Dit ontwerp maakt gebruik van verticale scheidingswanden die uitgelijnd zijn met de gewenste vezel oriëntatie. Door dit hulpstuk in een mal te plaatsen en er vezels in te deponeren, wordt de vezeloriëntatie veranderd van een willekeurige spreiding naar een die gecentreerd is om de gewenste oriëntatie te bereiken. Dit hulpmiddel is geschikt voor mallen van verschillende afmetingen en voor verschillende vezeloriëntaties. Voor het uitvoeren van de mechanische tests zijn vier proefstukken gemaakt met verschillende vezeloriëntatie distributies. Deze zijn willekeurig, 0° uitlijning, ±45° uitlijning (met scheiding film), en ±45° uitlijning (zonder scheiding film). Met de eerste twee proefstukken is het effect van de

uitlijning op de mechanische eigenschappen gemeten. Hierbij is een gemiddelde verbetering in trekstijfheid van 145% en 96% in treksterkte gemeten. Met de laatste twee type proefstukken zijn de afschuivingssterkte en afschuivingsstijfheid van het materiaal bepaald. Het gebruik van de scheiding film heeft een negatieve invloed op de gemeten mechanische eigenschappen.

Summary

With the objective of reducing fuel consumption and thus, polluting exhaust emissions, the aerospace industry has shifted to composites, often because of their high specific stiffness and strength. Within the composite materials, continuous fiber composites (CFC) are the most used and researched. Despite that these materials show the best mechanical properties, the geometries which can be created with them are mainly plate- and shell-based. Besides this, manufacturing with CFC requires pristine materials for the manufacturing process, a fact that makes them not suitable for recycling.

As an alternative, another group of composites called discontinuous fiber composites (DFC) can be used. This material is made out of smaller tapes of composite, which can be organized into a hierarchical material structure as can be found in nature. Because this material exists out of small elements, it is suited for the manufacturing of complex geometries and can be made from recycled materials. Until recently, the application of discontinuous fiber composites has been a less standard practice due to their lower mechanical properties compared to CFC. Moreover, this research and application gap is due to the complexity in determining the mechanical performance of DFC components with accuracy.

Interest in DFC has increased given that this material group is suitable for low-cost mass production and can be used as a solution for reducing composite waste. In order to increase the applicability of DFC into aerospace structures, deeper knowledge on the prediction and possible improvements of the material properties has to be obtained. One approach to improve the mechanical properties is to align the tape orientation with the loading direction, resulting in higher strength and stiffness in that direction. This thesis focuses on the design and production of a method that can be used to align DFC in the desired direction. Several alignment principles have been explored through the creation and testing of four proofs-of-concept based on selected working principles. Complimentary to this, a measurement system has been developed which can measure tape orientation by analyzing digital images. Manufacturing and investment times for each concept have been determined. Based on the alignment capabilities, manufacturing, and investment times of each concept, a design has been proposed.

The proposed design has been further developed for the manufacturing of test samples. The tape orientation has been altered to one that is mainly centered around the desired direction. This has been performed by placing the alignment tool inside a mold cavity and depositing

DFC tapes onto it. This alignment tool can be adapted to other mold shapes and sizes, as well as to different tape orientations. Four types of test samples have been manufactured to obtain data of different tape orientation distributions. These orientation distributions are: random, 0° centered, ±45° centered (with PEEK separation film), and ±45° centered (without PEEK separation film). The first two have been used to capture the effect of the alignment on the tensile strength and modulus. It was found that as a consequence of the alignment in the 0° direction, the average tensile modulus and strength increased with respect to the properties of the samples with a random tape orientation. With the latter two sample types, the shear modulus and strength of the material have been determined. By comparing the shear properties of these two types it was found that the separation film did not improve the mechanical performance.

Preface

This document is the final product of my master of science thesis. With this report I've tried to show some of the things I've learned during the master. I do not only see this report as the end of a thesis, but as the end of the last two years I was able to spend at TU Delft.

This project has been executed in the year where working on your own seemed the only thing that could be done as a student. I'm gratefully for the reasons this thesis has given me to still be able to get in "touch" with people. I would like to thank my supervisors Clemens Dransfeld and Deniz Gülmez for the time they have spent on me online and during the meetings we could have in person. From the first time we've talked about this project in January 2020 up till the end, I've felt support and enthusiast from both them. They have created the environment and tools (literally) for me in order to be able to make this report. During past year I've received help from many people from the workshop and the AMT research group of the faculty of aerospace engineering. I can't name them all but I want to thank all of them for making me feel welcome and helping me out.

I would like to thank my parents and family for supporting me with all the choices I've made the past 24 years and the friends that I have made in the meantime (amongst them Palak Sing Verma & Miguel Alonzo Diaz). Not only for helping me with my work but for being my friends during the past two years. Finally, I want to thank Irene Solbes Ferri for her support and comfort for which I'm extremely grateful.

Thank you all,

Delft, University of Technology — Huub H. Urselmann
June 30th, 2021

““ If you think you are invincible, you’re going to die””

— *Papa Rudy, The walk*

Table of Contents

List of Figures

List of Tables

Chapter 1

Introduction

In order to reduce fuel consumption and exhaust emissions, the aerospace industry uses composites because of their high specific stiffness and strength. Within the composite material family, multiple types exist. In figure 1.1 a simplified classification of fiber-reinforced composites has been shown. Here, two groups are shown, continuous fiber composites (CFC) and discontinuous fiber composites (DFC). The use of continuous fiber composites has been established for a long time due to their structural performance and the relatively high accuracy at which their properties can be determined. Although the manufacturing of CFC parts is labor intensive and time consuming, the number of identical parts that are normally manufactured is low as well which removes the need for a fast production process.

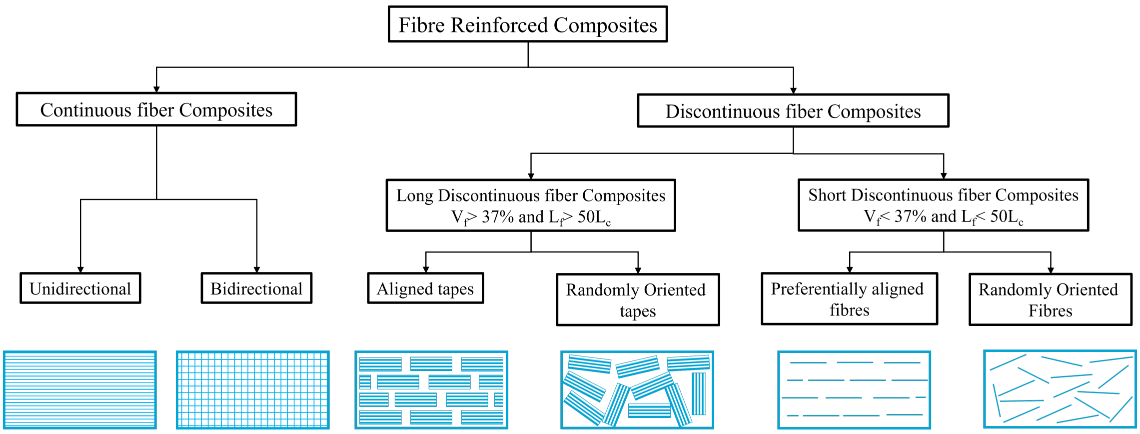

Figure 1.1: Classification of composites, inspired by Selezneva et al. [1]

The second group of fiber-reinforced composites is discontinuous fiber composites which are made out of multiple short fibers. This material group is suitable for low-cost mass production, can be used as a solution for the waste reduction of composites, and down-cycling of current composite structures. This group can be further classified based on the length and the alignment of these fibers. In figure 1.1, these types of DFC are shown on the right side.

This thesis project will focus on the aligned and randomly orientated tapes. These tapes can be aligned by means of mechanical alignment methods and are thus suited for large-scale manufacturing processes. Compared to short fiber CD, the mechanical performance of these materials is also better due to the high fiber volume fraction that can be achieved. In figure 1.2 the relationship between fiber length, processability, and material performance has been shown. Here the described area of DFC tapes is marked in blue.

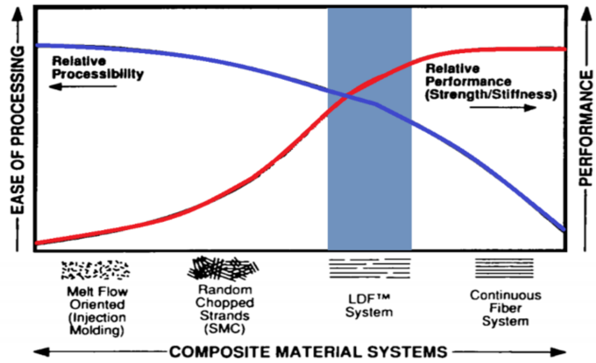

Figure 1.2: Relationship between fiber length, material performance and processability, chang et al. [2]

Compared to CFC, the material properties of DFC can not be predicted easily. This is caused by the complex structural hierarchy of the material. To apply this material group with higher confidence into structures, more knowledge needs to be gained on how to predict and improve the material properties of DFC. One approach to improve the material properties is to align the properties of the tapes with the direction of loading. This can be done by orienting the fibers inside the material in such a way that it becomes stronger and stiffer in the desired direction.

The manufacturing of DFC parts differs from CFC parts. Parts made out of CFC are mainly made by depositing the material onto a surface and making layers of fibers bond together by means of curing (TS) or melting (TP) of the matrix material. The manufacturing process of DFC with TP matrices uses high temperatures and pressures to shape tapes into the desired part. Firstly a batch of tapes is weighted and deposited into a mold. After the mold is closed, it is placed inside a heated press which heats up the material after which the press closes the mold fully, and the material flows into all the cavities of the mold. Because of the high viscosity of the material, a large pressure needs to be applied onto the mold in order to make this material flow. This high pressure limits the size of a part due to the force that is needed to shape the material. After cooling the mold, the matrix is consolidated, and the part can be removed. By optimizing the manufacturing process, multiple parts can be manufactured in one mold within a small time span.

When TS-based DFC are manufactured, multiple methods can be used for the manufacturing of parts. For example, a preform can be placed inside a mold after which a resin is infused. This method can be executed with a low pressure like with VIP or with a higher pressure for faster processing times with the RTM technique. In contrast to CFC, where mainly plate- or shell-like parts are manufactured, DFC can also be used to create 3D geometries [3–6]. Hereby it should be taken into account that a complex geometry in general also needs a complex (and thus expensive) mold. Although some parts could also be created with CFC, the use of DFC makes the manufacturing simpler due to the absence of phenomena such as wrinkling at the edges of a curved surface as can be seen in figure 1.3. Examples of DFC parts are shown in figure 1.5.

(a) (b)

Figure 1.3: Comparison CFC and DFC parts. a) CFC part with wrinkles, [7]. b) DFC part without wrinkles [8]

The alignment of the fibers inside the material influences the mechanical properties. In figure 1.4 the difference in stiffness and strength due to fiber alignment can be seen. With this, it can be seen that the performance of parts and structures can be improved by aligning fibers in a single direction. Although the effect of alignment on the mechanical properties such as the tensile modulus has been proven, there are many uncertainties that make the prediction of the mechanical properties difficult.

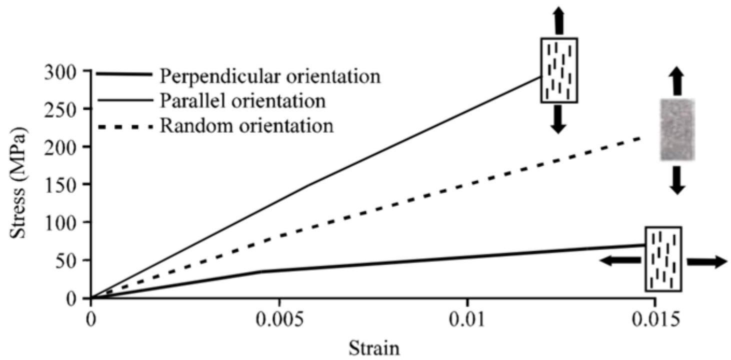

Figure 1.4: Differences in stress strain behavior due to fiber alignment, Osswald et al. [9]

Because the literature about alignment methods is limited and makes use of different measurement techniques and tape sizes (from a few millimeters [10] to centimeters [11]) it is not known which methods are the most suited for certain applications. Based on the availability of materials during the project, this thesis will focus on the alignment and manufacturing of DFC tapes with a thermoplastic (TP) matrix. The use of a TP matrix also enables faster manufacturing of parts due to the manufacturing steps, as will be described later. From the tape sizes that have been available, tapes of 22.5 by 7.5 mm have been used throughout the thesis. With these dimensions, the performance of the material is high while the processability is still possible. With a lower fiber length, the material performance could drop. If the fiber length gets higher, the processability of the material can become difficult.

For the comparison of alignment methods, the use of digital image processing has been found as a suitable method. This enables the execution of more measurements for each of the alignment methods compared to manual measurements. With the findings on the alignment methods, the influence of alignment on mechanical properties can be quantified. In the literature study has stated that the choices for alignment methods have been chosen arbitrarily. As a result of this, no good comparison between different methods with the same tape size has been executed. This raises the question of what the best method is for the production of DFC parts.

Figure 1.5: Examples of 3D shaped parts made from discontinuous fiber composites a) Rib stiffened structure with inserts [12], b) Door hinge [5], c) T-profile beam [3] , d) Demonstrator part of stiffened panel [4]

This thesis will focus on alignment methods for the alignment of CF/PEEK tapes. From a set of working principles, a selection will be made for further development and characterised. From these, a method will be selected, and further developed for manufacturing. Hereby the selection will be done in two stages. The first stage is based on feasibility while the second is based on quantified specifications of methods. With the selected method, samples will be manufactured for the determination of mechanical properties. These samples will be tested and compared to samples with random tape orientations. With the obtained data, an experimental relation can be found between the level of alignment and the mechanical properties.

Report structure

In this report, the activities that have been taken during the thesis will be described. Firstly, the results of the literature study will be summarized in chapter 2. Based on these results the thesis objectives with the related research questions have been formulated. In chapter 3 the process of concept creation and selection has been described which has resulted in the alignment tool that has been chosen for the creation of test samples. As part of this selection, a measurement system has been designed which is described in chapter 4. After the selection of the alignment tool, samples have been manufactured for tensile testing. The manufacturing and inspection of these samples have been described in chapter 5 after which the results of the testing are discussed in chapter 6. With the obtained knowledge and experience about the manufacturing process, a manufacturing outlook has been stated in chapter 7 for the application of the proposed alignment method on an industrial scale. Finally, the main findings of the report will be discussed by answering the research questions in chapter 8. Hereby recommendations for future research have also be given.

Chapter 2

Literature review

In preparation for the thesis project, a literature study has been done on discontinuous fiber composites. Hereby the interest in alignment methods of composite tapes and the effect of the alignment on the mechanical properties of the material have been taken into account. This chapter will give a brief overview of the most relevant findings of the literature review. After this, the found research gaps will be presented on which the objective of the thesis has been based.

2.1 Mechanical properties of discontinuous fiber composites

Discontinuous fiber composites have a hierarchical structure. On a nanoscale (figure 2.1a) are the fibers. When carbon fiber is used the carbon atoms within the fiber are arranged in 2D planes which are orientated in such a way that the best properties are in the axial direction of the fiber. At microscale (figure 2.1b), a structure of almost straight fibers can be seen which are encapsulated by the polymer matrix. This combination protects the fibers against cracks and notches while the loading forces are distributed between the fibers with help of the fiber-matrix interface. On the mesoscale (figure 2.1c), a brick-and-mortar structure can be recognized, hereby multiple tapes (bricks) are stacked onto each other with a polymer film in between them (mortar). This structure prevents crack-propagation in straight lines through the material and allows for shear failure between tapes which has the potential of absorbing energy.

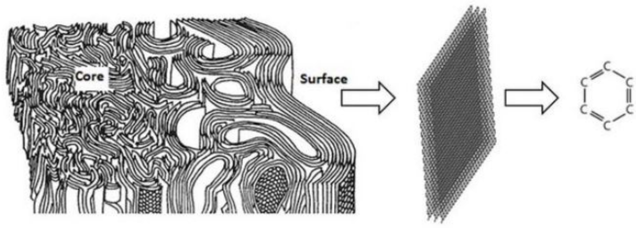

(a)

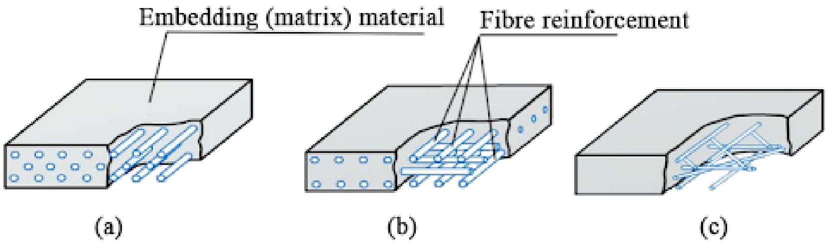

(b)

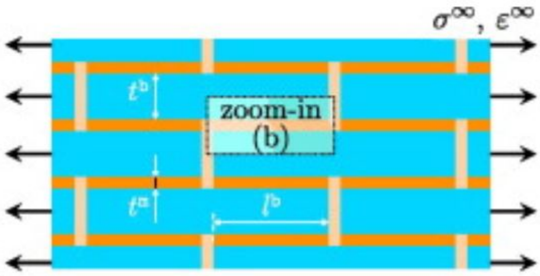

(c)

Figure 2.1: Different structure scales within discontinuous fiber composites, a) Nano-scale, the molecular structure within a carbon fiber [13], b) Macro-scale, the orientation of carbon fibers within a polymer resin, [14], c) Meso-scale, the brick and mortar structure of UD tapes, [15]

When looking at the material as a whole, the mechanical properties can more or less be compared with quasi-isotropic materials. According to [16] the tensile modulus is comparable (within scatter range) with a quasi-isotropic layup from the same material. During experiments, Selezneva et al. [16] noted that randomly orientated discontinuous fiber composites can even outperform quasi-isotropic composites in shear strength. This statement holds for the global elastic properties of the material inside a part. Locally there can be high differences when a random orientation is used. Within the material, some locations can have a very low stiffness (due to resin pockets and voids) and other spots can have properties compared to uni-directional composites (when all tapes are by chance aligned in one direction). With a higher thickness of a part, the probability that these opposites occur is lower than with thin parts. According to Feraboli et al. [17], the yield strength and ultimate strength of discontinuous fiber composites can be up to six times lower than a quasi-isotropic laminate in tension or compression dependent on the fiber length. Shorter fibers show lower strength than longer fibers. Due to the stochastic nature of the material, the actual failure load is dependent on the local (and global) orientations of the fibers. Due to the stochastic structure, DFC are less notch sensitive which makes them more suitable than continuous fiber composites which have stress concentrations around notches due to the anisotropy of the material [17,18]. The local layup of randomly placed tapes may decrease the in-plane tensile and compressive moduli of the material due to out-of-plane tape orientation [1]. Although this would make thinner tapes more preferable, thin parts have a higher chance of non-symmetric layups. This effect is more effective for thinner tapes where the lower number of through-thickness tapes enforces this effect. Another effect of this is that materials with thicker samples have less coupling between elongation and bending than materials with thin tapes.

2.2 Prediction of mechanical properties of discontinuous fiber composites

Numerical models can be used to predict the mechanical properties of discontinuous fiber composites and enable the option to execute more tests than with mechanical testing. Multiple methods for the prediction of mechanical properties have been developed. In this section, several of these methods have been described ranked from low to the high computational effort. It should be noted that all numerical models can only be used to determine the statistical behavior of the material.

1. 2D finite element analysis using equivalent laminate theory
   By using equivalent laminate theory [19], the tensile modulus can be calculated on a local scale. This method is suited to give an overall stiffness of the material [20] using finite element analysis. With this method, multiple random layups can be simulated which may yield insight into the scatter of the material properties. Because normally no information about the true fiber orientation in a part is known, this method can only give a statistical behavior of a plate. An overview of the process steps which have to be used for the creation of these models is shown in figure 2.2. When comparing these results with mechanical tests, it can be seen that the modulus of the material is comparable with a quasi-isotropic laminate. On the other hand, the predicted strength was 50% lower. This is caused by stress concentrations within the material due to its stochastic nature.

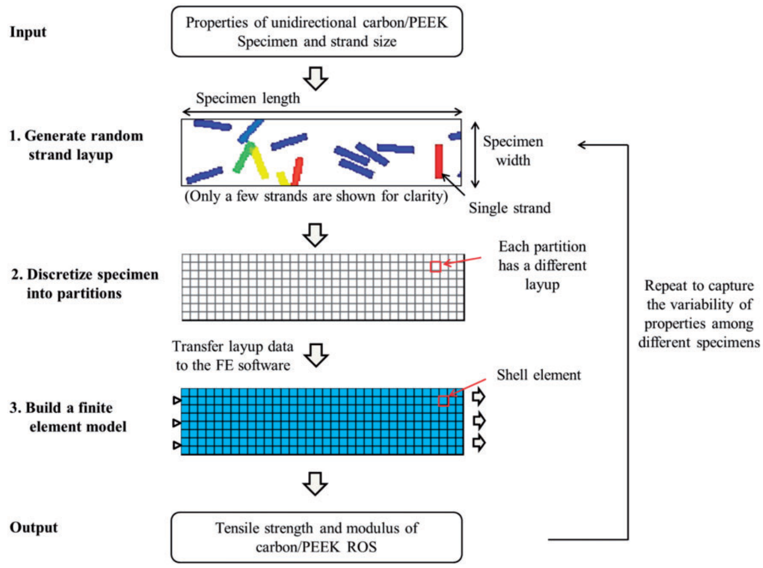

Figure 2.2: Process flow for creation of equivalent laminate finite element model, [1]

To create a model with this method, a random tape distribution (random location and orientation of each tape) has to be generated. The mechanical properties of a material are used to calculate the local in-plane elastic properties for the model. Finite element models with different randomized layups have shown that the lower strength of discontinuous fiber composites compared to quasi-isotropic laminates is caused by differences in local stiffness [1] in here it can be seen that the experimental scatter is higher than the analytical.

2. 2D finite element methods using improved equivalent laminate theory.
   Alves et al. [20] have shown an improvement on the equivalent laminate theory by implementing tape waviness into the numerical model. This is done by calculating the waviness of a tape when it is randomly placed in a virtual cavity. These improvements make the model under-predict the stiffness of the model compared to experiments. Figures 2.3 and 2.4 show the waviness of a tape and the waviness distribution of tapes inside a model.

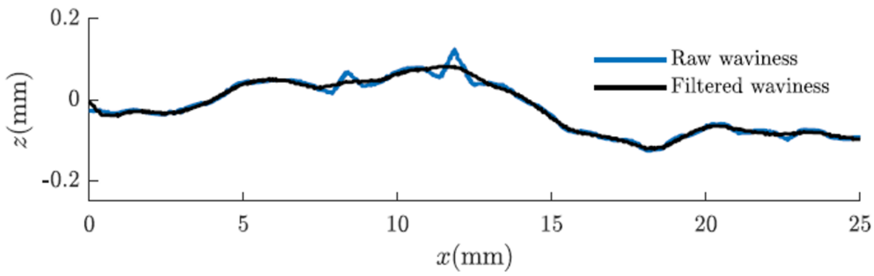

Figure 2.3: Waviness of tapes inside discontinuous fiber composite model, Alves et al. [20]

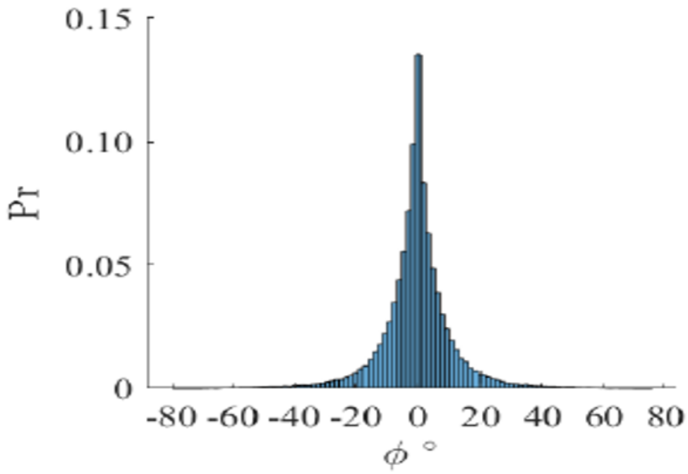

Figure 2.4: Out-of-plane angle distribution, Alves et al. [20]

The described method uses all the geometrical dimensions of the tapes. Before making a simplified 2D finite element model of the layups, the in-plane mechanical properties of the tapes are reduced based on the out-of-plane angle of each of the tapes. Because this is still a 2D representation of a part, the tape waviness is not fully taken into account for the strength [20].

3. 3D finite element model
   By making a 3D model of all the tapes in the material all the geometrical values and the orientation of tapes can be taken into account. This method requires a lot of computational effort [21] and is thus not suitable for large complicated parts. The results of this method can predict the strength and stiffness accurately. To make full use of the accuracy of this method„ a digital twin of a sample should be processed by the model instead of using it for calculating statistical properties. One of the reasons why this method is more accurate is the use of shear lag theory [22] which takes load transfer between tapes into account. With this method, the creation of stress concentrations inside the material can be better captured.

The most recent models can be improved by expanding the properties from only tensile, to compressive and shear too. This will give more insight into the material properties with regard to the tape size. For example, it is expected that discontinuous fiber composites that are manufactured from small tapes are less sensitive for fiber buckling due to their short length. Because different failure modes can appear for different load cases, more complex models have to be used that take local and global non-linearities into account.

2.3 Manufacturing of discontinuous fiber composites parts

Based on the interest in the use of TP-based DC, the manufacturing steps are only describing the manufacturing process of TP DC. In figure 2.5 a simplified schematic of the manufacturing process has been shown. For this manufacturing, firstly UD tapes will be cut into small tapes and compression-molded into a part. The part of the process cycle which happens inside the mold can be best described using a graph wherein the processing temperatures and pressures are shown. This cycle is shown with arbitrary values in figure 2.6 and is further described afterward.

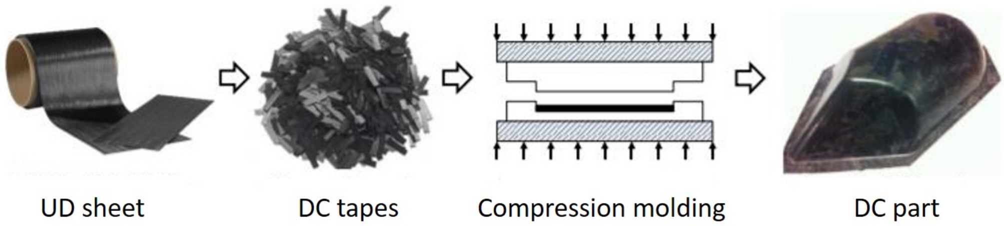

Figure 2.5: Schematic manufacturing cycle of DFC composites, Selezneva et al. [8]

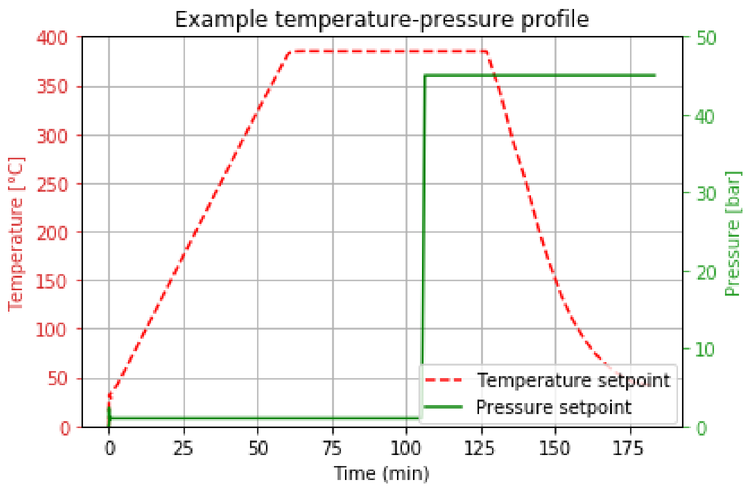

Figure 2.6: Example of temperature pressure cycle

The process for manufacturing parts out of discontinuous fibers can be divided into separate steps.

- Deposition
  During this step, the mold is prepared and the needed amount of material (mass of the part plus a few percentages to account for flashing [12]) is placed into the mold. When the geometry of the part has complex cavities it might be beneficial to ensure the material is already located near complex features to make the flow of material less needed [8]. The orientation of the tapes can be random or aligned with the desired direction.

- Heating
  Before the material can be shaped into the desired geometry, it needs to be heated till the material can flow. To decrease the time needed for heating, the mold can be closed

and contact pressure can be applied to improve heat transfer. In figure 2.6 this step can be seen at the start of the cycle where the temperature rises.

- Debulking
  During the debulking phase, high pressure is applied onto the mold to debulk the material. This step ensures that the material sufficiently heater up to the processing temperature. The debulking step can be seen in figure 2.6 as the phase where the temperature stays high and the pressure low.

- Consolidation
  During the consolidation, the matrix material is fully melted and will be pressed into the shape of the mold. Trapped air will be driven out of the material. The pressure during this phase is the highest of the process and will be applied until the mold is fully closed and cavities are assumed to be filled with the discontinuous fiber composite material (dwell).

- Cooling/ stabilization
  After the material is shaped, the matrix needs to cool down to be able to keep the shape of the mold after the pressure is removed. Hereby the cooling rate is important to control the crystallization and shrinking of the material. If this is not done correctly, the manufactured part can show warping or other unwanted deformations. During this step, it is almost inevitable to introduce residual stresses into the material due to thermal deformations caused by local differences in thermal expansion. Figure 2.6 shows this step as the end of the cycle where the temperature is decreased again. Because the cooling rate is limited by the cooling system, it is normally not constant.

- Extraction/demolding/post-processing
  After the part is cooled down, it can be removed from the mold and further cooled to room temperature [1,5]. The flashing of polymer material at the edges of the part will have to be removed. This can be done by using various simple tools such as knives or sanding paper.

Another method for the manufacturing of discontinuous fiber composites is to place the tapes without matrix in a mold and use vacuum infusion to bond them together [23, 24]. This method also allows using other types or combinations of composites (such as continuous fibers) in the same part and the use of thermosets is also possible. Hereby the known process for the creation of preforms can be applied. The pressure and temperature inside the mold are typically lower for thermoset matrices than thermoplastic matrices. The use of more viscous resins also enables a design with fine part features that can not be filled by the more viscous thermoset resins. During manufacturing, the used materials will dominate the parameters of the manufacturing process.

The change in orientation of the tapes due to the manufacturing process can vary based on the process parameters and execution of the manufacturing process steps. Li et al. [25] have shown that when the tapes are spread evenly in the mold before the pressure is applied, the alignment does not change a lot. During the heating and consolidating of the material, the tape orientation seems to stay the same on the surface of a part. This finding is of importance for the thesis when the tape orientation is measured during deposition.

2.4 Mechanical properties of discontinuous fiber composites

According to Ferabili et al. [17] the tensile modulus is comparable (within scatter range) with a quasi-isotropic layup from the same material. During experiments, Selezneva et al. [16] noted that DFC with randomly orientated tapes can even outperform quasi-isotropic composites in shear strength. This statement holds for the global elastic properties of the material inside a part, but locally there can be high differences due to the randomness of the orientations. Within the material, some locations can have a very low stiffness (due to resin pockets and voids) and other spots can have properties comparable to uni-directional composites (when all tapes are by chance aligned in one direction). With a higher thickness of a part, the probability that these opposites occur is lower than with thin parts. According to Feraboli et al. [17], the yield strength and ultimate strength of DFC can be up to six times lower than a quasi-isotropic laminate in tension or compression dependent on the fiber length. The actual failure load is dependent on the local (and global) orientations of the fibers which thus results in a lower overall strength. On top of this, DFC are not notch sensitive [26] which can cause a failure at other places that are normally seen as stress concentrations. This makes them more suitable than CFC in some cases. The local layup of randomly placed tapes may decrease the in-plane tensile and compressive moduli of the material due to out-of-plane tape orientation [1] Although this would make parts with thin features more preferable, these parts will also have a higher chance of non-symmetric layups due to the lower number of through-thickness tapes. Dependent on the manufacturing process the alignment of the tapes can be higher at the boundaries of the part. This creates a stiffer skin (outside of the part) [27] than the core of the part.

Just as with CFC, the fibers are dominating the stiffness of DFC as well due to their high tensile modulus compared to the matrix material [19]. For continuous fiber composites, the fibers also influence the strength greatly and the material can even carry loads after the matrix has failed [19]. Most of the failure mechanisms of DFC in tension are matrix-dominated [16, 28, 29], the properties of the matrix will influence the strength properties of the material more. The inter-tape stresses that cause the failure of the material are dependent on the interface area and thus dependent on the tape size and orientation. Haper et al. [30] have shown, through experiments and analytical predictions, many relationships between the material design properties and mechanical properties. Hereby, the stiffness and tensile strength are linked to parameters such as fiber volume fraction, tow length, and specimen width. Hereby most of the parameters that influence the mechanical properties have been proven with the use of mechanical testing, numerical modeling of the materials [1, 20, 21] or assumed based on knowledge of continuous fiber composites [18, 19]. With numerical models [1, 20–22, 25] and experimental studies [11, 24, 25, 29, 31–35], it is clear that the stiffness of the material increases with an increasing alignment (which is also applicable with continuous fiber composites [19]).

2.5 Alignment definition for discontinuous fiber composites

The alignment of fibers within the material can be defined by using various methods. With an alignment definition, different orientation distributions can be expressed and compared to other orientations easier. The literature study has compared multiple definitions for alignment which will not be discussed in this report. For this thesis, the definition of the orientation tensor has been used. Li et al. [25] have described a method to quantify the tape alignment in a laminate employing the orientation tensor. Kravchenko et al. [36] have shown utilizing numerical models that there is also a clear link between the orientation tensor and the stiffness and strength of the material. This makes the use of the alignment tensor suitable. This method makes the use of the orientation tensor [37] for which the calculation has been stated in equation 2.1 whereby p_i and p_j are first-order orientation tensors. An in-plane orientation tensor is a 2 by 2 matrix, hereby the terms a11 and a_{22} describe the level of alignment with the two-axis, while the a_{12} and a_{21} terms are equal and are used to quantify the bias of the fibers towards one direction. Although this method does make use of all tapes and their orientation values, this method can not be used to directly calculate the values of relevant properties of the material.

$$a_{\mathrm{ij}} = \sum \frac{p_i p_j}{N_{\mathrm{tapes}}} \tag{2.1}$$

2.6 Alignment methods for discontinuous fiber composite tapes

Until now, several methods are used to align the orientation of fibers into the desired direction. Gan et al. [11] have described a technique where tapes were dropped into a container with rectangular openings (slits) at the bottom. With the aid of vibrations, the tapes keep re-orientating until they fall through one of the slits. Another method has been described by Harper et al. [24]. With this method, tapes are cut and directly placed on a mold surface. With the use of airflow (sucking the tapes onto the surface) the tapes are kept on the deposition surface. Besides these three methods that are based on mechanical interaction, the most primitive method is the use of placement by hand. Hand placement has been used by Li et al [25] to fully control the fiber orientation and distribution. This can be done by placing tapes in designated locations with the help of lasers or guide paper. Even randomly dropping tapes will tend to create a biased orientation distribution. An example of a method to create an orientation distribution that is assumed to be random has been shown by wan et al. [38] whereby tapes are dispersed into water and collected onto a grid.

A method that is not directly applicable on long tapes but only on small fibers of less than 5mm long is the use of liquid current to align particles. This method uses fibers dispersed into a liquid and lets them flow through a slid onto a surface with vacuum holes to remove the water. Although this method has been used by many researchers, it does not seem to be a suitable method for larger tapes with a length longer than 5 mm. This length is below the critical fiber length for stiffness and strength. [31–34]. Besides this, Harper et al. [24] have described this process as slow due to the low number of tapes and the need for drying the tapes before molding. Methods that seem to be even more complex and less practical for the application of tapes are also found in the literature. Scholz et al. [35] describe a method whereby short fibers (particles) are being aligned with the use of ultrasonic waves. This method is appropriate for small particles. For small fibers, a magnetic field can be applied to re-orientate them in the unconsolidated matrix. Chung et al. [39] state that this method is only suitable for short fibers although small improvements can be achieved with this method.

Improvement of alignment can be obtained by applying shear flow forces, this naturally occurs when forming the material in a mold and is only effective for longer flow distances. Martulli et al. [29] have improved a random tape distribution to a slightly aligned distribution due to polymer flow during the manufacturing process. Hereby the first position of the orientation tensor was measured at 0.668.

All the mentioned methods have not been compared with each other. Some of these methods have specifications on the alignment although this is only measured by measuring an-isotropic of the tensile modulus. Besides this, all the methods make use of different tape sizes and some are not fit for manufacturing. Some methods that are used in other industries are based on the geometrical properties of particles.

2.7 Relevant knowledge gaps

The mechanical properties of DFC can be compared to a quasi-isotropic CFC. One of the methods to improve the mechanical properties is by aligning fibers within a material. Although this will improve the mechanical properties, the exact effects are unknown because these properties are also largely dependent on matrix-dominated failure modes.

Based on the literature study it has been found that the determination of the mechanical properties of DFC is difficult. With the use of numerical models, statistical properties can be determined. Different models exist and can be suitable for only the determination of elastic properties to the failure load for complex loading's. For the most reliable simulations, more knowledge should be gained about fiber orientations within a part. This has not been done due until now.

The manufacturing of DFC is well known due to its similarities with other processing techniques such as RTM and VIP. Where the knowledge about the RTM process can be used for the mould design and handling, the VIP process shows similarities with the molding phase. The effect of the manufacturing process on the mechanical properties (such as fiber alignment) has been determined experimentally but should be more understood at a later point. It has been found that the alignment of the fibers inside DFC influence the mechanical properties. To quantify these influences, a suitable method has to be developed that fits the manufacturing process of DFC. Because the literature about these methods is limited and makes use of different measurement techniques and tape sizes (from a few millimeters [10] to centimeter-scale [11]) it is not known which methods are the most suited for a specific case.

To improve the production process, a comparison between alignment methods has to be executed. Besides this is the known the data about these alignment methods limited due to the manual measurement methods that have been used. The use of digital image processing can be a suitable method to execute more measurements for each of the alignment methods. This will give data with a high confidence interval about the distribution of tapes. Different alignment methods will have to be compared for tapes with the same length scale. This will give insight into the manufacturing process. With the findings on the alignment methods, the influence of alignment on mechanical properties can be measured for a known orientation distribution. With the found date state of the art numerical models can be validated with a higher level of certainty which makes the application of discontinuous composites more attractive for real applications.

2.8 Objective and research questions

Based on the knowledge gaps the thesis objective has been formulated. This objective will focus on some parts of the described knowledge gaps. The objective aims to fit within the broader interest of the AMT research group of TU Delft. Because of the exploratory character of the thesis, two objectives have been formulated that together form the thesis project. Hereby the objectives will be an extension of each other and will all be based on the interest of the research group. Throughout the thesis research questions will be discussed and answered. The two objectives have been based on the findings of the literature review and will focus on the development of an alignment method for DFC tapes and the mechanical properties of the material. The first objective is stated below:

"Manufacture a prototype of an alignment system of single layer unidirectional CF/PEEK tapes for making molded specimens."

This objective will be completed by experimentally exploring methods that have the potential to align chopped CF/PEEK tapes and develop multiple proofs-of-concept. The measurement technique for the tape orientation is through optical characterization using computer vision by OpenCV [40]. With this method, a large-scale measurement can be executed and the alignment of the tapes can be defined. Besides this, the manufacturing process of the proof-of-concept is evaluated based on the gained experience. In combination with this objective, the following main research questions are formulated: *"Which alignment methods is suitable for discontinuous fiber composite tapes?"*. This research question will be answered using the sub-questions below. These questions will be discussed in chapters 3 and 4.

- What methods can be used to improve the alignment of discontinuous fiber composite tapes?
- How can the orientation distribution of discontinuous fiber composite tapes be quantified?
- How can the orientation distribution of discontinuous fiber composite tapes be measured?
- How could the chosen alignment method be implemented in an automated production line for discontinuous fiber composite parts?
- Can numerical simulation be used for the verification and validation of alignment methods and how does this compare to measurements?

After these questions have been answered, the focus of the thesis project will be shifted to the effect of different orientation distributions on the elastic properties. Hereby the concept that has been developed for the previous objective will be used to manufacture multiple samples. The objective for this is:

"Experimentally investigate the tensile stiffness and tensile strength of a discontinuous fiber composite material with random, 0° centered, and ±45° centered tape orientation distribution."

By manufacturing samples with different tape orientation distributions, the effect of the alignment can be measured employing tensile tests. During these tests, the strains and stresses can be measured which will give insight into the mechanical properties. Below the related research questions are stated. Firstly the application of the alignment method will be of interest to be able to manufacture samples. With these findings, the remaining research questions, that focus on the tensile elastic properties, is *"What are the elastic properties of a discontinuous fiber composite material with an aligned tape orientation distribution compared to a random tape distribution?"* Hereby the following research questions will be used:

- How can the chosen alignment method be used to manufacture samples that are suited for mechanical testing?
- What are the tensile strength and stiffness of a discontinuous fiber composite material with an aligned orientation distribution?
- How can multiple tape orientations be combined in a single material?
- What are the mechanical properties of a discontinuous fiber composite material with combined tape orientation distributions?
- How do the found elastic properties compare to a discontinuous fiber composite material with a random orientation distribution?
- How do these elastic properties compare to continuous fiber composite models?

Chapter 3

Creation of alignment method

For this thesis, it has been decided to focus on mechanical methods which are suited for the alignment of CF/PEEK tapes. Based on the time that is available for the project and the availability of tape sizes, the choice has been made to only focus on one tape size. The dimensions of this tape, as mentioned in the introduction, are *22.5 x 7.5 x 0.2 mm*. The use of a single tape size makes the comparison between alignment methods easier with a higher certainty.

3.1 Methodology

For the creation of a final alignment method, the following project flow is chosen. Firstly, multiple concepts are created to explore possible working principles. These concepts are based on principles that have been created during the thesis or principles that have been found during the literature study. To select the most promising concepts, a selection has been done based on simple criteria. The concepts that have been are further developed and manufactured into working proofs-of-concept. After the proofs-of-concept have been tested and reviewed, a final design is selected and further developed for the manufacturing of test samples.

3.2 Working principles for alignment methods

As a first step, basic working principles have been created without details for design or solutions of potential problems, each principle has briefly been described in table 3.1. Here, the most prominent advantages and disadvantages of each concept have been stated. In table 3.2, concepts have been described that are assumed to be infeasible for this thesis (due to the high level of complexity) or the ones that are assumed to have a low chance of being effective (due to the chosen tape size). These working principles could be used for research on alignment on a smaller length scale.

Table 3.1: Description of working principles for alignment methods

Nr.	Name & Description	Sketch
1	**Vibrational box:** This concept is based on the design of Gan et al. [2]. The design consists out of a box with inside vertical plates (with different heights). These plates are all aligned in the desired direction of the tapes and create slits in between which the tapes have limited possible orientations. Possibly with the use of vibrations, the tows can be rotated due to interaction with each other and the walls of the box. **Pros:** Flow possible, Easy design (few parameters), Suited for multiple tape sizes. **Cons:** No in-plane orientation, No constant tape spreading.	
2	**Sliding slope:** A tilted slope is positioned at an angle whereby channels are introduced from top to bottom. The walls will constrain the tape movements more the further down the tows slides (by increasing wall heights and decreasing channel width). At the end of the plate, the tows should all be aligned. **Pros:** Constant flow possible, Scalable. **Cons:** Many process parameters, Low flow.	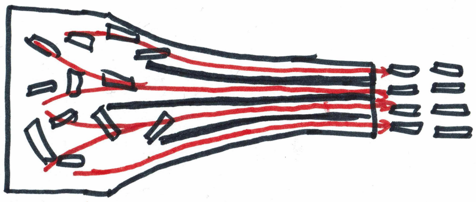
3	**Rotating drum (batch-wise):** A drum loaded with tows will be rotated. Because the tows keep falling they probably start aligning with the rotational axis of the drum. The drum can be opened after a while and the tows come out more aligned than before. With this principle, the volume and size of the tows and radius of the drum will influence the effectiveness. **Pros:** Low number of process parameters, Simple design, No vibrations. **Cons:** Batch-wise process, Large drum needed.	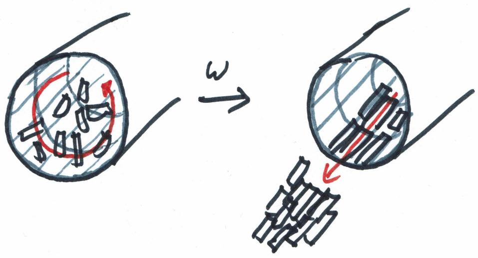

4 **Rotating drum (flow-wise):**
For flow-wise alignment, tapes will be separated when falling from a certain position within the drum. The drum will be loaded once or with a flow of tapes. When the drum is rotated, the profile in the inner wall will carry good orientated tows higher than badly orientated tows. Tows that fall from higher locations can be captured with a gutter-shaped surface. **Pros:** Scalable, Simple design. **Cons:** Uncertainty before testing, Dimension specific, Complex design.

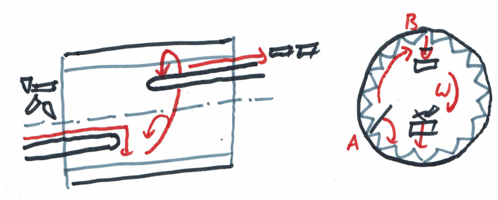

5 **Vibrational plate:**
Placing a small number of tows on a plate and vibrating it in a mode where all waves are in one direction. Tows will probably realign with the wave direction. Wave amplitude and tow size might interfere with efficiency. **Pros:** Can be combined with pick and place. **Cons:** High amplitude vibration needed, Wanted vibration modes hard to obtain consistently.

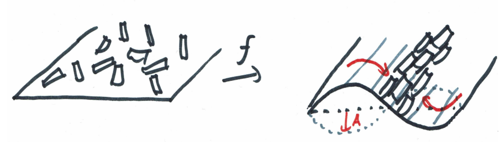

6 **Slope with slits:**
A plate under an angle and covered with spots or lines with a higher coefficient of friction which realign the tows. This can imitate the forces of viscous alignment on the tapes. Dependent on how small the spots can be compared to the tows. The capturing of the aligned tapes can be done using slits on the surface of the plate. **Pros**: Simple design, High flow rate possible, Multiple tape lengths possible. **Cons:** Less control over orientation, Electronics needed, Risk of clogging.

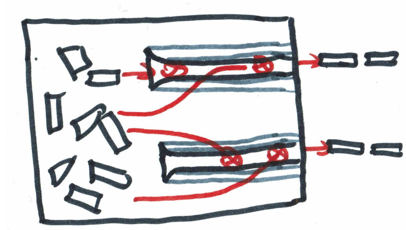

7 **Air/Liquid assisted:**
Employing air or water flows, the tapes are aligned through shear alignment within a medium. Till now this technique is mainly used for small fibers [24, 31]. **Pros**: High flowrate possible. **Cons:** Water-removing (drying) needed afterward, Complicated design, Suitable for small tapes.

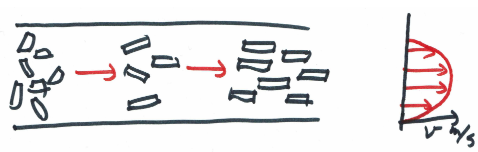

8 **Pick and place:**
With the use of pick and place, robots can place material as a cluster of tapes or single tapes inside a mold cavity. **Pros**: Very accurate, All tape sizes, Option to create digital twin during manufacturing. **Cons:** Slow, Expensive, High computational effort (needs computer vision software.

9 **Wind vortex:**
A funnel with wind suction/pressure so force alignment into a tube. **Pros**: High flow-rate. **Cons:** Complicated design, Probably water needed, Mainly with small tapes, Transition from fast to slow-moving speed after alignment.

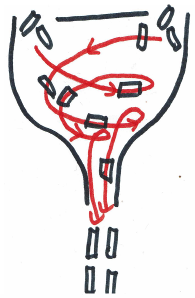

10 **Increase wall effect:**
At the edges, the fibers are normally better aligned [27]. With "temporary" walls during production this could increase the alignment of the tapes. **Pros**: Direct deposition into mold. **Cons:** Complicated mechanical design, One design means one tape width, Only one-dimensional tape orientation, only works for thin layers.

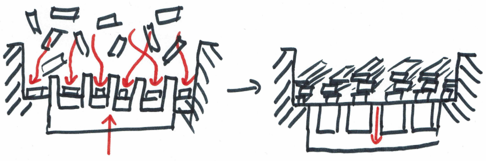

11 **Mechanical interference:**
Using a moving object to filter which tape orientations are able to pass. **Pros**: Can be changed to different tape sizes, Filter on layer height also possible. **Cons:** Small mechanical parts, Wear sensitive, Chance of damaging tapes, Low flow rate.

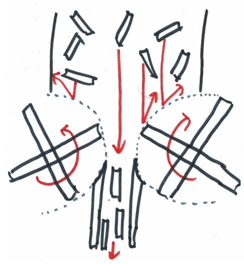

12 **Revolver:**
A rotating drum under an angle where the outside has slots where a tape can sit in. when the drum rotates, some of the tapes fall by chance in the slot and are carried to the higher part of the drum where they are released by gravity in a tube or conveyor belt [41]. **Pros**: Scalable, Reliable orientation. **Cons:** One design means one tape size, Slow process, Based on chance.

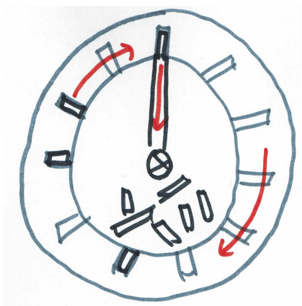

13 **Vibratory bowl feeder:**
An already existing concept for an assembly where parts are fed into another machine with a particular orientation. Berkowitz et al. [42] have shown a method that is suited for rectangular shapes. **Pros**: Known process, Can be outsourced. **Cons:** Not scalable, Expensive, Low flow.

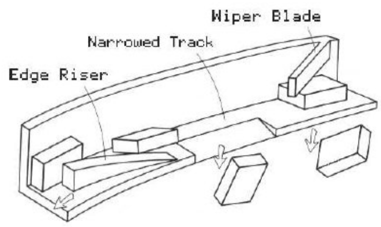

principle vibratory bowl feeder, [42]

14 **Morphing surface:**
Comparable to concept 2, but where the sliding surface, morphs from a V-shaped surface to a flat surface with channels. **Pros**: Simple design, Scalable. **Cons:** Low accuracy (probably).

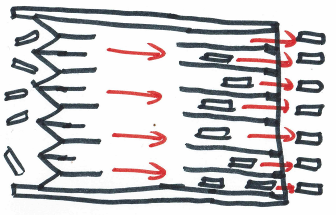

15 **Controlled cutting:**
Thinking about the alignment earlier in the production process can make the orientation easier to control. Because the tapes are made from a continuous tow, a flow can be created. A comparable system is presented by Harper et al. [30]. **Pros**: Full control, No need for new manufacturing stage. **Cons:** Need for cutting next to placement.

16 **Stretching:**
The tapes are placed on lines of elastic material (like rubber bands). When stretching the lines, each orientation will be more aligned with the direction of the rubber band. When tapes are more aligned, they fall between the lines. To de-stretch, the tows will have to be lifted from below. **Pros**: Scalable. **Cons:** Never full alignment, Low reliability, Wear sensitive.

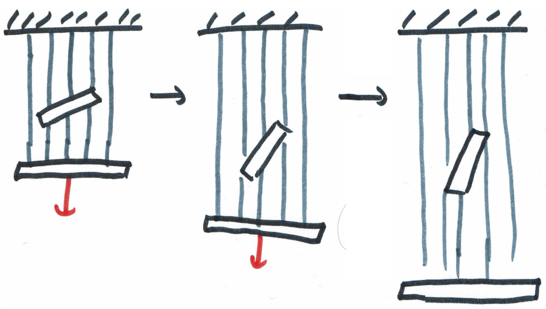

Table 3.2: Description of infeasible working principles for alignment methods

Nr.	Description
17	**Shear flow:** This is a method that is already in use for the alignment of small tows with a fiber length between 0.1 and 5 mm [24, 31]. this makes the method unsuitable to directly implement and would need further development in the medium and extrusion mechanism to also become suited for larger tow length and width. Besides this does this method also needs post-processing to remove the used liquid.
18	**Magnetism:** Magnetism is already used to align small fibers and particles [43, 44] in polymer matrices. This method can be applied by coating tapes with magnetic particles. This way, the tapes are more sensitive to the magnetic influences on the outside and can be reoriented. This method is very elaborate and can be a thesis project on its own. Because of this, there will be no further development done on this matter.
19	**Ultrasonic levitation:** With the use of controlled sound waves, it is possible to levitate small particles [35]. This can be used to control the position of tapes that are able to be levitated. This method needs a lot of development before it can be used for manufacturing. The expected time for this is too much to be feasible for this thesis project.

3.3 Decision criteria for working principles

Based on three criteria a selection of concepts will be made that will be further detailed and tested on a suited scale. This selection is done to lower the effort of further detailing of unfeasible concepts. If a concept has a rating of two or lower for any of the criteria the concept will be excluded from further development. Because the three criteria seem equally important for the feasibility of a concept, there are no weighing factors used. Below, the three criteria are described with their corresponding grading tables. Afterward, the scoring for each concept is shown in table 3.6, for each of the working principles.

Flow-rate or batch size

One of the main advantages of DFC is the speed of manufacturing, the alignment method should preferably match this speed. For each concept, the manufacturing speed is assumed to be scalable with the size of the hardware. This has resulted in the choice to judge the concept based on the size in which it will be manufactured if it were made as proof-of-principle. The grading is based on table 3.3. Here it can be seen that a non-linear grading has been chosen for the scoring system.

Table 3.3: Scoring criteria flow-rate and batch size

Score	Flow-type $[\frac{tows}{s}]$	Batch-type [#tows]
1	≤ 2	≤ 25
2	≤ 5	≤ 50
3	≤ 10	≤ 100
4	≤ 20	≤ 250
5	>20	>250

Design complexity

The number of parts that a design consists of is an indication of the feasibility of a concept. Concepts with many parts, electronics, or parts with many features make the design and working normally more complex and probably less feasible. This can cause problems in later stages of design and manufacturing. The grading is shown in table 3.4. Hereby three categories have been made based on the presence of electronics in the concepts.

Table 3.4: scoring criteria design complexity (N.A. = no grading possible)

Score	Without electronics [#parts]	With simple electronics [#parts]	With complex electronics [#parts]
1	> 5	> 5	> 5
2	≤ 5	≤ 5	≤ 3
3	≤ 3	≤ 3	≤ 1
4	1 (complex)	1 (simple)	N.A.
5	1 (simple)	N.A.	N.A.

Process complexity

When a concept has many independent parameters that have to be tuned, it makes a concept less feasible for optimization. A design that has many tunable parameters will take more effort during the designing and testing phases, while the presence of just a few parameters makes optimization of a concept more feasible. It is assumed that concepts with fewer parameters are more suited for different tape sizes or can be altered easily because of their simplicity. The grading for this criteria is shown in table 3.5. For these criteria, the frequency of rotation or vibration is not included.

Table 3.5: Scoring criteria process complexity

	Number of independent parameters
1	> 6
2	≤ 6
3	≤ 4
4	≤ 2
5	≤ 1

3.3.1 Concept determination for proofs-of-principle

In table 3.6 the scores for each of the concepts have been given. Based on these results, the final concepts will be chosen. In the table, it can be seen that six concepts scored higher than a 2 for all of the criteria. Because the *"vibratory bowl"* concept scored relatively low overall, this won't be taken to the next stage. For the *"rotating drum"* concept, the flow option has been selected due to the higher flow rate score.

Table 3.6: Grading working principles

	Concept	Flow rate	Design complexity	Process complexity	Total	Grade
1	Vibration bucket	3	5	4	12	80%
2	Sliding slope	4	4	4	12	80%
3	Rotating drum (batch)	2	3	5	11	73%
4	Rotating drum (flow)	3	3	5	12	80%
5	Vibrational plate	2	5	4	11	73%
6	Slope with slits	4	4	3	11	73%
7	Air/liquid assisted	4	2	3	9	60%
8	Pick and place	1	3	5	9	60%
9	Wind vortex	5	3	2	10	67%
10	Increased wall effect	4	2	5	11	73%
11	Mechanical interference	2	3	4	9	60%
12	Revolver	2	4	4	10	67%
13	Vibratory bowl feeder	3	3	3	9	60%
14	Morphing surface	4	5	5	14	93%
15	Controlled cutting	5	1	4	10	67%
16	Stretching	2	4	5	10	67%

During the manufacturing and testing of the first concepts it was found that the concepts *"sliding slope"* and *"slope with slits"* have lots of resemblance with the *"morphing surface"* and flow-variant of the *"vibrational box"* concepts. Because of this, these mentioned concepts will not be developed any further. Based on the experiments with testing the *"vibrational bucket"* concept, it was found that this concept can effectively be used for flow-based and batch-based alignment. The four concepts that will be further developed and are listed below.

1. Vibrational box (flow–wise)
2. Vibrational box (Batch-wise)
3. Rotating drum (flow-wise)
4. Morphing surface

3.4 Design and manufacturing of proofs-of-concept

In this section, the working principles of the concepts will be described and presented as they are manufactured for the testing phase. During this project phase, multiple iterations have been made. Based on the relevance of this for the objective of the thesis, only the final designs will be presented. The final designs have been used as the prototype for the measurements of the orientation distribution. In appendix B.1 technical drawings are shown of each of the three concepts. Here, the overall dimensions and geometries have been described.

3.4.1 Vibrational box (batch-wise & Flow-wise)

The design of this concept is based on the design presented by Gan et al. [11] but has been altered to fit the tape size that will be used in this study. In the design, three different wall heights are used in a specific order to constrain tape movement in the sideways direction. By dropping the tapes in the box, the tapes will interfere with the walls and rearrange until they can fall between them. At the bottom of the box, a surface captures the tapes. When this surface is stationary, the box has to be moved upwards after deposition. If the surface is moving, a gap is needed between the box and the surface to allow the tapes to move away.

According to the design of Gan et al. [11], four vibration motors were synchronized to create an upwards vibration. Because this is a relatively complex solution, another solution has been chosen. Instead of constant vibration, the bucket will be shaken by hand if needed. During testing, it was found that the majority of all the tapes fall through the slits without vibrations. The final design can be mounted above a moving or stationary surface. The design is shown in figure 3.1. Hereby the flanges on the bottom are used for mounting. In here, it can be seen that the concept is printed as one part. which resulted in a low design and manufacturing time.

With the batch-wise method, the surface underneath the alignment tool does not need to move. This version of the concept has as advantage that no complex systems are needed for the placement of aligned fibers inside the mold. As a result of this, it is expected that the process can be faster and cheaper.

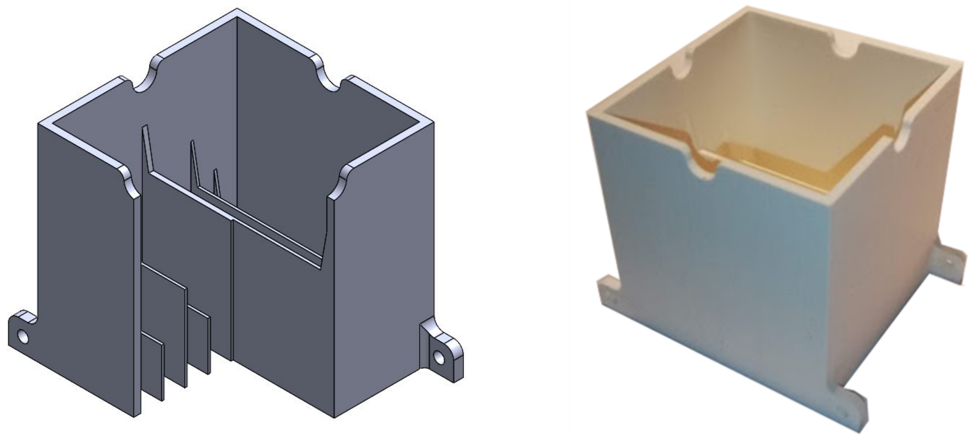

(a) (b)

Figure 3.1: Vibrating box concept. a) Isometric view of CAD model. b) Photo of manufactured part

3.4.2 Rotating drum

The flow-wise version of the rotating drum aims to change the location of a falling tape based on the orientation of that tape. The idea is to carry the well-orientated tapes higher in the drum so that they can fall on a collecting surface that is stationarily positioned within the drum. The badly orientated tapes must fall before this and thus not on the collection surface.

Figure 3.2 shows different types of falling behavior inside a rotating drum. Badly orientated tapes should behave according to "a", the tapes that are well orientated should behave more like "b". What should be avoided is the behavior of "c" hereby the rotation speed of the drum will be the main parameter to avoid this. In figure 3.3 the final shape of the inside surface has been shown whereby the well orientated are expected to fall higher than point A and the bad orientated tapes around point B.

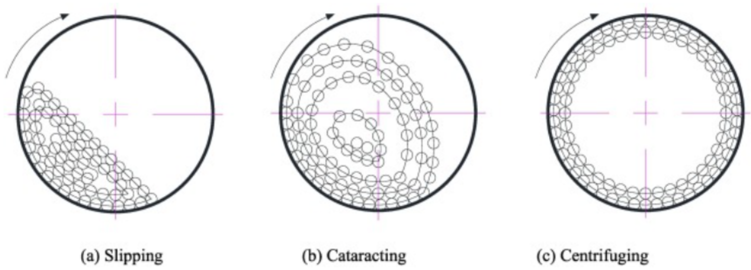

Figure 3.2: Different types of fall behaviour of particles in a rotating drum [Jiang et al. [45]]

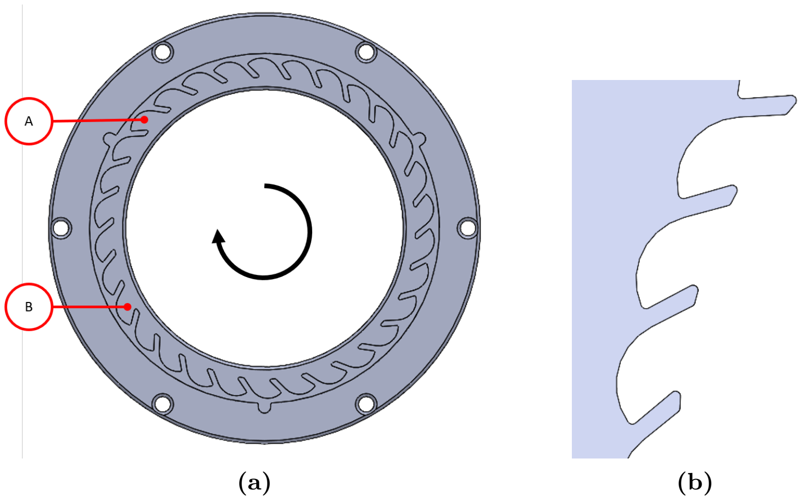

Figure 3.3: Surface geometry inside rotating drum, a) Cross-section. b) Closeup of inner profile

In figure 3.4a an isometric view of the design is shown whereby the described inner profile can be seen (4). The drum is placed on two frames (3) with bearing contacts (2). To avoid the drum slowly moving off the frames, slopes have been designed on the outer surface of the outer edges (1a). The frames will be fixed on a rigid surface to maintain equal spacing. The drum will be rotated using a geared electric motor that is connected to the drive surface of the drum (1.b) with an elastic band. Figure 3.4b shows the manufactured assembly.

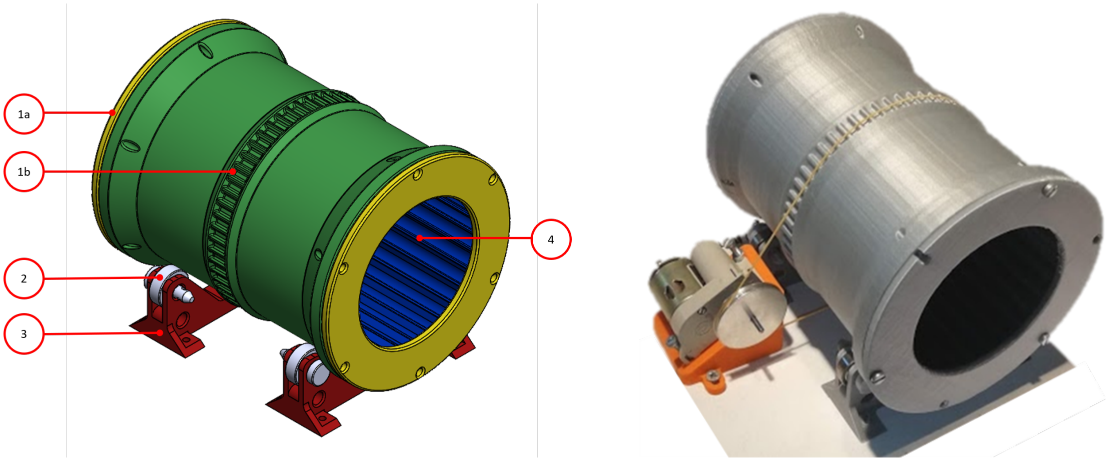

(a) (b)

Figure 3.4: Rotating drum concept. a) Isometric view of CAD model. b) Photo of manufactured part

3.4.3 Morphing surface

The morphing surface concept is a surface that changes its cross-section over its length. This can give different functions to different parts of the surface. These functions can be alignment, transportation, and transfer of tapes to another part of the manufacturing process. The surface will be placed under an angle and vibrations will cause tapes to slide over the surface. The start (top) of the surface has the shape of V's. This shape will transform into multiple square channels over the length of the surface. A better image of this morphing is shown in appendix B.1.

The design has been assembled out of multiple segments. At the high end of the surface, a box is attached where an electronic motor rotates two asymmetric weights to generate vibrations. Figure 3.5a shows how the surface is modeled. At the top, the surface consists out of V shapes. The bottom of the surface consists out of rectangular-shaped channels. Because the morphing surface can only be used to create a flow of aligned tapes, the lower end has a circular end to give room for a conveyor belt. Figure 3.5b shows the manufactured surface. Although the printed layers introduced additional roughness of the surface, this did not seem to restrict tape movement.

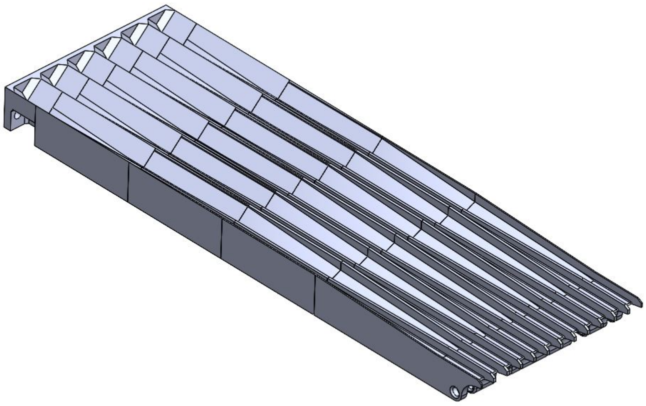

(a)

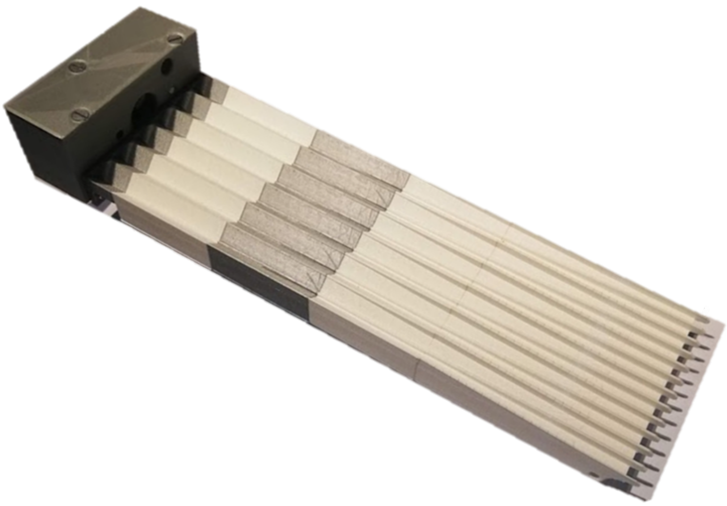

(b)

Figure 3.5: Morphing surface concept. a) Isometric view of CAD model. b) Photo of manufactured part with vibration generator

3.5 Selection criteria for the final concept

After the creation of the concepts, a second selection has been done to choose the final design. It has been argued that different applications can have different methods that are the best for the alignment of tapes. For example, the load on the material can ask for different alignments. A highly concentrated alignment is very suitable for axial loading but probable not for shear or bi-axial loading. Because of this complication, it has been chosen that the methods of alignment should be suitable for the manufacturing of tensile test specimens with the available mold.

3.5.1 Grading function

During the determination of the final alignment method, not only the level of alignment will be taken into account, but also the process that will eventually lead to the test specimen. The ranking of the concepts will be done by using equation 3.1. Hereby the values w are the weighing of different parts. The scoring for the manufacturing time and cost is normalized to the maximum values of all concepts.

$$score = w_1 alignment + w_2 cost_{\text{manufacturing}} + w_3 t_{\text{manufacturing}} \tag{3.1}$$

The tape alignment has been given a weighting value of 3. After this, the manufacturing time has a weighting of 2 and finial the manufacturing cost a value of 1. It should be noted that the determination of this scoring function and the weighing values are chosen arbitrarily. Because of this, it is required that the "winning" concept should also make sense based on own judgments. In the remainder of this chapter, the three criteria will be determined except for the alignment which will be discussed in chapter 4.

3.5.2 Grading criteria: Level of alignment

According to the literature study, the alignment of fibers in one direction improves the stiffness of the material in that direction. In the literature study, it is stated that there are multiple ways to express the alignment. Li et al. [25] describe a method to quantify the tape alignment in a laminate as stated in equation 3.2.This method is a simplification of the orientation tensor [37, 46] which can be in 2D and 3D.

$$a_{11} = \sum \frac{cos^2(\phi)}{N_{\text{tapes}}} \tag{3.2}$$

For this definition, a value of 1 means that all tapes are aligned in the 0° direction. For randomly orientated tapes, this value will be between 0 and 1 dependent on the orientations. For random orientations, a value of 0.5 is assumed. This method is a simplification of the use of the orientation tensor [37, 46] which can be in 2D and 3D. A reason for the use of this method is that it is widely used within the literature and is thus also more suitable as a value to compare to other measurements and relations that are found between physical properties [27, 37, 46]. The value a_{11} of the orientation tensor will be used as expression for the tape alignment. The measurement of the alignment distribution of each of the concepts is discussed in chapter 4. This chapter will describe the measurement technique as well as the results that were measured.

3.5.3 Grading criteria: Manufacturing cost

Because the thesis is not focusing on cost reduction of the manufacturing process, this criterion is taken to be the least important. The manufacturing cost will be based on the design and manufacturing time of the process. This includes the manufacturing of the parts that are needed for the alignment method but also that of all the other manufacturing steps that are dependent on the concepts. This criterion can be seen as the investment cost needed for each concept.
An estimation has been done on the time it takes to manufacture the production line for the proofs-of-concept. This will be done by describing the expected manufacturing process and estimating the time that is needed for designing and manufacturing each of these processes.

The design and manufacturing of this process are expected to need a large number of hours which are originating from different actions that have to be taken. For this comparison, multiple aspects of the are taken into account which will be discussed for two product categories which are batch-based production and flow-based production.

Flow-based production

For flow-based production, the process will be based on the creation of thin plates which consist out of aligned tapes in between two polymer films. These plates will have to be cut to size before they can be placed inside the mold. This production method gives the possibility to scan the plates separately before stacking them in the mold. In figure 3.6 a sketch of this process is shown. It has to be taken into account that a production line like this has to be designed and manufactured when samples have to be made. Based on the three actions that are taken into account for this comparison, the design and manufacturing times of the three flow-based concepts are given which are stated in table 3.7.

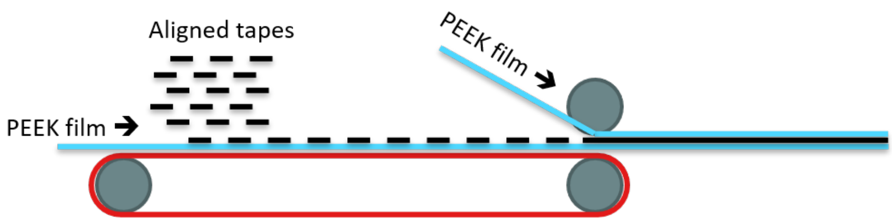

Figure 3.6: Flow based tape capturing

Table 3.7: Manufacturing time for flow-based concepts

	Vibrational box (flow)	Morphing surface (flow)	Rotating drum (flow)	Unit
Concept manufacturing	15:00	40:00	50:00	[hh:mm]
Deposition mechanism	5:00	10:00	10:00	[hh:mm]
Tape capturing	15:00	15:00	15:00	[hh:mm]
Total	35:00	65:00	75:00	[hh:mm]

Batch-based production

Batch-based production is a more straightforward method. Hereby the tapes will be deposited inside the mold cavity. Although this method is faster, it does not allow for inspection of the tape orientations during the manufacturing process. The time estimations of the flow-based production of the batch-based vibrational box shown in table 3.8.

Table 3.8: Manufacturing time for batch-based production

	Vibrational box (single batch deposition)	Unit
Concept manufacturing	10:00	[hh:mm]
Deposition mechanism	01:00	[hh:mm]
Tape capturing	00:15	[hh:mm]
Total	11:15	[hh:mm]

3.5.4 Grading criteria: Manufacturing time

The third term in the scoring formula is the manufacturing time of the concept. This time is based on the time it takes to align a given number of tapes that are needed to manufacture a single plate (1800 tapes) and the time needed for the execution of the concept-dependent actions. The manufacturing time is dependent on the size of the wanted part (volume and area). A rough estimation of the manufacturing time will be based on the case of creating a plate with the dimensions of 140 x 100 x 4 mm. These are the inner dimensions of the mold currently used to manufacture a plate out of DFC tapes.

The manufacturing time has been split into alignment time and process time. The alignment time is based on the observations during the testing of the concepts. The processing time is estimated by breaking down the manufacturing process and estimating the times for each process step. Actions that do not contribute to the comparison such as the pressure and temperature cycle will be left out of this comparison because these are assumed to be the same for all alignment methods.

Alignment time

The alignment time has been based on the observations that have been done during the testing of the concepts. These alignment times have been stated in table 3.9. It should be noted that these observations are inaccurate but can still be used due to the large differences between the concepts.

Table 3.9: Alignment times concepts

	Alignment time [mm:ss]	Unit
Vibrational box (single batch deposition)	01:00	[mm:ss]
Vibrational box (flow based production)	03:00	[mm:ss]
Morphing surface (flow based production)	12:00	[mm:ss]
Rotating drum (flow based production)	06:00	[mm:ss]

Process time

The manufacturing time of all the concept-dependent actions has been based on a function breakdown. With these estimations, the process times have been given a value in table 3.10. The function breakdown for the steps that have been anticipated for each of the concepts has been given in figure 3.7. These times have been based on the assumption that the plate that is manufactured with the flow-based concepts is the width of the mold. Because this can not be the case for the rotating drum concept 10 extra minutes have been added for the plate production. In table 3.10 it can be seen that the batch-based concepts are faster than the flow-based processes. This is mainly due to the simplicity of the manufacturing process.

Table 3.10: Manufacturing times concepts

	Alignment time	Unit
Vibrational box (batch-based deposition)	00:16	[hh:mm]
Vibrational box (flow-based production)	00:45	[hh:mm]
Morphing surface (flow-based production)	00:45	[hh:mm]
Rotating drum (flow-based production)	00:55	[hh:mm]

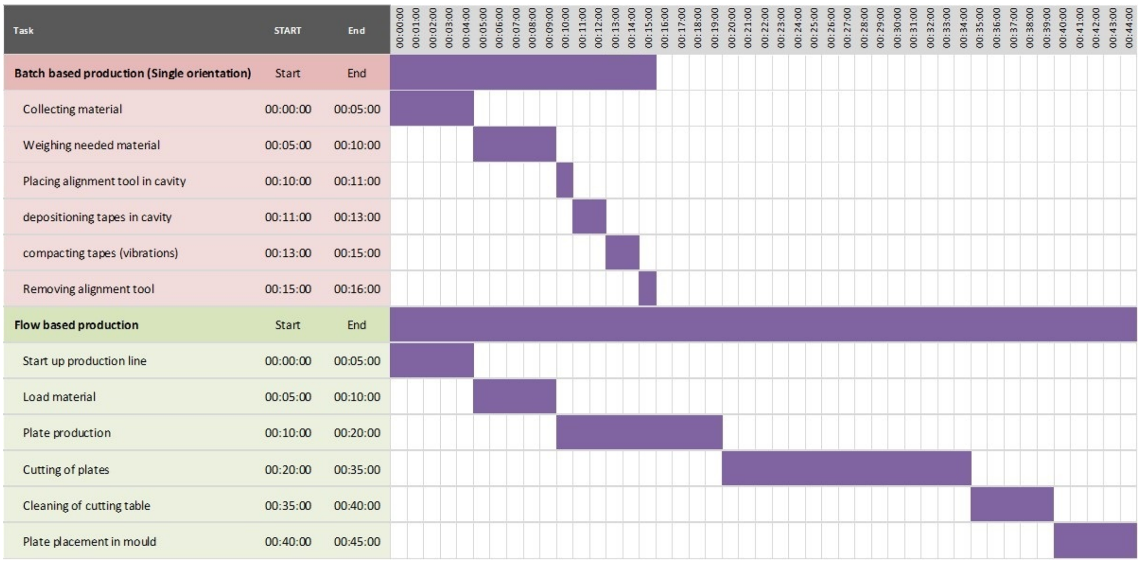

Figure 3.7: Function breakdown for determining process time

3.5.5 Grading alignment methods

Based on the scoring concept and the values that have been stated in the previous sections, the scores for each concept can be calculated and are shown in table 3.11.

Table 3.11: Overview concept scores

	Vibrational box (batch-based)	Vibrational box (flow-based)	Morphing surface (flow-based)	Rotating drum (flow-based)	Units
Alignment	0.8726	0.9485	0.9763	0.9584	[-]
Man. Cost	11:15	35:00	65:00	75:00	[hh:mm]
Man. Time	0:17	0:48	00:57	01:01	[hh:mm]
Score	4.97	3.87	3.27	2.94	[-]

It can be seen that the *"vibrational box (batch-based)"* scored the highest compared to the other concepts. With this, it has been chosen to use this method for the alignment of tapes during the production of test samples. Due to the high overall score of the concept, the uncertainty of the tape alignment method (as discussed in chapter 4) will most likely not change the outcome of the concept selection.

One advantage of this concept is that it can easily be designed such that multiple batches are deposited. This can be used to introduce the creation of different orientations. The argumentation why this concept scored the best despite that it scored the lowest on alignment, is its fast process time and simplicity within the manufacturing line. Also because the alignment of all the concepts is good, the scoring of this becomes less decisive. During the next steps of the thesis, this method will be used to manufacture samples that are suitable for mechanical testing.

3.6 Concept simulation

During the development and testing of the concepts, the possibility for simulation with numerical methods was explored. The use of this would enable the option for design optimization without the need for manufacturing and testing in real situations. The method that has been used is Rhino 6® in combination with the Grasshopper plug-in. During this exploration, the vibrational box concept was tested first because of its potential as a final alignment method and because the model could be designed with a few parameters. Because the needed model was more complex than anticipated (due to the need for aerodynamic forces) the exploration with this concept was abandoned. To showcase the potential of simulation the morphing surface concept had been modeled. The results from these simulations were not realistic enough to be used but did show potential for simulation of simple physics. In appendix C the full process and results of the simulations are described.

3.7 Proposed alignment method

Based on the selected concept, an alignment tool has been designed for the creation of test samples inside the mold. In total, three different tools have been designed and manufactured. With these tools, the tapes can be orientated in the -45°, 0°, and 45° direction. Due to the low requirements on mechanical properties and dimensional accuracy the tools have been manufactured using the FDM technique with Ultimaker 2+®. This process allowed for fast prototyping and manufacturing. The changes that had to be implemented on the proof-of-concept are the dimension of the tool to fit the size of the mold and the height of the outer wall for an easier deposition of tapes (without spillage). Because the wall spacing is not fully compatible with the mold, it has been chosen to have larger spacing between the outer walls. Hereby the walls in the middle have the same spacing as the proof-of-concept. The effect of the height of the inner walls has not been examined. Because the height is larger than the tape length, it is assumed that this will not influence the alignment. With a wall height that is lower than the tape length, tapes could stick out and block the tool. For the tools with a ±45° angle, the cavities at the corners of the tool have been given a larger spacing to make tape deposition there possible as well. In figure 3.8 the designed tools have been shown. For a more detailed description, technical drawings have been shown in appendix B.2. In here it can be noticed that the 0° tool has three different wall heights whereby the ±45° tools only have two. The highest wall originates from the original design of Gan et al. [11]. Hereby the width of a box segment was halved by walls that decreased in height which constrains movement of tapes across walls. This design strategy was not possible for the ±45° tools due to the spacing of the walls and the size of the mold. During testing, it was found that the tapes can not move sideways because the spacing between walls is too large for a tape to bridge them.

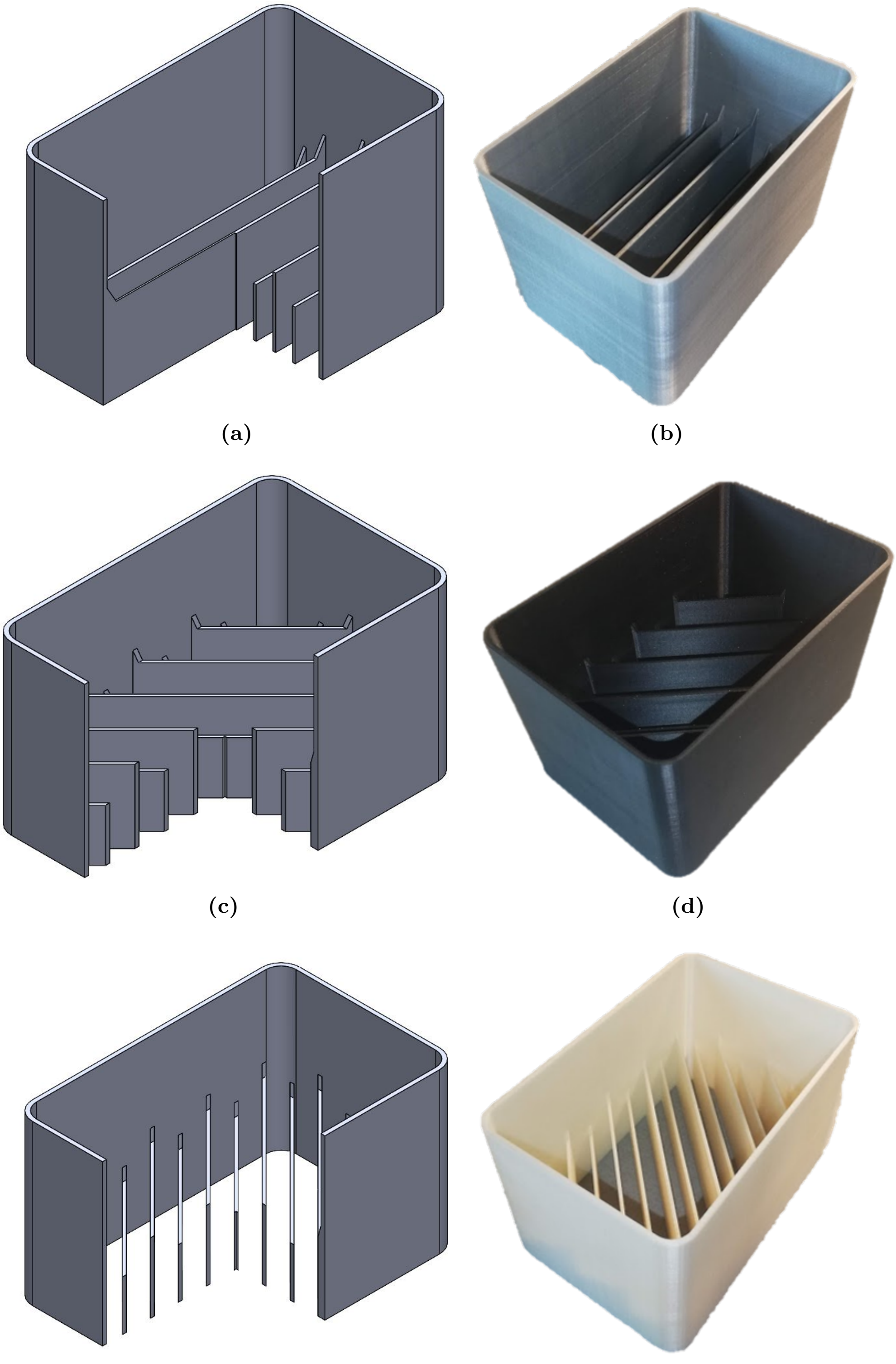

(a) (b) (c) (d) (e) (f)

Figure 3.8: Alignment tools for manufacturing, isotropic CAD model and manufactured part, a-b) 0° orientation, c-d) +45° orientation, e-f) -45° orientation

Chapter 4

Orientation Measurements and Digital Image Recognition

In parallel with the development of the concepts, a measuring system has been developed which enables large-scale measurements of tape orientations. With this system an important feature of the concepts, the orientation distribution of tapes, becomes quantifiable. The system can measure the in-plane orientation of single tapes or orientations of tapes within small groups of overlapping tapes. This chapter will firstly describe the measurement methodology and setup that has been used. Afterward, the validation and verification process has been described. Finally, the results of the measurements of each of the concepts have been presented. Here, the alignment definition that is used for the determination of the final concept has been stated.

4.1 Methodology

The thought behind the working of the measurement system is relatively simple. By capturing images of a tape and processing these with image recognition software, the orientation of the tape can be determined. This section will describe the test setup and codes that have been developed.

In figure 4.1a, a schematic representation of the setup has been shown. The measurements of the tape orientations will are performed by capturing a picture of tapes (4) that are located on a white background (5). This image is captured utilizing a USB webcam camera (1) that is connected to a computer. By recognizing the tapes with OpenCV [47], the orientations can be determined in large quantities. A frame (3) has been constructed for the positioning of the camera (1) and lights (2). LED lights (2) have been attached to the frame for the illumination of the tapes. At the bottom of the frame, a wooden plate (5) is used for the mounting of the background surface of the tapes. During the measurements, the setup is placed in a darkened room where other light sources should introduce less noise in the view of the camera. In figures 4.1b and 4.1c the used setup has been shown.

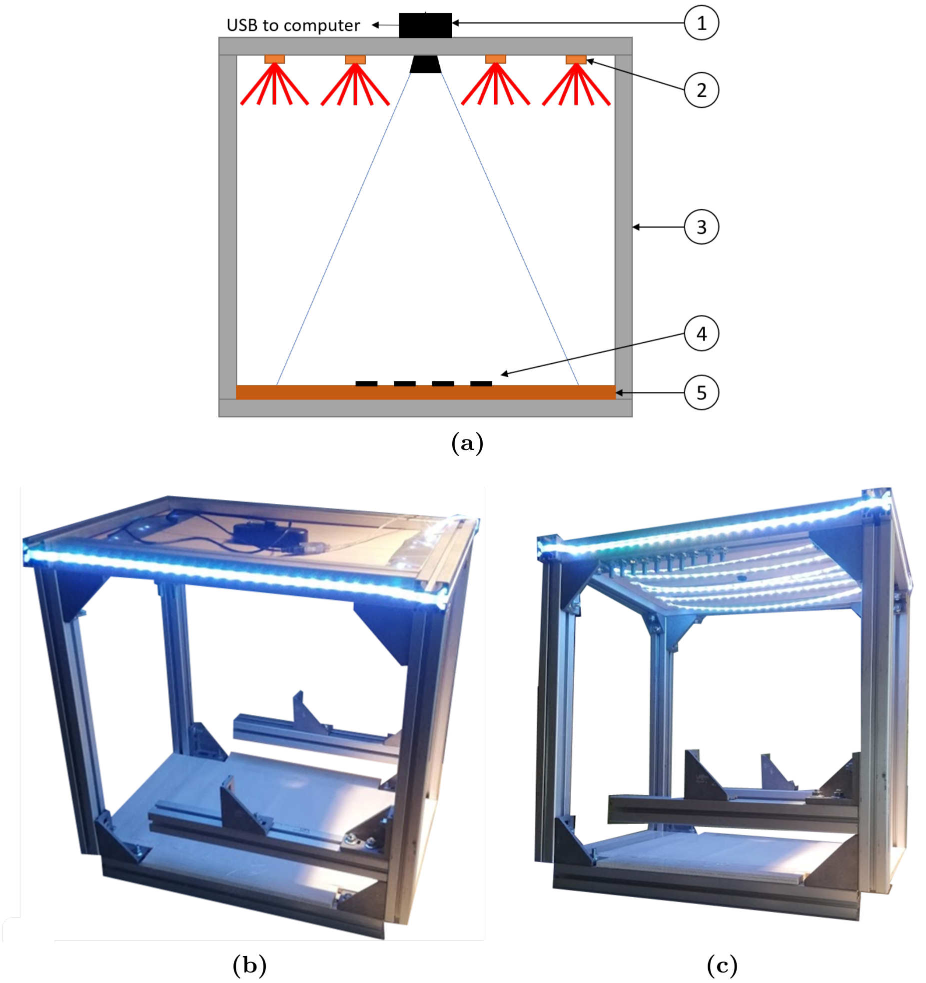

Figure 4.1: Measurement setup for tape orientation measurement. a) Schematic, b) Upper view of setup, c) Lower view of setup

To obtain the desired data from the measurements, multiple codes have been written. An overview of the "collaboration" between these codes has been shown in appendix E. These codes each have separate functions which will be described for a few of them below.

The most important code is developed to recognize tapes and return the orientation of each tape and is given in appendix F. The image that is captured by a camera is first cropped to only focus on the area of interest and transformed into a gray-scale image for the reduction of computational effort. After this, the grey image is turned into a black-and-white image based on a threshold value that has been found during the background analysis of appendix A. The determination of the threshold values is dependent on the background and light which has also been described in this appendix. This has resulted in the use of white paper as background and red lighting has been described. To recognize tapes within a group of overlapping tapes, basic patterns are identified.

The code will create a *.txt* file to collect all the measurements. Because the created text file consists out of all the measurements that have been taken, a single tape can be represented by multiple data points in the text file. This data is refined to remove "double" readings from the same tape. For this, a second code has been made. This code creates series of measurements that are considered to be from the same tape which will be simplified to one single value. The code that is used to filter the raw data is shown in appendix G.

4.2 Validation and verification of the measurement setup

To know the reliablilioty of the measurements, the test setup and code have been validated and verified. In this section, the action will be described that have been taken to state if the system does what it is designed for (validation) and how accurate the system this does (verification).

4.2.1 Validation of tape orientation measurement system

During validation of the system, it is proven that the system can identify the composite tapes and determine the orientation of these tapes. This validation has been completed early in the development process by producing an image of tapes and utilizing the code to determine the orientation of the tapes. In 4.2a the results of this experiment are shown. It can be seen that the tapes are recognized.. The code was also able to determine the tape orientation which has been confirmed by a manual angle measurement of the tapes (with a different image) as shown in figure 4.2b.

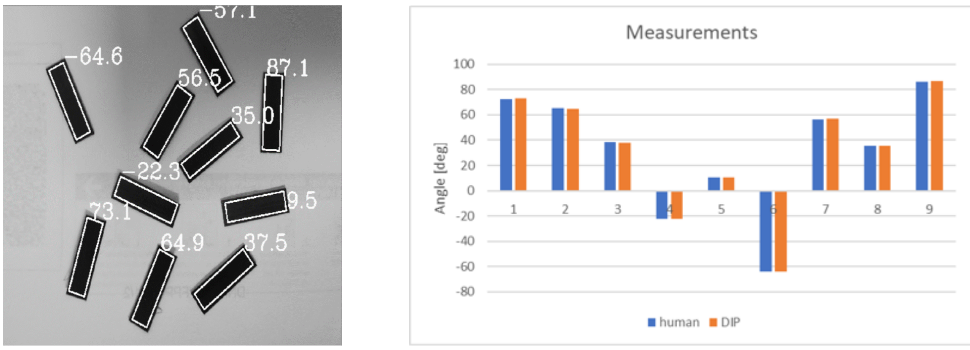

(a) (b)

Figure 4.2: Validation of tape orientation measurement system, a). Recognition of tapes with orientation readings, b) Measurement of angles, manual measurement (Blue) code measurement (orange)

4.2.2 Verification of tape orientation measurement system

The verification of the measuring setup will only be performed on the area in the image that will be used by the measurement of the concepts. It was observed that within the full view of the camera, straight objects become curved (distorted) at the edges. Within the area that will be used during the measurements, the influence of this distortion on the measurements has been addressed. A pattern as shown in figure 4.3a has been located in the center of the camera view. The total width and height of the pattern are 135 mm which is greater than the used measurement area during the concept measurements. Figure 4.3b shows the image that is captured by the camera. When the pixel locations of the pattern were examined, it was clear that the lines were not curved significantly. To show this, the pixel indices of nine points (all corners and center points of the red lines) of the pattern are shown in tables 4.1 and 4.2. It can be observed that these points form an almost perfect grid. With these measurements, the assumption of an undisturbed image in the center part of the camera view is accepted.

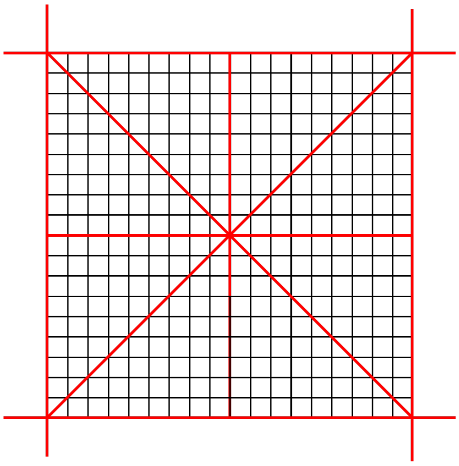

(a)

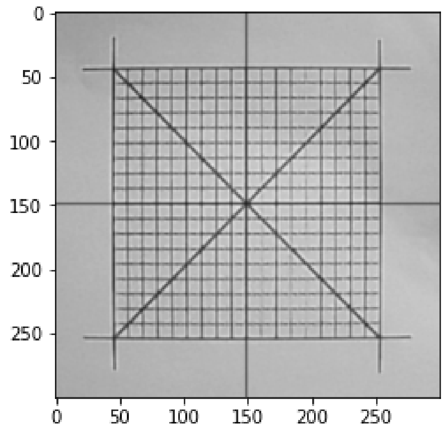

(b)

Figure 4.3: Camera field distortion, a). Test pattern, b) Camera capture, x- and y-axis show pixel indices

Table 4.1: X-indices distortion pattern

	X-coordinate		
	Left	Center	Right
Top	45	149	253
Center	45	149	254
Bottom	46	149	253

Table 4.2: Y-indices distortion pattern

	Y-coordinate		
	Left	Center	Right
Top	44	43	44
Center	149	149	149
Bottom	254	254	253

Followed by the acceptance of the assumption of the undisturbed camera, measurements have been taken from five locations in the area of interest (as shown in figure 4.4a) for the determination of the system accuracy. Hereby location 1 is in the center of the camera view. During each measurement, a servo motor is positioned on one of these locations. This servo rotates a paper surface with a single CF/PEEK tape stepwise . For each step, the measurements are read and the average and standard deviation of the measurements (more than 100 per step) are calculated. For ilustration, a small selection of these measurements is shown in figure 4.4b. In here, the red lines represent the average of the measurements per step, furthermore the blue lines display the standard deviation of these measurements. When for all the locations and steps, the mean angle is plotted over the standard deviation as shown in figure 4.4c. With this, it is found that the standard deviation does not exceed 2.8° with an average of proximately 1°. It is noted that there seems to be a lower overall standard deviation around the ±45° angles. This can be explained by the change in angle due to a change in pixel index is smaller when a line is orientated at a 45°. Because of this, it is expected that the observed scatter in measurements will decrease when a camera with a higher resolution is used for the measurements. If a particular range of angles is more of interest, the diagonal of the camera view can be aligned with the center of this range. This has not to be done for the concept measurements.

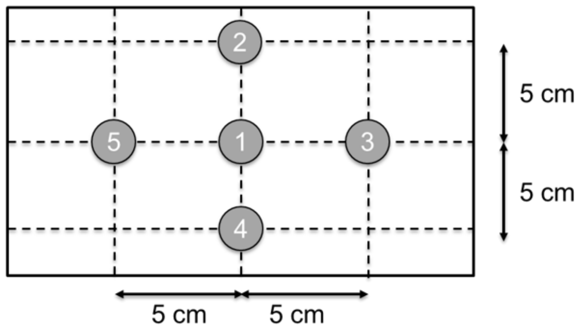

(a)

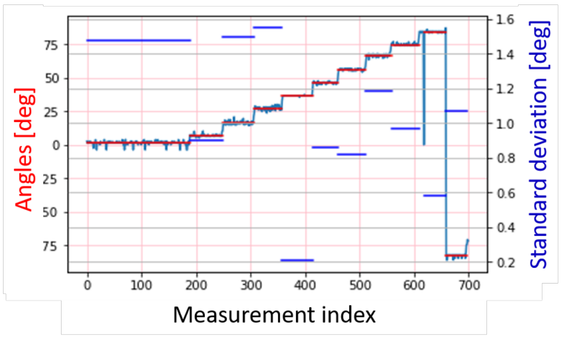

(b)

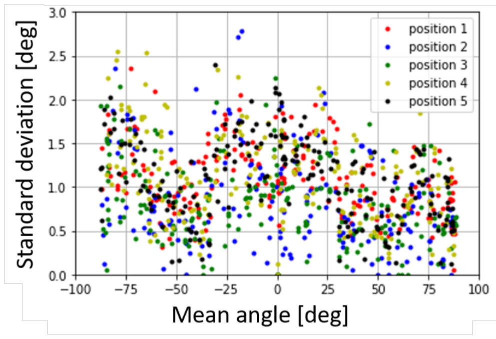

(c)

Figure 4.4: Validation measurement, a). Measurement locations, b) Measurement processing example, c) Measurement mean angle and standard deviation

4.3 Effect of batch-wise deposition on Vibrational box concept

Although Gan et al. [11] have used the concepts of the vibrational box to create a flow-wise tape deposition onto a surface, it was found that the concept is also able to align tapes as a batch-wise process. One difference between the two deposition strategies is that the batch-wise deposition will create tape orientations perpendicular to the desired orientation. This is caused by tapes that can stand straight up against the walls of the alignment tool. During tests, it was found that the percentage of perpendicular tapes is dependent on the batch size of tape deposition, hereby smaller batches will result in a lower number of perpendicular tapes. Besides this is has been observed that the "shaking" of the alignment tool will lower this percentage although it will not necessarily become zero. The difference between batch- and flow-wise deposition will be discussed below.

4.3.1 Tape perpendicularity

The characterization of the batch-wise tape deposition with the vibrational box concept consists out of two steps. First, the orientation distribution of the flow-wise deposition will be measured. This distribution is assumed to be the same for all the tapes that are not perpendicular. To create the orientation distribution, a chosen percentage of perpendicular tapes will be added to these measurements based on small-scale experiments.

By depositing batches of a known number of tapes into the vibrational box, the number of perpendicular tapes can be determined. During the test, three batch-sizes have been tested. The batch sizes are 10, 21, and 40 tapes. Each batch has been tested ten times to create a data set that is assumed to be representative. When depositing the tapes in the alignment tool, the tool has not been shaken although this will likely happen during a manufacturing process. The batches have respectively 8.0%, 11.4%, and 13.3% perpendicular tapes which implies that smaller batch sizes have a lower percentage of perpendicular tapes. Because it is assumed that the alignment tool will be shaken, the percentage of perpendicular tapes is assumed to be part of the flow-wise orientation distribution is 8%.

4.4 Measurement results of proofs-of-concept

In this section, the orientation distribution of each concept will be displayed employing histograms and the in-plane orientation tensor. In the remainder of this section, these methods will be used to characterize the alignment of the four concepts.

Vibrational box (flow-wise)
During the measurements, the alignment tool is positioned above a conveyor belt which moves the tapes underneath the camera of the measurement system. A second conveyor belt was used to supply tapes into the tool. The outcomes of the measurements are displayed in figure 4.5 and with the in-plane orientation tensor.

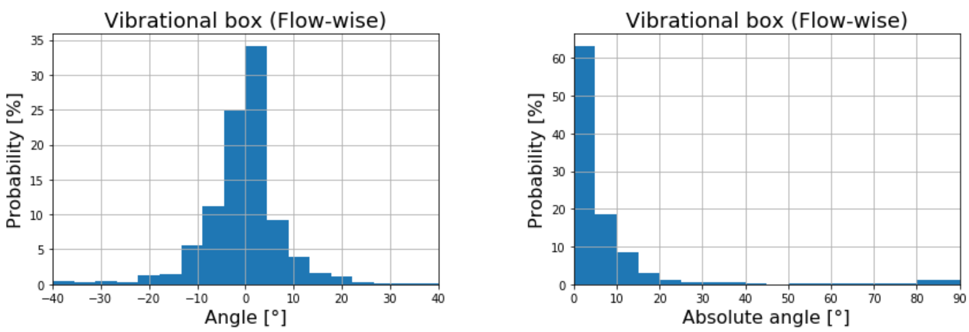

(a) (b)

Figure 4.5: Measurements orientation distribution flow-wise vibrational box, a) Orientation distribution range [-40°,-40°], b) Absolute orientation distribution

$$a_{\text{in plane}} = \begin{bmatrix} 0.9485 & 0.0051 \\ 0.0051 & 0.0515 \end{bmatrix}$$

Vibrational box (batch-wise)

When adding the percentage of perpendicular tapes, the characterization of the batch-wise variant changes slightly compared to the flow-wise version. Because of this, the batch-wise variant of the vibrational box has the lowest alignment of the concept that has been tested. The results are shown in figure 4.6.

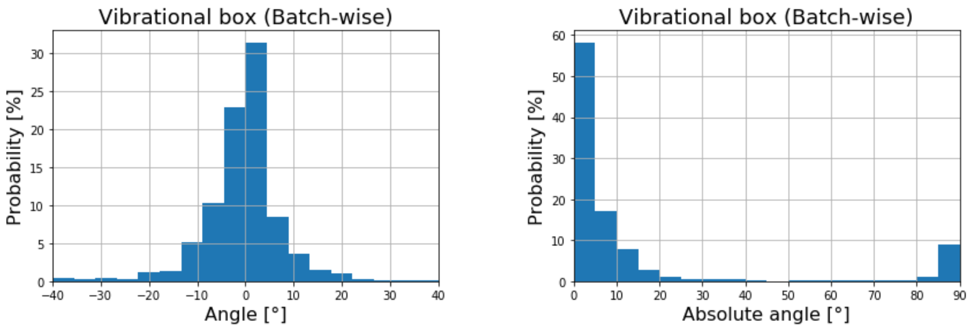

(a) (b)

Figure 4.6: Measurements orientation distribution batch-wise vibrational box, a) Orientation distribution range [-40°,-40°], b) Absolute orientation distribution

$$a_{\text{in plane}} = \begin{bmatrix} 0.8726 & -0.0047 \\ -0.0047 & 0.1274 \end{bmatrix}$$

Morphing surface

By placing a conveyor belt at the end of the morphing surface, the aligned tapes have been measured. Based on the orientation tensor of these measurements, it has been concluded that this concept has be best alignment. The resuts of the measurements can be seen in figure 4.7.

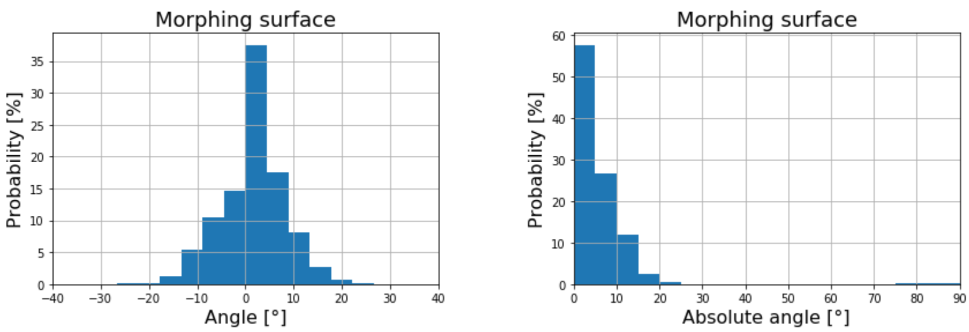

(a) (b)

Figure 4.7: Measurements orientation distribution morphing surface, a) Orientation distribution range [-40°,-40°], b) Absolute orientation distribution

$$a_{\text{in plane}} = \begin{bmatrix} 0.9763 & 0.0195 \\ 0.0195 & 0.0237 \end{bmatrix}$$

Rotating drum

By employing two conveyor belts for the feeding and extraction of the tapes into and out of the rotating drum, the tapes have been aligned and measured. During the measurements on the rotating drum, it was found that the flow-rate of the process was the lowest of all the concepts. This is caused by the small width of the extraction conveyor belt.

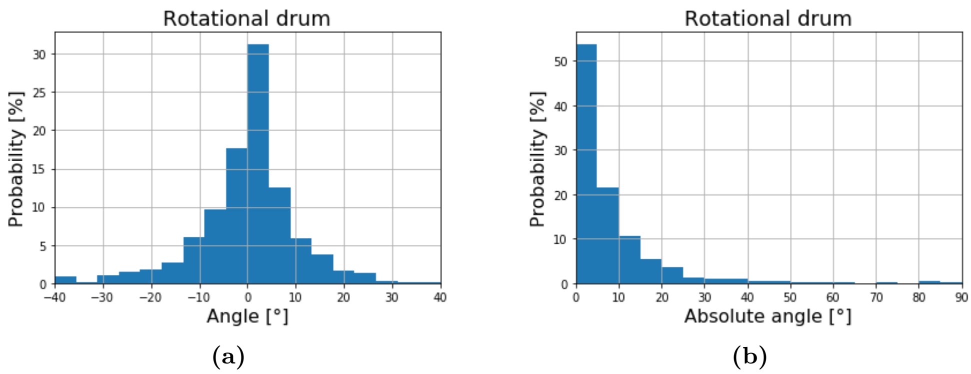

Figure 4.8: Measurements orientation distribution rotating drum, a) Orientation distribution range [-40°,-40°], b) Absolute orientation distribution

$$a_{\text{in plane}} = \begin{bmatrix} 0.9584 & 0.0027 \\ 0.0027 & 0.0416 \end{bmatrix}$$

4.4.1 Comparison

Based on the orientation measurements of the concepts, it can be concluded that the orientation tensors don't differ considerable from each other in absolute terms. The morphing surface shows the best alignment of the four concepts and the batch-wise vibrational box concept shows the least alignment. When calculating the homogenized material properties by using CLT, it can be seen that the methods differ more than in just the alignment in one direction. A wider spread in orientations (such as with the rotating drum concept) leads to better tangential and shear stiffness. For some cases, this could be preferred based on the application.

Chapter 5

Application of the alignment method for specimens preparation

For the mechanical characterisation of DFC, test specimen have been manufactured. To obtain the test samples, multiple plates have been manufactured. Hereby, the random orientation will serve as a baseline for the comparison with the 0° aligned samples. With the ±45° sample, the shear properties can be obtained by testing the mechanical properties. From within the research group, there has been an additional interest in combining different orientation layers of DFC with different alignment orientations, a side experiment has been performed with the ±45° plates. For one of these plates, a separation layer has been placed in between the different layers to see if this feature is needed for the protection of layers during deposition and what the effect will be on the mechanical properties. The result from the mechanical test will be discussed in chapter 6. The manufacturing of samples has also given the possibility to gain knowledge about the manufacturing with DFC.

5.1 Discontinuous plate manufacturing

The manufacturing process of the plates has been based on the research knowledge of Deniz Gülmez and has not been investigated extensively apart from the work that has been done during the literature review. The literature review in chapter 1 has described the manufacturing process of TP-based DFC by using the same figure as figure 5.1. After the manufacturing of UD tapes from UD strands, the material is deposited into a mold after which it is heated and pressed into the desired shape. The use of the alignment tool is used during this deposition. Besides this addition to the process, the same steps can be used. In this section, the manufacturing process will be further described.

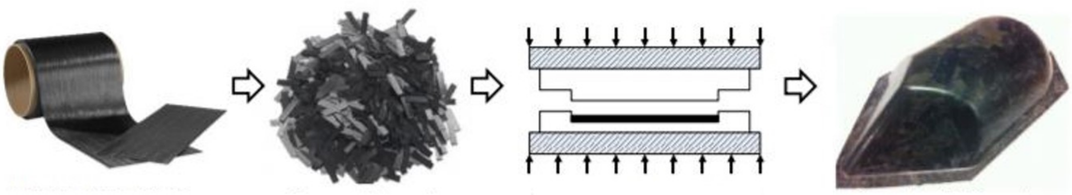

Figure 5.1: Schematic manufacturing cycle of DFC composites, Selezneva et al. [8]

5.1.1 Mold preparation

For the preparation of the production, firstly, all the surfaces of the mold have been cleaned after which two layers of release agent (marbocote®) are applied to all working areas. After this, the lower plate and frame of the mold will be assembled followed by another layer of release agent.

5.1.2 Tape deposition

The orientation distribution of the tapes can be random or aligned utilizing an alignment tool. If an alignment tool is used, it will be placed inside the mold cavity, as shown in figure 5.2. As next step, 90 grams of the CF/PEEK tapes will be deposited into the cavity or alignment tool. To keep the tapes compact inside the cavity, this is done in batches . After the deposition of tapes, the tapes that can obstruct the closing of the mold are pushed inwards and the mold closed. In the sections below, the process of tape deposition will be discussed in detail for each of the orientation distributions.

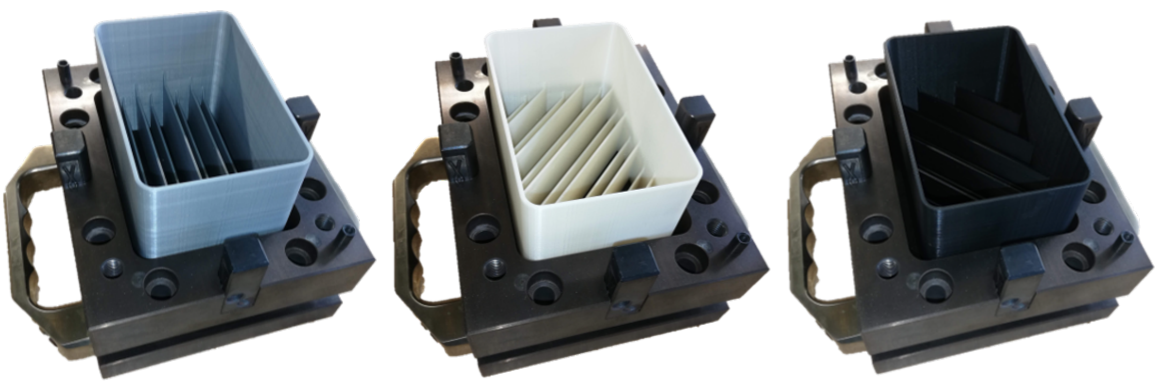

(a) (b) (c)

Figure 5.2: Alignment tools in mold cavity, a) 0° alignment tool, b) +45° alignment tool, c) -45° alignment tool

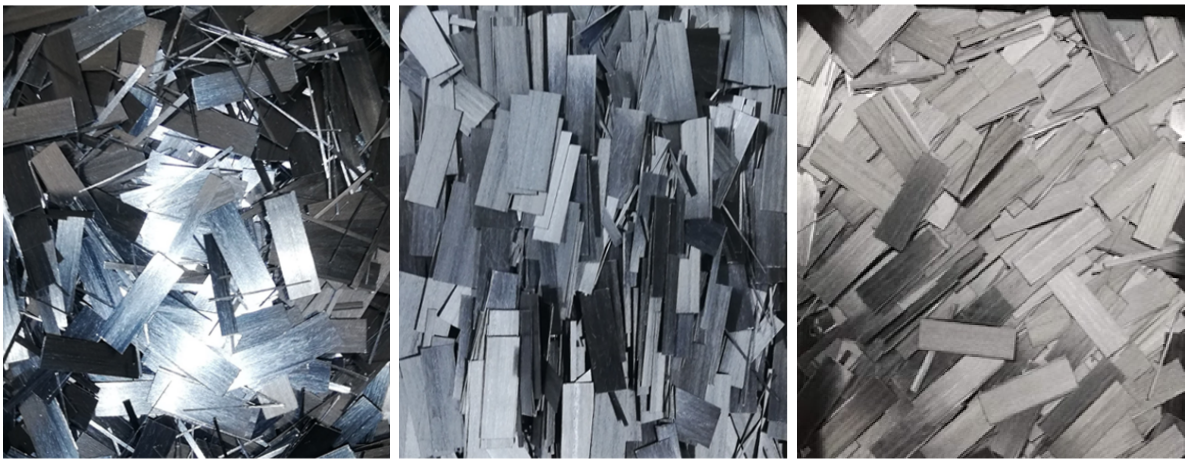

(a) (b) (c)

Figure 5.3: Deposited tapes inside mold, a) Random tape distribution, b) 0° centered tape distribution, c) ±45° centered tape distribution

Random tape orientation

For the plates with randomly orientated tapes, small batches of tapes have been placed by hand inside the mold cavity. While doing this, the focus was to not create any bias to a single tape orientation. After all the tapes were deposited, it was observed that the height of the tapes exceeding the edge of the mold which lead to blocking during the closure of the mold by tapes. This resulted in a higher percentage of tapes that had to be deposited in the center. An image of randomly orientated tapes inside the mold can be seen in figure 5.3a.

0° centered tape orientation

To align the tapes in the loading direction, the 0° alignment tool has been used. The use of the alignment tool is as follows:

1. The tool is placed inside the mold cavity
2. A small batch is dropped inside the tool such that tapes are spread evenly
3. The tool is shaken to make the tapes align and lower the number of perpendicular tapes
4. The tool is removed carefully in order not to disturb the tape orientation

This process of tape deposition is repeated until the required amount of tapes is deposited inside the mold. The location of tape deposition has been changed based on where a lower number of tapes observed. When the tool was placed again in the mold, any straight-upstanding tapes have been flattened. The use of the alignment tool resulted in a lower number of tapes at all the edges of the cavity. In figure 5.3b the tapes after deposition are shown. When comparing this to the randomly orientated tapes it was noted that this technique makes the tapes more compact inside the mold which made it easier to close.

±45° centered tape orientation

For the ±45° tape orientation, the same process as with the 0° orientation has been adopted with different alignment tools. Hereby two tools have been used that have been designed for a [+45°,-45°,+45°] stack. Firstly 25% of the material is deposited with one tool, followed by 50% of the material with the other and the remaining 25% with the first tool again. For one of the three plates that have been manufactured PEEK films have been placed inside the cavity between different orientations. In figure 5.4c the stacking sequences have been shown for the plates with and without PEEK film. Because of the tape orientations, large gaps have been observed at the corners of the plate. The compaction of the tapes was in between the random and 0° centered orientations. Hereby the addition of the PEEK film made the compaction even less although better than with randomly orientated tapes. In figure 5.3c the tapes after deposition have been shown.

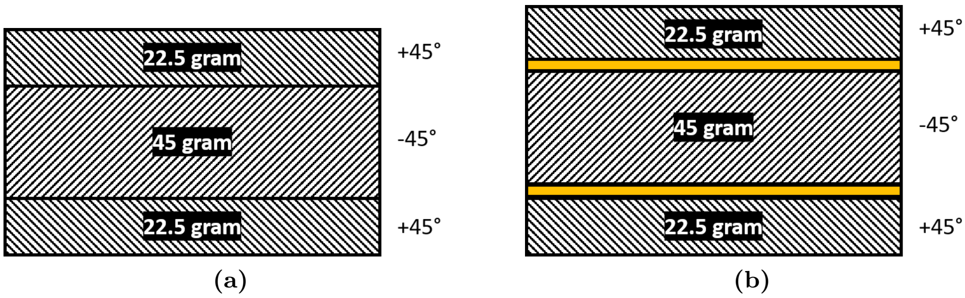

Figure 5.4: Stacking sequence ±45° centered tape orientation, a) Stacking sequence without PEEK film, b) 0°Stacking sequence with PEEK film (yellow)

5.1.3 Temperature pressure cycle

After the tape deposition, the mold is closed and placed in the press. Thermocouples are connected and checked followed by the start of the temperature/pressure cycle. The programmed cycle steps are stated below.

1. Application of contact pressure
   After the mold is placed in the press, the press is closed and the initial contact pressure is applied. This is needed to create a better conductivity between the press and the mold, and between the mold and the tapes inside.
2. Heating of mold
   After the contact pressure is reached (directly at the start of the cycle) the contact plates of the press are heated with a temperature ramp till 385°C.
3. Dwell time
   Until both of the thermocouples give temperature readings of 383°C or higher, the plates of the mold will be kept at a constant temperature. When the 383°C threshold is reached, it will be kept at this temperature for 15 minutes to ensure that the material inside the mold is molten. For all the plates (except plate 9) the same threshold temperature has been used. To avoid polymer degradation, the heating phase of plate 9 has been stopped at a lower temperature.

4. Increase of mold pressure
   After this dwell time, high pressure of 45 bar is applied inside the mold and kept like this for 20 minutes to let the material flow to all the corners of the mold cavity.
5. Cooling of mold
   After the high pressure is applied, the mold will be cooled down with a temperature ramp. During this phase, the plate inside the mold will consolidate and become dimensional stable.
6. Removal om mold pressure
   When the readings of the thermocouples are below 40°C (dimensional stable and safe to handle) the pressure on the mold will be removed and the press can be opened

An example of the temperature/pressure cycle is shown in figure 5.5. Hereby the period between the end of the temperature increase ramp and the increase of the pressure is dependent on the time it takes to heat the mold. During the manufacturing of the plates, it was noticed that the time at which the pressure is applied can differ significantly between plates (100 to 200 minutes).

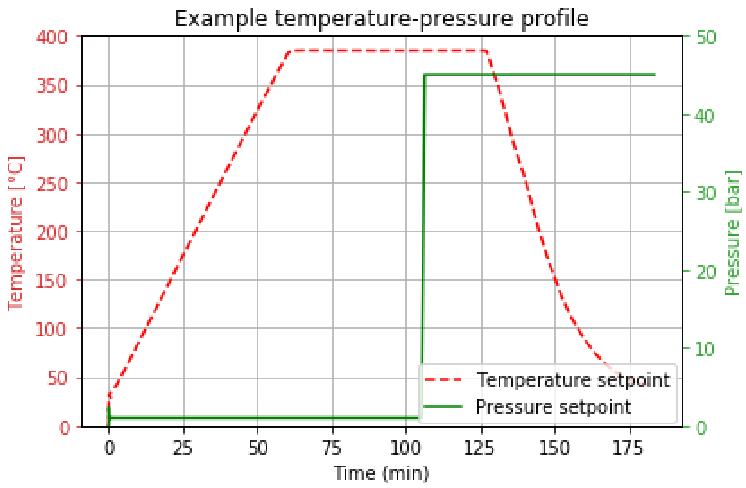

Figure 5.5: Example of temperature pressure cycle

5.1.4 Plate removal

When the mold is cooled down, the mold is clamped and opened. With the use of bolts, the upper and lower part are separated from the frame. The plate had to be forced out of the mold due to differences in thermal shrinkage between DFC and the mold frame. In figure 5.6 three manufactured plates have been shown for each different tape orientations. With the plate removed, the mold parts are cleaned (removal of polymer resin flashing) and stored. After this, the manufacturing of the plate is finished and can be inspected with different techniques before manufacturing the samples from it. These topics will be discussed in the next section and chapter 6.

(a) (b) (c)

Figure 5.6: Manufactured plates, a) Randomly orientated tapes, b) 0° centered orientated tapes, c)±45° centered tapes

5.2 Plate inspection after manufacturing

Before the manufactured plates are cut into samples and mechanical testing is performed, three different types of non-destructive inspections are performed on the manufactured plates. These inspections are optical inspection, plate dimension measurements, and the use of a C-scan. The first two of these will be discussed in this section. The results of the C-scans will be discussed in chapter 6 in combination with the failure analysis.

5.2.1 Optical surface inspection of manufactured plates

Optical inspection has been performed by inspecting all sides of the plates by eye and if needed with a digital microscope. For all plates, it was observed that around the edges of the plate, the surface seemed wrinkled (which could also be felt by touch at some locations). This wrinkling could be caused by the difference in thermal shrinkage during cool-down or by the limited flow of material from the center to the side of the plate.
At the top-side of plate 8, a spot was found that felt rougher than other surfaces. After the surface area was inspected with the use of a *Digimicro 2.0 USB microscope* as shown in figure 5.7c , the surface was identified to be a dry spot. One cause of this can be the shrinkage of the material which caused the separation of the resin from the fibers.

Plate 9 showed clear signs of poor material flow during manufacturing. By utilizing the *Digimicro 2.0 USB microscope*, an image of these defects has been obtained. Although the corners have many flaws, the center region of the plate that will be loaded during the mechanical tests seems to be free of defects. In total, 9 areas at the edges of the plate have been found where defects could be seen as indicated in figure 5.7a. Figures 5.7d, 5.7e, and 5.7f show some of these flaws. In here it can be seen that the separate tapes have been moved and deformed during molding but not to the extent to fill the cavity of the mold. After the temperature-pressure cycle of this plate was examined, it was found that this plate was kept for the longest time at an elevated temperature above 380°C. When this was taken into account with the absence of resin flashing, it was suspected that the matrix might be degraded during the process which caused an increase in viscosity and decrease in material flow.

In literature [48–50], it was found that PEEK degrades at temperatures above its melting temperature. It is assumed that the increase in viscosity has influenced the flow during this process cycle. Besides plate 9, plate 7 also had a relatively long heating time but showed no signs of bad material flow. A reason that plate 7 does not have these defects could be due to the PEEK separation layers which likely increased the flow of matrix due to more viscous polymer material. The extended heating time of plate 9 is most likely caused by the degradation of the thermocouples which seemed to converge to lower temperature values.

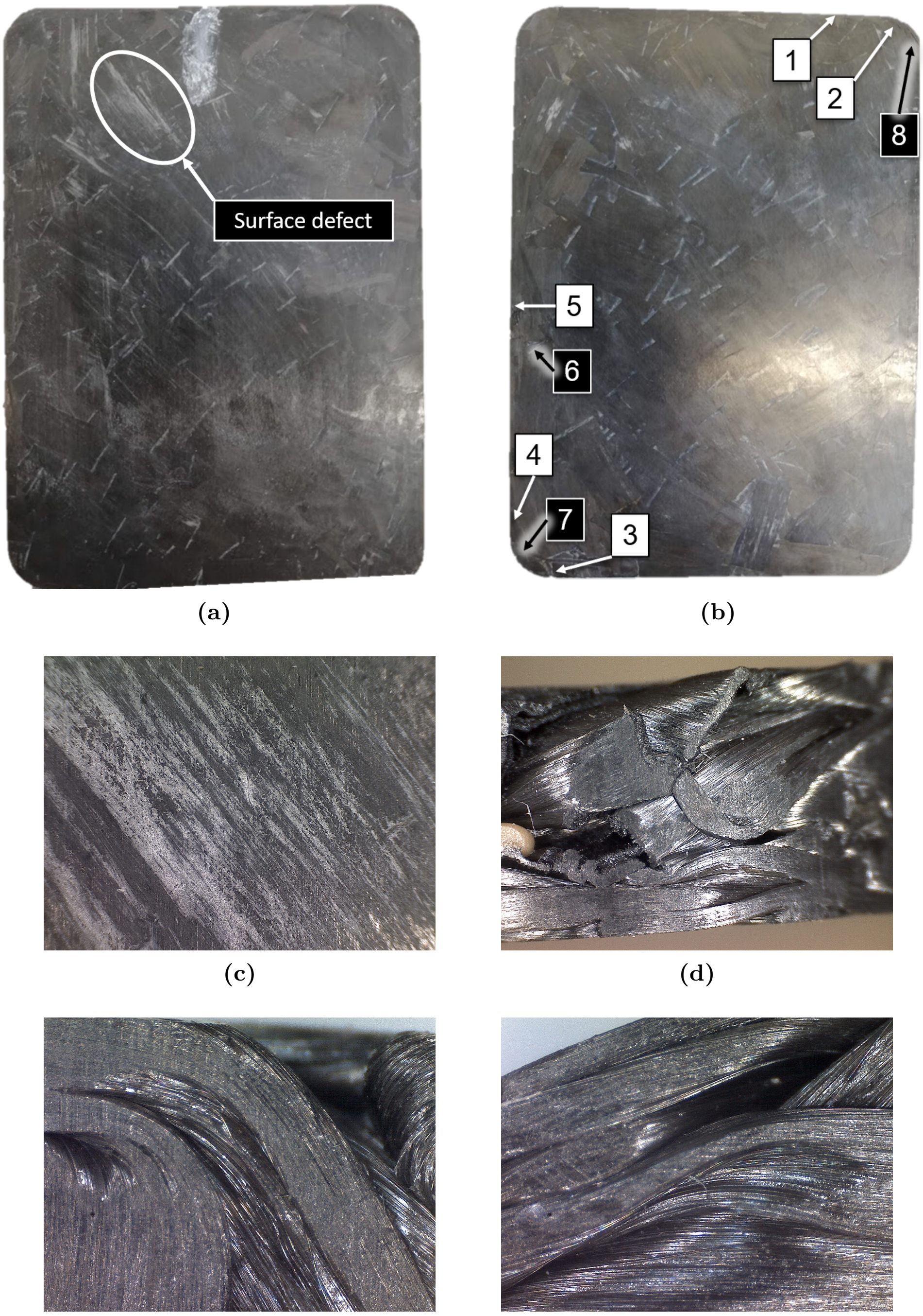

(a) (b) (c) (d) (e) (f)

Figure 5.7: Optical inspections of manufactured plate 8. a) Location of dry spot on top surface plate 8. b) Location of dry spot on surfaces plate 9 (black box is front surface, white box is back surface. c) Close-up of dry spot. d) Close-up of defect on position 2 of plate 9. 2) Close-up of defect on position 7 of plate 9. d) Close-up of defect on position 8 of plate 9

5.2.2 Plate dimensional measurements

The outer dimentions of all plates and samples have been measured. This has for the calculation of the mechanical properties and to collect data for the creation of knowledge about the manufacturing. What was noticed during the measuring of the plates was that the width and length in the middle were usually smaller than at the corners. The thickness also seemed to change from one side to the other leaving one side thinner than the other. Besides the plates, each sample for mechanical testing has been measured in, length, width, and thickness. These measurements have been used to estimate the net stress in a cross-section.

5.3 Plate cutting into samples

After the plates have been manufactured and inspected, they are cut into samples. Based on Gan et al [11], it has been assumed that the area within 20 mm of the edges is affected by the walls of the mold. Within this area, the tapes are probably more aligned with the direction of the wall. This makes them unsuitable for the mechanical tests and restults in a limited amount of material per plate can be used for mechanical testing.

The size of a sample should not be too small because of the size of the tapes within the material. On the other hand, if a too larger sample is used the production and testing will be more expensive for a fixed number of tests. The choice in sample size during the project is even more important because the material is also limited available, therefore bigger samples mean fewer test results. This can result in lower certainty of the results. Based on the tapes that are used and the literature [11, 28, 51], a sample width of 25.4 mm (1 inch) has been chosen.

Based on these arguments, two samples for mechanical testing can be produced from the middle section of the plate. On both long sides, a cut will be made on the edge to ensure a straight line after which a strip with an 8 mm width will be cut from the edge. This is done to be able to see the extent of alignment near the walls of the mold. The remaining material (between the samples for mechanical testing and wall alignment) can be used for inspection with optical microscopy. In figure 5.8 the cutting lines that have been machined for each plate have been represented with the red dashed lines.

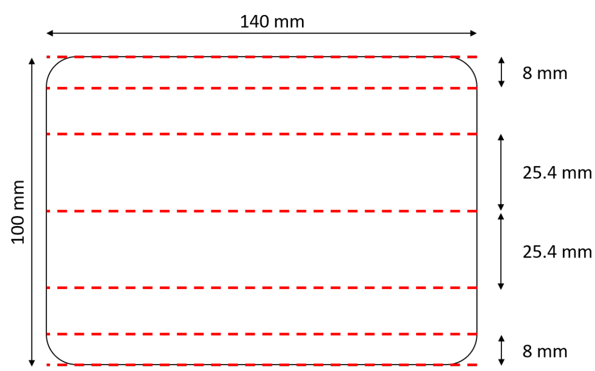

Figure 5.8: Cutting lines for sample manufacturing

Chapter 6

Structural characterisation and mechanical performance

This chapter has been devoted to answering most of the second part of the research questions concerning the determination of the mechanical properties of DFC and the effect of alignment. This report will discuss the methodology and test setup that has been used. After this, the results concerning the UTS and USS and modulus in shear and tensile loading will be discussed followed by a failure analysis based on the failure surfaces.

6.1 Methodology and test-set-up

To determine the elastic properties of the samples, tensile tests have been performed on the different samples. For this, six samples have been tested for the randomly orientated tapes, six for the 0° orientated tapes, four for the +45° orientated tapes without PEEK film, and two for the +45° orientated tapes with PEEK film. Hereby a *250 kN Zwick tensile testing machine* has been used to obtain a force-displacement curve. During the tests, a strain rate of $\frac{mm}{s}$ has been used. Because the displacement of the readings from the tensile test machine also contains the deformations of the whole machine, DIC readings have been performed on the surface of the samples which has been linked to the forces from the tensile test machine. For this, two 5MP cameras with a focal length of 50 mm have been used. During the testing, the DIC system has been calibrated twice by means of a calibration sample. The calibration scores were 0.023 and 0.027 which was well within the acceptable range. The strain data obtained from the DIC system and the force readings can characterize the difference in tensile stiffness for each orientation distribution. To collect enough data to be representative, the area that is visible for the DIC cameras has to be as large as possible. This has been done by using a clamping length of 30 mm. This leaves roughly 80 mm of gauge length visible for the DIC cameras. In figure 6.1 the test set-up is shown. After all the data is obtained, it will be post-processed. The actions taken for this will be discussed in the next section.

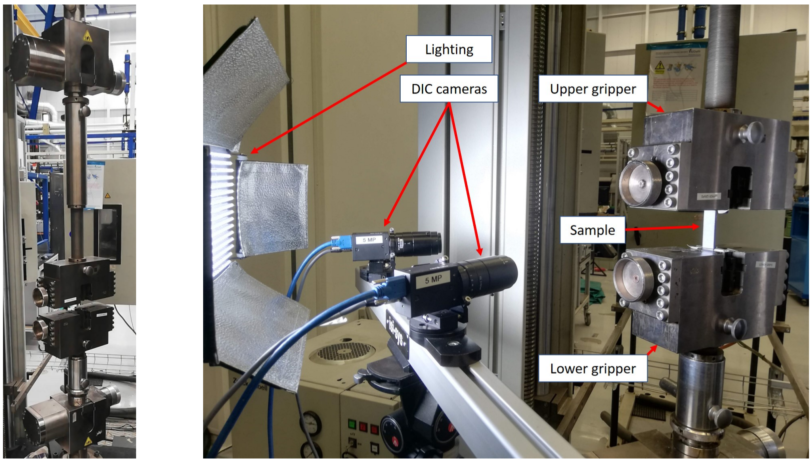

(a) (b)

Figure 6.1: Tensile testing setup. a) Grippers between cross-heads. b) Grippers and DIC measuring set-up

6.2 Post-processing of test measurements

By combining the force readings with the measured sample dimensions the average stress in the sample has been calculated. With the maximum value of the measurements, the UTS of each sample has been determined. With the average of the strain readings that have been captured by the DIC system, a stress-strain relation has been created and the tensile modulus is determined. Because there is no suitable norm for determining these properties for DC, a combination of two sources has been used. Hereby the lower bound of 1000 micro-strain used by Siddiqui et al. [52] has been used to remove the noise at the start of the testing. The upper bound has been used from Cuartas et al. [53] which is the strain at half the failure load. Between these bounds, a linear curve fit has been made whereby the slope is the value of the tensile modulus.

Because the DIC system can also be used to measure the strains in the direction perpendicular to the loading direction, the poison ratio of each of the samples has been calculated. By taking the negative of the ratio between the average strains in the transverse and longitudinal direction. In the same strain range as mentioned before this ratio seems to be relatively constant.

With the testing of the ±45° samples the shear properties of the material can be calculated. This has been done by rotating the coordinate system by 45° which transforms the global longitudinal normal stress into shear stress by using equation 6.1 [19]. Hereby the assumption that has been made is that the remaining normal stresses are not coupled with shear deformations. The shear stress and strain is calculated with the formulas in equation 6.1, 6.2 and 6.3 [19]. After this, the USS and modulus are determined in the same manner as with the UTS and tensile modulus have been obtained.

$$\tau_{12} = \frac{\sigma_{yy}}{2}, \tag{6.1}$$

$$\gamma_{12} = \epsilon_{xx} - \epsilon yy, \tag{6.2}$$

$$G_{12} = \frac{\tau_{12}}{\epsilon_{12}}. \tag{6.3}$$

By using the measured tape orientation distribution and calculating a homogenized material stiffness with CLT, a comparison has been made to see how well these methods can be used to predict the material properties. This method has been used by Selezneva et al. [1] for the creation of FEM-models of DC. With the use of the in-plane properties for this comparison, three sets of angles have been used based on the measurements to see how big the scatter of the properties is. Hereby the angles have been moved away and towards the direction that causes the best stiffness properties. This has been done with an increase or decrease of 3° which is roughly three times the average standard deviation of the tape orientation measurements as described in chapter 4.

6.3 Results from tensile testing

This section will present the results that have been found based on the processing of the test measurements. Here, the tensile properties will be discussed followed by the shear properties of the ±45° samples. Each of these properties will be determined according to section 6.2.

6.3.1 Tensile response

With the processed data, stress-strain curves have been obtained for all the samples. These are shown in figure 6.2. In the graph, a clear difference in mechanical behavior can be seen hereby the samples with a higher tensile modulus have a low strain at failure. Besides the ±45° centered samples, all curves seem more or less linear.

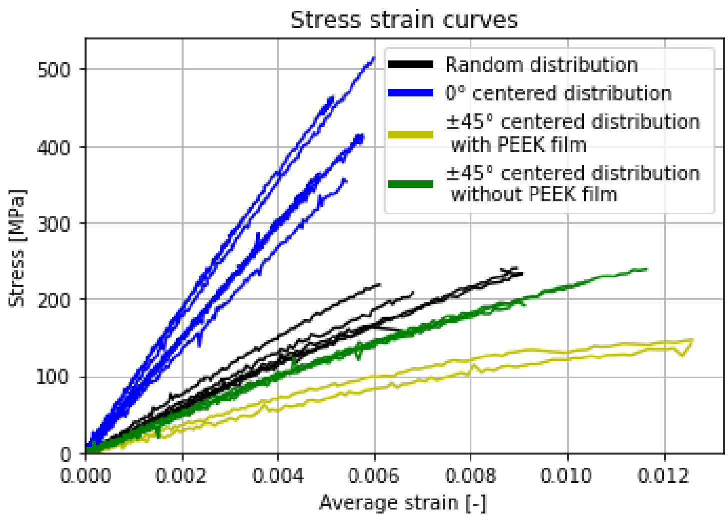

Figure 6.2: Stress strain curves of tested samples

Ultimate tensile strength

The UTS of the material is determined by using the maximum stress that has been read from the stress-strain curves. In figure 6.3 the difference in UTS can be seen between different tape orientations. The samples with a random tape orientation showed an average UTS of 202 MPa. The effect of the alignment of the tapes on the UTS is clear in the difference in UTS between the random and 0° centered tape samples. The 0° centered tape samples show an average UTS of 396 MPa which is approximately 96% higher than that of the random samples. The real UTS of this material is most likely higher because the tabs of the samples (with a lower level of alignment) failed instead of the fully aligned material. Hereby the samples with and without PEEK film showed UTS of 144 MPa and 210 MPa respectively which is a reduction of 33%.

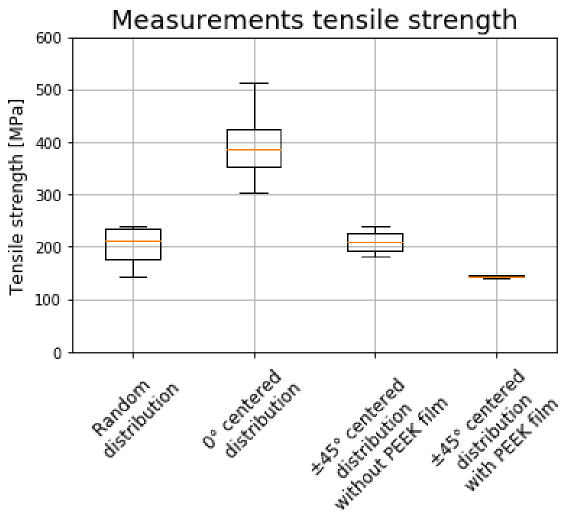

Figure 6.3: Ultimate strength of samples

Tensile modulus

In the figure 6.4a the tensile stiffness of the samples are plotted next to each other. It was found that the benchmark samples with randomly orientated tapes have an average tensile modulus of 32.5 GPa. The samples with tapes aligned in the loading direction showed a 145% higher tensile modulus of 79.7 GPa. These results show clearly that with an improved alignment, the tensile stiffness of the material improves. Because the error bars of the data are not overlapping, this statement agrees with the literature [1, 20, 21, 36]. The ±45° specimen showed the lowest tensile modulus with an average of 15.9 GPa and 25.3 GPa for the samples with and without PEEK film.

When comparing the 0° centered orientated samples with the others, it is noticed that the 0° centered samples show a larger scatter. A reason for this larger scatter could be found within the deposition technique that has been used. When assuming there is a difference in orientation distribution between the plates, this would be most visible with the 0° centered samples. The difference in properties due to the changes in a deposition could be seen in a single plate which can be seen in figure 6.4b. The two samples from each plate did have more similar properties than the whole population of samples (especially for samples 6.3 and 6.4 whereby the elastic modulus of both samples was 13% above the average of the whole population). This would mean that the differences in deposition due can cause the scatter in properties. With the random and ±45° centered samples this effect will influence the mechanical properties less because their angles are already spread over a larger range. The same conclusion is not applicable to the UTS because the properties differ more between samples of a single plate.

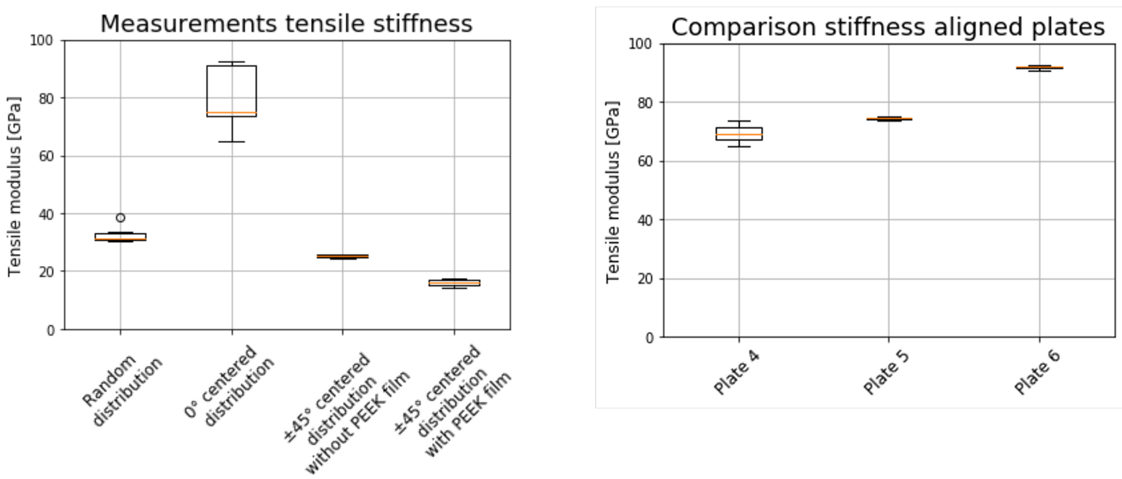

(a) **(b)**

Figure 6.4: Tensile stiffness of samples. a) Tensile stiffness of orientation distributions. b) Tensile stiffness of plates with 0° centered orientation distributions

Poisson ratio

The Poisson ratios of the material have been calculated with the strains at the surface of the sample and are shown in figure 6.5. The results for the samples with random tape distributions are as predicted by CLT around 0.30. The poison ratio of the ±45° samples has a value of 0.59. The effect of the PEEK film in between the orientations has lowered the poison ratio of the samples to a value of 0.39. The 0° samples show unexpected values which are higher than expected. Hereby an average value of 0.49 has been observed. These results will be further discussed in combination with the comparison with CLT.

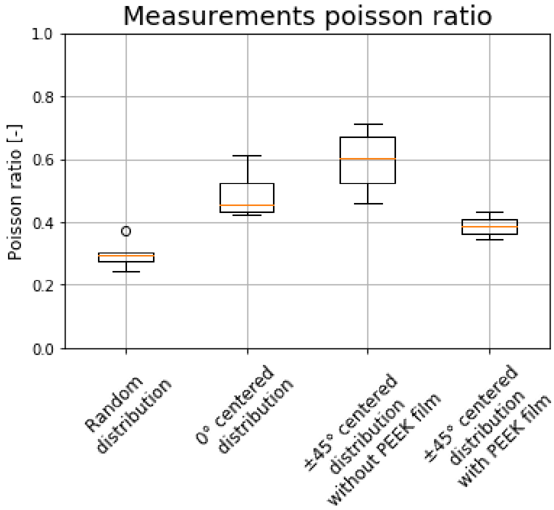

Figure 6.5: Poisson ratio of tested samples

Comparison with CLT

By using CLT, the tensile modulus, shear modulus, and mayor Poisson ratio are tried to be predicted. This section will discuss results on the tensile modulus and mayor Poisson ratio. The tensile modulus of the randomly orientated samples has been estimated between 49.7 and 57.2 GPa, For the 0° aligned samples these values are between 104.9 and 107.9 GPa and for the ±45° samples (without PEEK film) 37.8 and 48.0 GPa. With this, it can be concluded that the use of a homogenized CLT simplification will result in an over-prediction for all the samples.

One of the causes for the difference between the measured stiffness and the expected stiffness (based on classical laminate theory) was expected to be the out-of-plane angles of the tapes inside the material. Out of each plate, two strips of material were cut during the manufacturing of the mechanical test samples. With these samples, images were made to inspect the cross-section. The images have been used to characterize the average out-of-plane angles of the tapes for the random, 0° and ±45° tape distributions which are 4.5°, 2.9°, and 3.2 respectively. Hereby it was found that the decrease in stiffness due to tow-waviness is relatively small compared to the difference between the measured stiffness and the estimations based on classical laminate theory. Although it was expected that these angles were causing a relevant percentage of the stiffness reduction, it was found that this could only account for 1.6%, 0.8%, and 1.2% of the stiffness. The methodology and images that have been used are described in section 6.7.

Besides the tow-waviness inside the plates, the transfer of loads from one tape to another is also likely to be a cause of the stiffness differences between the material and CLT. In section 6.8, the effect of shear lag on the stiffness has been examined by the use of a model of a single lap joint. Here it has been described that due to the shear lag, the effective stiffness of a lap joint can vary between 1.2% and 4.0%. It has been found that parameters such as the contact length between tapes, tape stiffness, and film thickness between the tapes are important parameters. The average stiffness reduction that has been found was 2.1%.

With CLT, the Poisson ratio was also tried to be predicted. For the random tape orientation, the prediction was accurate between 0.29 and 0.33 compared to the 0.3 average of the measurements. For the ±45° samples this value was estimated between 0.61 and 0.79. Hereby the measured value of 0.59 is just outside this range. This difference could be because the matrix is more dominant with DFC and will thus lower the properties. The 0° centered samples showed a large difference between the CLT prediction and the measurements. Where the prediction was in a range between 0.20 and 0.24, the measurement showed a value of 0.49. The reason behind this difference has not been found.

6.3.2 Shear response

With the testing of the ±45° samples the shear properties of the material have been calculated as has been described in the post-processing section. With this, the shear stress-strain curves and shear modulus can be obtained. These curves of the six samples are shown in figure 6.6.

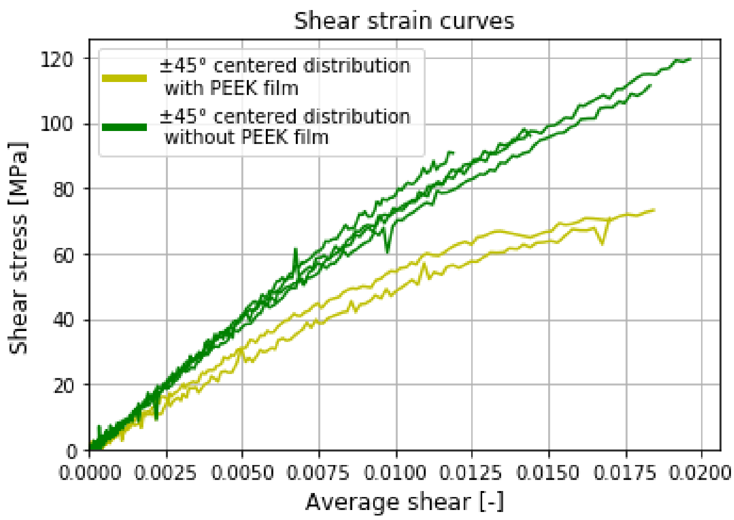

Figure 6.6: Shear stress strain curves of tested samples

Ultimate shear strength

The USS of the material has been determined by taking the maximum shear stress of the material. In figure 6.7 the results are presented. Hereby it can be seen that the addition of the PEEK film decreases the USS of the material from 105 MPa to 72 MPa which is a decrease of 32%. It should be noted that this ratio in USS decrease is more than the difference in thickness increase due to the addition of the PEEK layers. In the failure analysis, it is mentioned that the failure mode of these samples is shear failure. With this, it is assumed that the maximum calculated shear stress is the USS of the material.

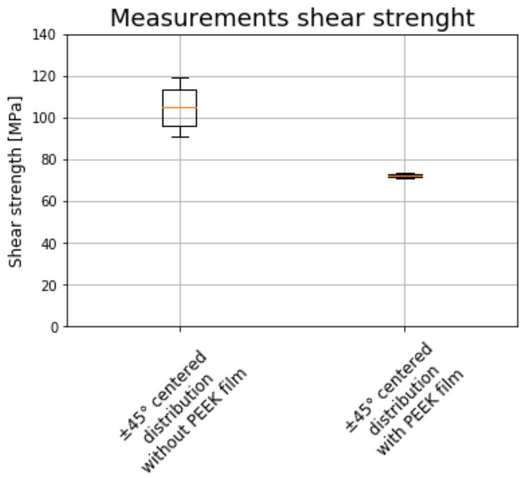

Figure 6.7: Shear strength of samples

Shear modulus

In figure 6.8 the results of the measurements can be seen. The samples that have been manufactured with a PEEK layer in between different tape orientations show a lower stiffness of 5.7 GPa compared to 7.9 GPa of the samples without PEEK film.

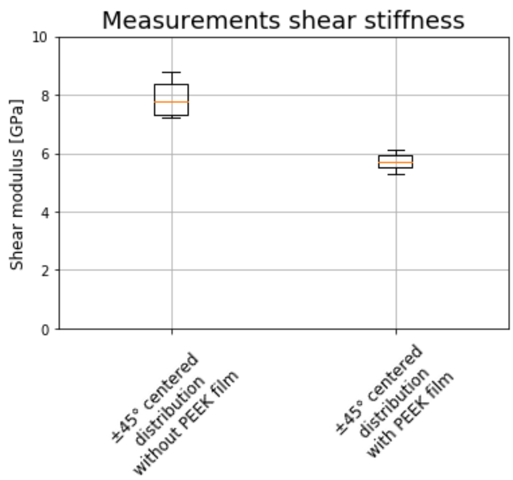

Figure 6.8: Shear stiffness of samples

Comparison with CLT

For this comparison, only the results of the sample without PEEK film have been used. When estimating the shear modulus with CLT, the expected value for the shear modulus is between 7.8 and 8.4 GPa. Because the difference between CLT and the measurement is smaller in shear this might indicate that his property is more influenced by the matrix than by the discontinuity of the fibers.

6.3.3 Optical inspection of PEEK film inside samples

Optical microscopy has been used to examine the distribution of material inside the manufactured plates. The main goal of this inspection (in combination with the mechanical testing) is to see the effect of the separation film between the two plates with a ±45° tape distribution. Hereby the area where the two distributions are in contact with each other is of interest. During the optical inspection, it was found that there was no clear boundary layer between different tape orientations. The PEEK film was present in the material in the form of large (compared to the tape thickness) volumes. Because these volumes probably cause local drops in stiffness, stress concentrations around them could be the reason for lower overall material strength. This, in combination with the lower stiffness and strength of the material, suggests that the use of a PEEK film will not contribute to better material properties. What could be further examined is the use of thinner films. Because the total thickness increase due to the two PEEK films was large (estimated 12% of the plate) a thinner film could be used to reduce the accumulation of the polymer inside the material. This would still separate layers with different tape orientations but has a lower impact on the mechanical properties.

6.4 Comparison of failure location with DIC measurements

In this section, the evolution of the strain readings during the testing will be discussed. Hereby the strain values halfway and at the end of the test have been presented for one of each sample type. The aim of this analysis is to see if the failure location can be predicted at a relatively low load. The strain readings for each sample will be presented in two formats, an image of the sample surface where the color of the surface indicates the strain. The other is by means of a graph with three lines which indicate the strain values over the length of the sample at a certain width. The lines are located at one fourth, half, and three fourth of the width of the sample. In these images, the vertical lines indicate the failure location.

For most of the samples, the highest peak in strain resulted in the initiation of the failure at that location. After a crack has been formed, the stresses in the material changed and a crack propagates from that point through the width of the sample in a short time. Only for sample 7.4, the first crack did not propagate and a second one was formed. The initiation of this crack was not at a location with the highest strains and could be caused by a local weakness due to the separation films.

It was noted that the cracks (most likely) always started at the edge of the sample. This is probably the result of the edge effect of the sample and due to the cutting of the sample. due to this, the length of tapes at the edges is not their full width which reduces the load transfer capabilities and introduces stress concentrations in these areas.

With this analysis, it can be concluded that the failure location can be predicted by means of the local strains. By applying a load that is below the failure load, the failure location can be predicted. It should be noted that the use of this technique can not be used for real application because this should be done with each part due to the local differences in tape orientations.

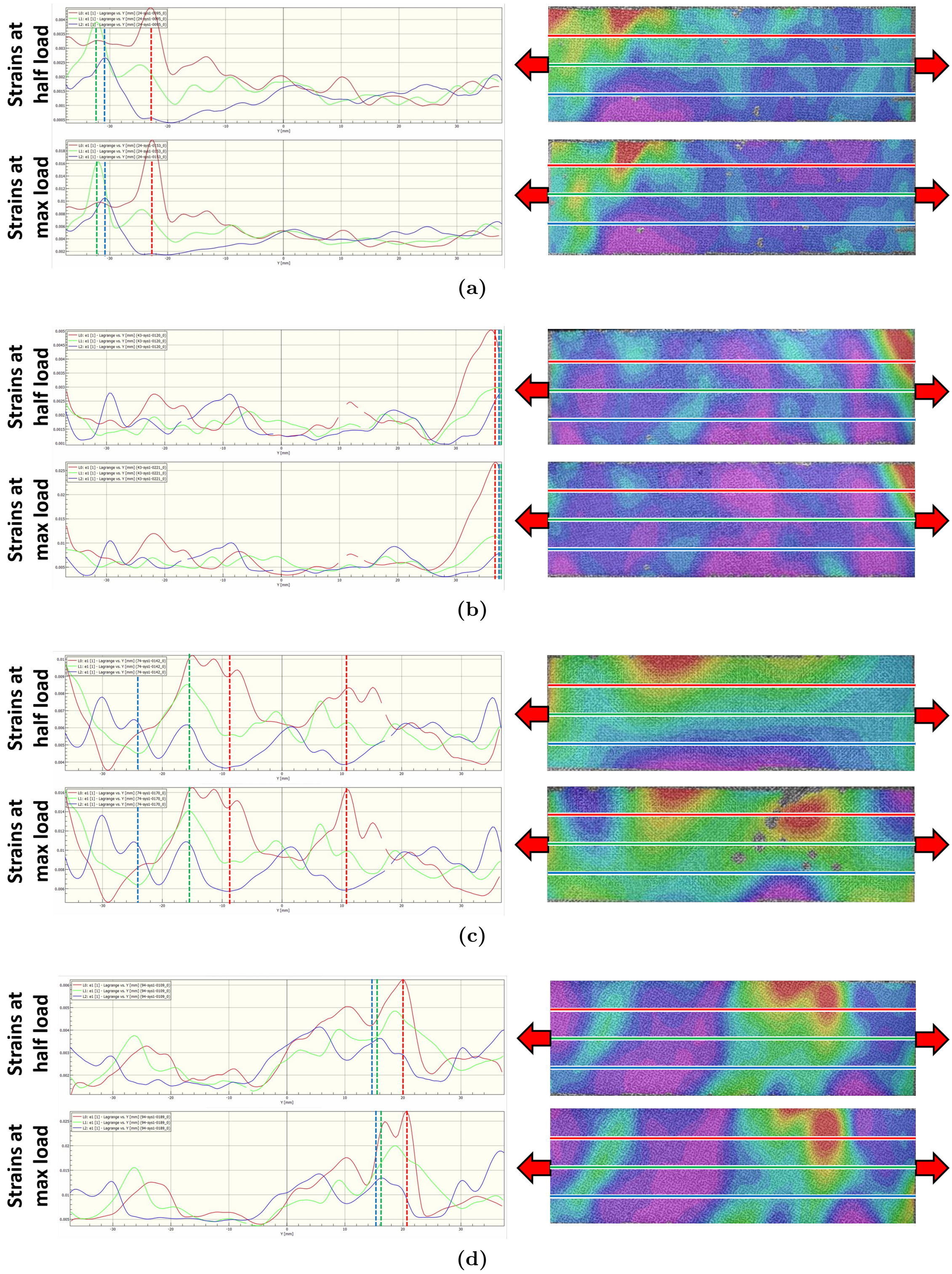

Figure 6.9: Strain evolution halfway and at the end of the test, left are strain-plots over lines. Vertical lines indicate where failure occurred. Right are strain images of the sample, a) Sample 2.4 randomly orientated tapes, b) Sample 4.3 0° orientated tapes, c) Sample 9.4 ±45° without PEEK film, d) Sample 7.4 ±45° with PEEK film

6.5 Analysis of failure surfaces by optical microscopy

To gain insight into the failure modes that have been present during the testing, the fracture area of samples has been inspected employing optical microscopy. This has been determined for each of the four sample types. In the literature review, it was found that different failure mechanics can occur based on the loading that is applied and the orientation of the tape with respect to that loading [16, 28, 29]. Because the information that can be obtained from the fracture decreases with an increase in handling activities and storage time, it has been chosen to document these with a 5x amplification with the "*Keyence laser scanning confocal microscope*". Below, the fracture surfaces will be described for each of the sample types.

6.5.1 Randomly orientated tapes

The failure mode of the material is dependent on the orientation of the tape. Because the random tape orientation can contain all orientations, this sample shows most of the failure modes. Although matrix failure at the interface between the tapes showed to be the most present, other failure mechanisms have also been observed. These are listed below:

- Shear failure has been recognized by the presence of cracks inside the tapes. These cracks were at 45° with respect to the loading direction. An example has of this has been shown on location A in figure 6.10.
- Local fiber buckling is seen on a small scale in a tape that was orientated at roughly 45° with respect to the loading. Because this failure did not happen at the surface it is expected that the buckling occurred during or after the failure initiation inside the material. An example has of this has been shown on location B in figure 6.10.
- In location C in figure 6.10, fiber failure has occurred at the tips of the failure surface. Hereby the fracture line of a tape contains multiple fibrous tape ends (top).
- Matrix failure at the interface is the most prominent failure mode that is observed. One of these areas is location D in figure 6.10. Hereby flat tape surfaces are seen with the microscope. Because this failure mode has the biggest surface, it is assumed to be the most dominant one when using a random tape distribution.
- Tape splitting occurred inside tapes that are orientated perpendicular to the loading direction and has been observed at the start of the failure surface (bottom). An example has of this has been shown on location E in figure 6.10.

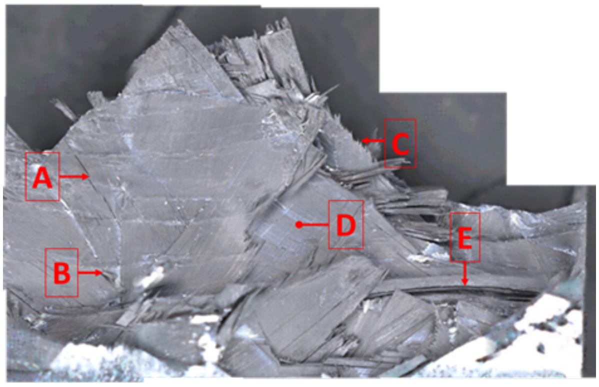

Figure 6.10: Fracture surface sample 1.4 (random tape orientation)

6.5.2 °0 centered orientated tapes

The samples that were made with a 0° centered alignment all failed at the ends of the samples where the alignment of tapes is expected to be less. With this in mind, the failure modes for aligned DFC are less certain. During the inspection of the failure areas, many tapes seemed to be curved (in-plane as well as out-of-plane) which reinforces this statement. The observed failure modes are not the same as for the randomly orientated tape samples. Although the failure modes of matrix failure (location A in figure 6.11). has been observed, failure modes such as fiber breakage (location B) and tape splitting (location C) have been observed more frequently, which could be an indication that these failure modes are more applicable with aligned DC. In figure 6.11 one of the failure areas is shown.

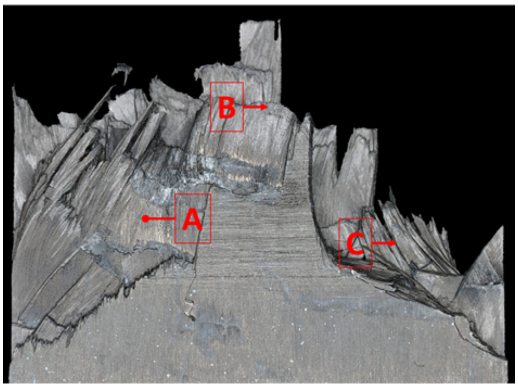

Figure 6.11: Fracture surface sample 4.3 (0° centered tape distribution)

6.5.3 ±45° centered orientated with PEEK film

The failure surface of the ±45° samples that have been manufactured with a PEEK layer shows a relatively small failure length whereby the failure line at the surface is at 45° to the loading direction. Over the whole of the failure surface, the resin can be seen (location A in figure 6.12) which is most likely originating from the PEEK separation film. Besides this, tape splitting (location B) and matrix failure (location C) have been observed as the main failure modes.

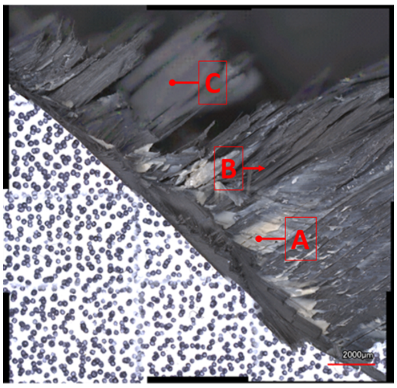

Figure 6.12: Fracture surface sample 7.4 (±45° centered tape distribution with PEEK film)

6.5.4 ±45° centered orientated without PEEK film

The samples that have been manufactured without a PEEK layer in between different orientations have clear characteristics of the failure of a cross-ply. When inspecting the failure area, three different layers are distinguished. All of these layers have a failure line that is orientated at ±45° of the load. These three layers are two thin ones at the outside and a thicker one in the center of the thickness. Because of this, it is assumed that these layers are the layers inside the material that have different tape orientation distribution. For the sample, the main failure mode is matrix failure (location A in figure 6.13). Tape pull-out is also suspected to be present at the end of the middle layer based on location B in figure 6.13. This failure surface is significantly smaller than that of the matrix failure.

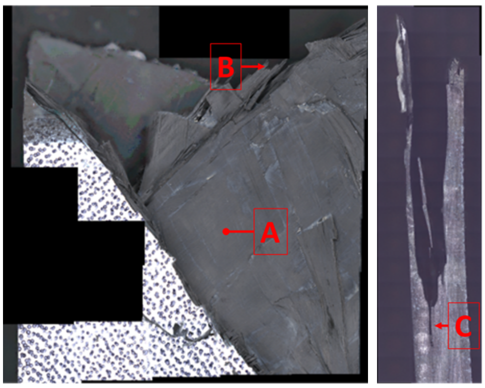

(a) (b)

Figure 6.13: Fracture surface sample 9.4 (±45° tape orientation without PEEK film). a) top view, b) side view

6.6 Comparison of failure location with C-scan

After the manufacturing of the plates, C-scans have been made to see any possible defects in the material. The scan is performed inside a water medium with a 5MHz signal. With an estimation of the speed of sound through the material of 3000 $\frac{m}{s}$, the wavelength of this signal is approximately 0.6 mm. If defects are large enough compared to the wavelength of the signal, they can absorb or scatter the signal coming from the scan and can thus be seen as a drop in signal strength on the receiving side of the signal.

A phenomenon that has been observed from the results is that the edges of the plate seem to be more prone to show defects. This is most visible with the 0° tape orientation plate. This can be caused by the difference in local tape orientation at the edges compared to the overall tape orientation. The difference in thermal expansion between DFC and the mold creates a compressive force on the plate when it cools down. Because at the edged of the plate the tapes are more aligned in this direction, the matrix will be dominant and is thus more prone to create defects in these locations under compressive loading.

For each of the samples, the failure location of the samples has been compared to the results of the C-scan. Although Yamashita et al. [28] have shown no strong relation between the location of a defect and the location of the failure, this non-destructive inspection can help with finding possible outliers in the event of an early failure. Besides this, this study has only been performed on samples with randomly orientated tapes. In figure 6.14, the DIC images of each sample will be presented. In each of these images, the failure location is indicated. By doing this comparison, it has been concluded that no features can be observed with the C-scan which can be used for the prediction of the failure location. It has been observed that most of the samples of the same plate have a failure location at the same length. This could be an indication of "weak spots" in the material that are big enough to exist in two samples.

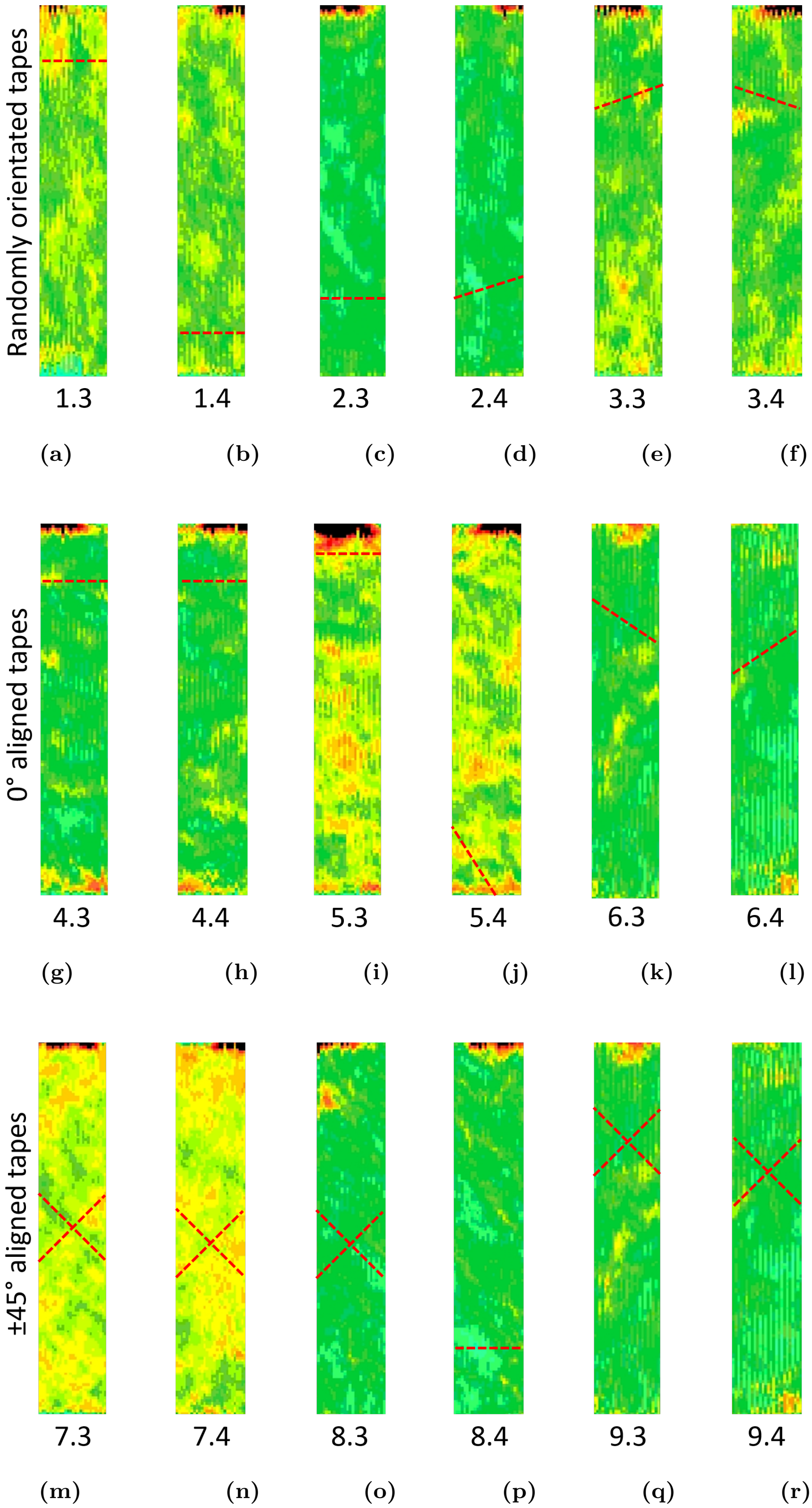

Figure 6.14: Comparison failure location with C-scan. Red line indicates failure area, a-f) Randomly orientated tapes, g-l) 0° aligned tapes, m-n) ±45° tape with PEEK separation layer, o-r) ±45° tape without PEEK separation layer

6.7 The effect of tape waviness on the tensile modulus

Alves et al [20] have stated that tow waviness reduces the in-plane elastic properties of a panel. Because this tow-waviness has been observed with the use of optical microscopy it is expected that the difference in measured stiffness and calculated stiffness (based on CLT) is partially caused by this. This section will describe the method that has been used to quantify the waviness inside the material and the expected effect of this on the elastic properties of the material. Because CLT does not make use of the out-of-plane stresses and material properties, this method has been used to determine the change. As a side-product of this method, the homogenized material properties can also be estimated.

In order to quantify the reduction in stiffness of the fibers, the properties are rotated around the z-axis with the in-plane angle and with a second angle around the y-axis. After this, the new global elastic properties are calculated.

6.7.1 Local compliance matrix of CF/PEEK

The calculation of the local compliance matrix has been based on the mechanical properties that have been based on literature [54–57]. Because the used tapes have a fiber volume fraction of 55% the stiffness properties have been scaled with the fiber volume fraction if needed. These properties are shown in table 6.1. To reduce the number of independent material properties, the tapes are assumed to be orthotropic. The compliance matrix are shown in table 6.2 whereby equation 6.4 gives the formulas for the specific locations.

Table 6.1: AS4-PEEK elastic properties, based on [54–57]

Property	Value	Unit	Property	Value	Unit	Property	Value	Unit
E_{11}	121.60	GPa	G_{12}	6.30	GPa	ν_{12}	0.29	-
E_{22}	10.2	GPa	G_{13}	6.30	GPa	ν_{13}	0.29	-
E_{33}	10.2	GPa	G_{23}	3.60	GPa	ν_{23}	0.47	-

Table 6.2: Local compliance matrix for orthotropic materials

S_{11}	S_{12}	S_{13}	0	0	0
S_{12}	S_{22}	S_{23}	0	0	0
S_{13}	S_{23}	S_{33}	0	0	0
0	0	0	S_{44}	0	0
0	0	0	0	S_{55}	0
0	0	0	0	0	S_{66}

$$S_{11} = \frac{1}{E_{11}} \qquad S_{44} = \frac{1}{G_{13}} \qquad S_{12} = -\frac{\nu_{12}}{E_{11}}$$
$$S_{22} = \frac{1}{E_{22}} \qquad S_{55} = \frac{1}{G_{23}} \qquad S_{13} = -\frac{\nu_{13}}{E_{11}} \tag{6.4}$$
$$S_{33} = \frac{1}{E_{33}} \qquad S_{66} = \frac{1}{G_{12}} \qquad S_{23} = -\frac{\nu_{23}}{E_{22}}$$

6.7.2 Effect of fiber orientation

For this exercise, it has been chosen to rotate the compliance around two axes, first, the in-plane angle is applied like is done when determining the properties of a laminate. This rotation is around the z-axis. After this, the properties get rotated around the y-axis with the out-of-plane angle. These two transformation matrices are used in equation 6.5 to calculate the new compliance matrix.

$$S_{\text{global}} = T_z \; T_{y\prime} \;\; S_local \; T_{y\prime}^{T} \;\; T_z^T \tag{6.5}$$

In figure 6.15 it can be seen that the fiber waviness can affect the tensile modulus significantly. Hereby this effect seems to be larger at 0° while in-plane angles of 90° are not affected. With this, it has been proven that the fiber waviness of the tapes inside the material can affect the properties. The next step for this is to measure the out-of-plane angle of the tapes inside the plates. This will be discussed in the next section.

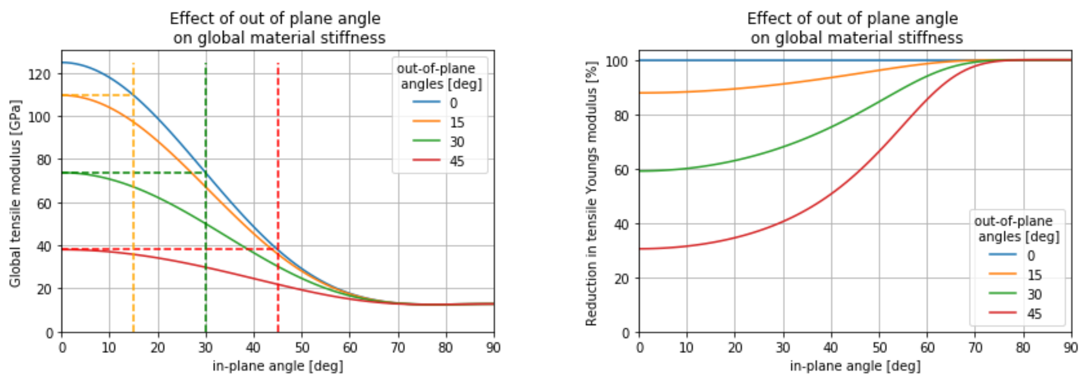

(a) (b)

Figure 6.15: Stiffness reduction due to the out-of-plane angles, a) Absolute tensile modulus, b) Tensile modulus compared to 0° out-of-plane angle

6.7.3 Measurement of out-of-plane angle

With the use of optical microscopy, cross-sections of the material have been examined and the angles of the tapes within are measured. Because the tapes inside the material are not all in the same orientation (in-plane and out-of-plane) the average value of the out-of-plane angles has been chosen to characterize this for the random, 0° and ±45° orientation distributions.

The angles are measured manually over a fixed width. For all three types, a location has been chosen for each of the samples that have been captured. In figure 6.18 lines have been drawn in the image of the cross-section which captures the average out-of-plane angle over a constant width. This resulted in the average angles as shown in table 6.3.

Table 6.3: Average out-of-plane angles

Orientation	Average angle
Random	4.5°
0° centered	2.9°
±45° centered	3.2°

Because these angles are measured in the global coordinate system, the rotation angle around the local y-axis can be calculated with equation 6.6. Hereby α is the average of the measured out-of-plane angles and β the in-plane angle of the tapes as given by table 6.3. The value of α' is used in equation 6.5 for the out-of-plane rotation around the y-axis.

$$\alpha' = \arctan(\tan(\alpha)\ \cos(\beta)\ ) \tag{6.6}$$

With these angles, new stiffness reduction plots can be made which are shown in figure 6.16. Although the out-of-plane angle seems to have a small effect on the stiffness due to the small angles that are measured, this effect can be larger because the tapes are also in-plane curved which could reduce the stiffness with the same magnitude. This in-plane curvature was noted during the optical inspection whereby fibers of a single tape had different cross-sectional shapes on different locations (see figure 6.17). Because the deformation of the tapes is less constrained in-plane these angles could be larger than the out-of-plane angles.

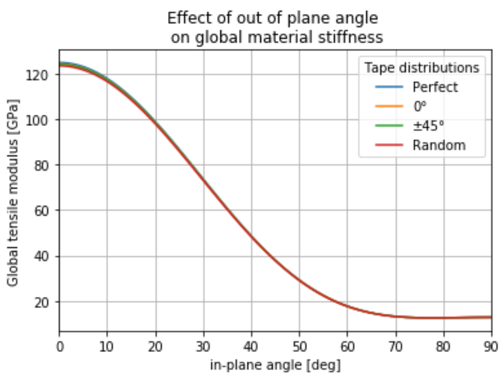

(a)

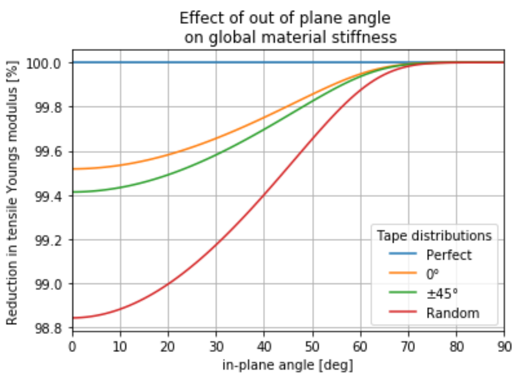

(b)

Figure 6.16: Stiffness reduction for the three orientation distributions due to the out-of-plane angles, a) Absolute tensile modulus, b) Tensile modulus compared to 0° out-of-plane angle

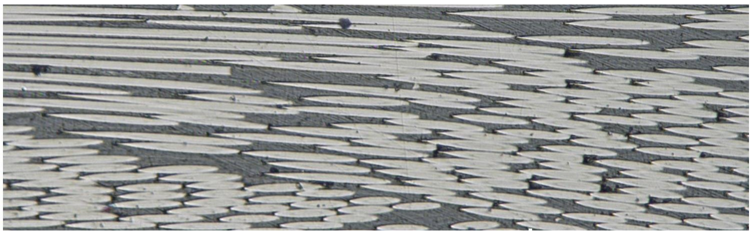

Figure 6.17: In-plane curvature of tapes inside the material observed by the difference in fiber cross-section

6.7.4 Material properties

By using the orientation distributions that have been found in chapter 4 the material properties with and without tape waviness are estimated. In table 6.4 the stiffness reductions in loading direction are shown that have been found by using different methods. This has been done by using the average out-of-plane angle and by using the average stiffness reduction for each out-of-plane angle that has been measured. It can be noted that the difference between these is small are relatively large which is caused by the non-linearity of the stiffness with an increase of the out-of-plane angle. With this, it can be concluded that the use of CLT will not introduce large uncertainties due to the out-of-plane angle.

Table 6.4: Comparison stiffness reduction with different methods

	Stiffness reduction with average angle	Stiffness reduction with average reduction
Random	0.72%	1.19%
0°	0.43%	1.59%
±45°	0.27%	0.77%

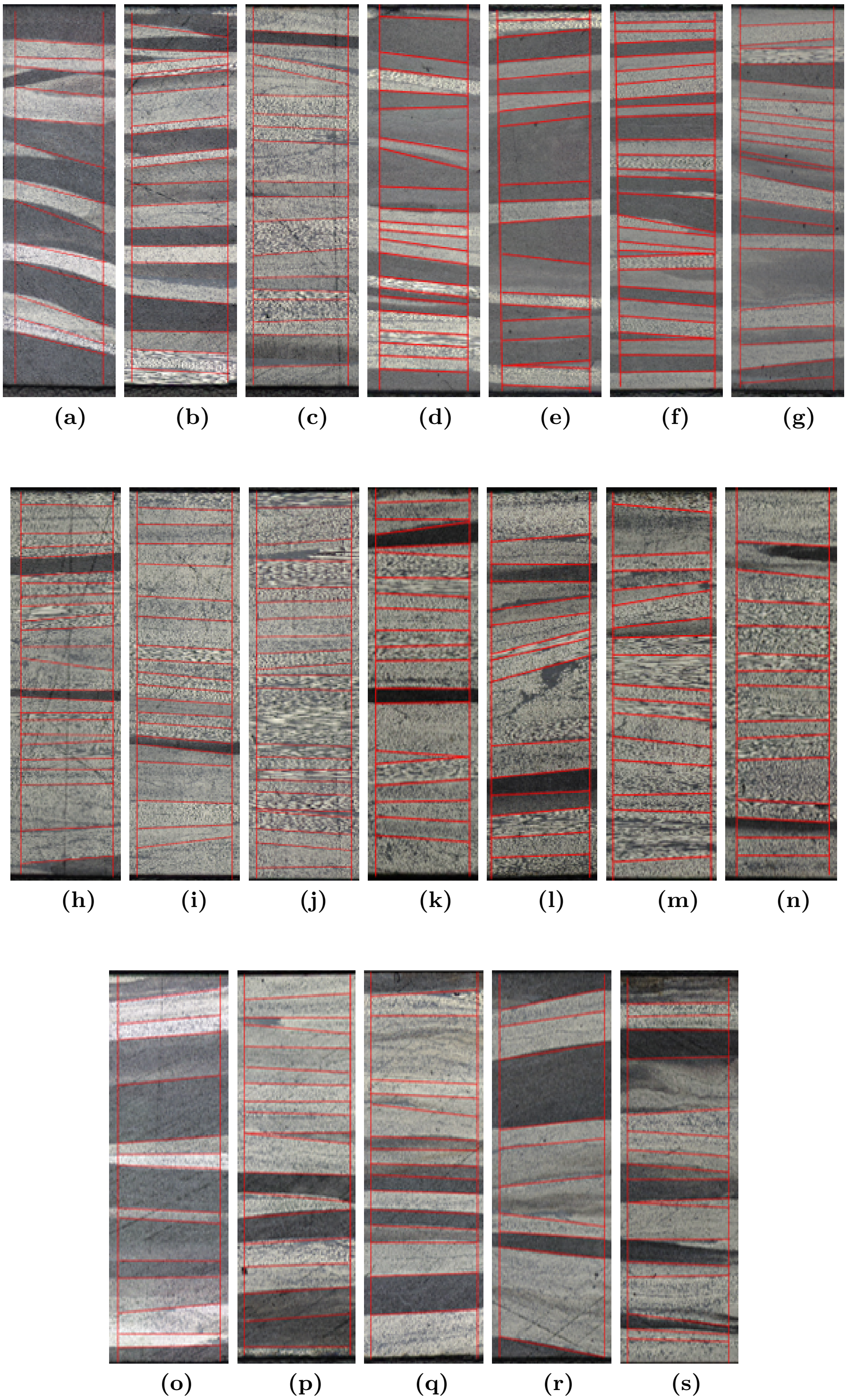

Figure 6.18: Measurements of out-of-plane angles in cross-section image, a-g) Random distribution, h-n) 0° aligned plate, o-s) ±45° plate without PEEK film.

6.8 The effect of shear lag on the tensile modulus

In section 6.3, it was found that the estimated material stiffness (with CLT) was overestimating the material stiffness that has been measured during the mechanical testing. It is expected that the load transfers within the material could cause a reduction in the overall material stiffness. In this section, a simplified model will be used to estimate the reduction in stiffness. Based on this model, a study on the effect of the bond length and tape stiffness on the material stiffness will be executed. The results will be used to see the effects of the load transfers inside the material on the stiffness. The code that has been developed for the execution of calculations has been shown in appendix D.

For this derivation, a tape thickness between 20 and 140 GPa (for different tape orientations) has been used. The bond layer is assumed to have a shear modulus of 1.4 GPa [58] has been assumed.

6.8.1 Simplified lap joint model

The model that will be used for this exercise is based on the assumption that DFC are build with a brick-and-mortar structure as shown in figure 6.19a. Based on the assumption that all load transfers within the material happen due to a thin polymer film between the tapes, a double lap joint has been chosen as a simplified model. This model can be simplified again to a single tape and polymer film. In figure 6.19c the model that has been chosen is shown. Hereby, three parts can be distinguished:

- The PEEK interface, this part is assumed to be only loaded in shear
- The CF/PEEK tapes which are loaded with an arbitrary force (P) in the x-direction and are assumed to only be extended in the x-direction.
- The interface layer between the PEEK film and the tape, over the length of this surface, forces are transferred between tape and film.

The boundary conditions of the system are that the tape is loaded on the left side with a force P, the right side of the tape is not constrained. The bottom part of the tape is constraint by assuming a roller joint. The PEEK film will be fixed on the upper boundary which will cause the load transfer at the interface.

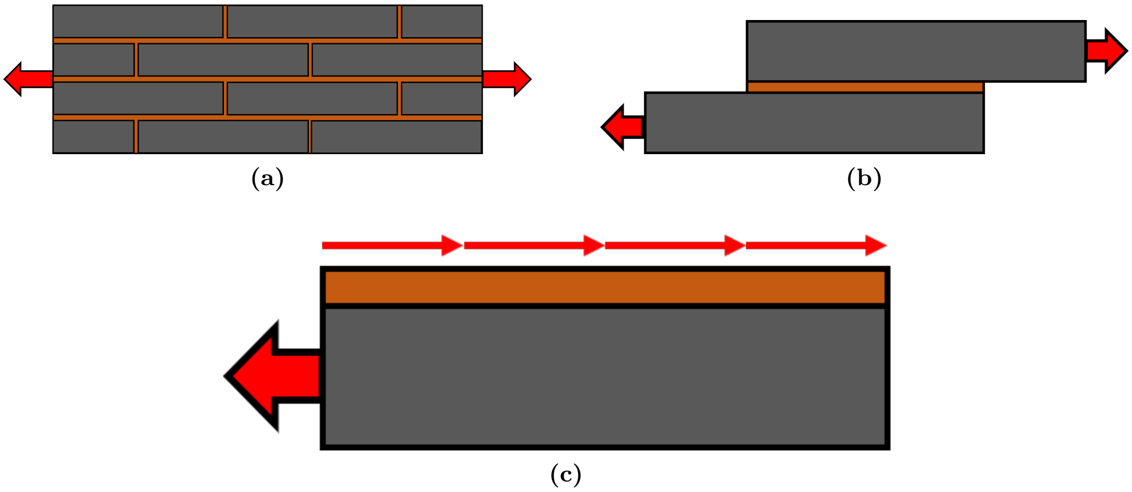

Figure 6.19: Lap joint model withing discontinuous fiber composites. a) Simplified brick and mortar structure b) Bond between two tapes c) Simplification of bond lap joint.

6.8.2 Measurements of film and tape thickness

In order to obtain reliable results, two measurements have been executed to define the dimensions of the model. Hereby the thickness of the tapes and the PEEK film has been obtained by means of optical microscopy. In figure 6.20 three images are shown which have been used to determine the average tape and film thicknesses. Because of the stochastic nature of the material, the bond length is unknown and has been assumed to be between 7.5 mm (width of a tape) and 15 mm (length minus width of a tape). Below, the results of these measurements are discussed.

- Tape thickness
  When measuring the thicknesses of the tapes it was noticed that the minimum tape thickness in samples with a random orientation distribution was thinner than others (0.1 mm for random samples and 0.16 in others). This is probably caused because of tapes with the same orientation stack onto each other during deposition. The average thickness for all the samples was found to be 0.145 mm.
- PEEK film thickness
  During the observations, it was found that there was not always a PEEK film to be distinguished between the tapes. Where a film was observed (sometimes with a low number of fibers inside) the average thickness was roughly 1 micrometer.

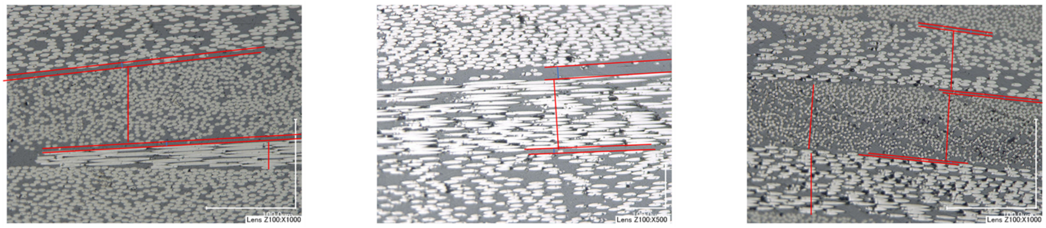

(a) (b) (c)

Figure 6.20: Measurements of tape and bond thickness, red lines are used for measurements. a) Sample 4.4 b) Sample 8.2 c) Sample 8.6.

6.8.3 Derivation

In order to determine the strains in the tapes, the stresses will be calculated based on the shear stresses at the interface layer. The shear stress will be determined by finding the suitable differential equation based on the energy equations as stated in equation 6.7 till 6.11. These are based on the energy equation and the Euler-Lagrange equation [59]. When solving these equations with the boundary conditions of the model, the shear stress, axial stresses, and strains can be calculated. For this case, the value for C1 has been determined by numerically integrating the shear force and making it equal to the given axial force. Figure 6.21 shows the shear stresses over the length of the interface for different bond lengths. It was found that the length of load introduction at the ends of the bond is limited affected by the length of the bond itself.

$$U* = \iiint_V \frac{\tau_{xy}}{\gamma_{xy}} dV + \iiint_V \frac{\sigma_{xx}}{\epsilon_{xx}} dV \tag{6.7}$$

$$U* = \iiint_V \frac{\tau_{xy}^2}{G} dV + \iiint_V \frac{q(x)^2}{Et_{tape}} dV \tag{6.8}$$

$$U* = \int_0^l \frac{\tau_{xy}(x)^2}{2G} t_{bond} + \frac{q(x)^2}{Et_{tape}} dx \tag{6.9}$$

$$\frac{d\sigma}{dx} h = \tau_{xy} = \frac{dq(x)}{dx} \tag{6.10}$$

$$\tau_{xy} = C_1 \sinh \frac{x}{\sqrt{\frac{t_{bond} t_{tape} E}{2G}}} \sinh \frac{w}{\sqrt{\frac{t_{bond} t_{tape} E}{2G}}} \tag{6.11}$$

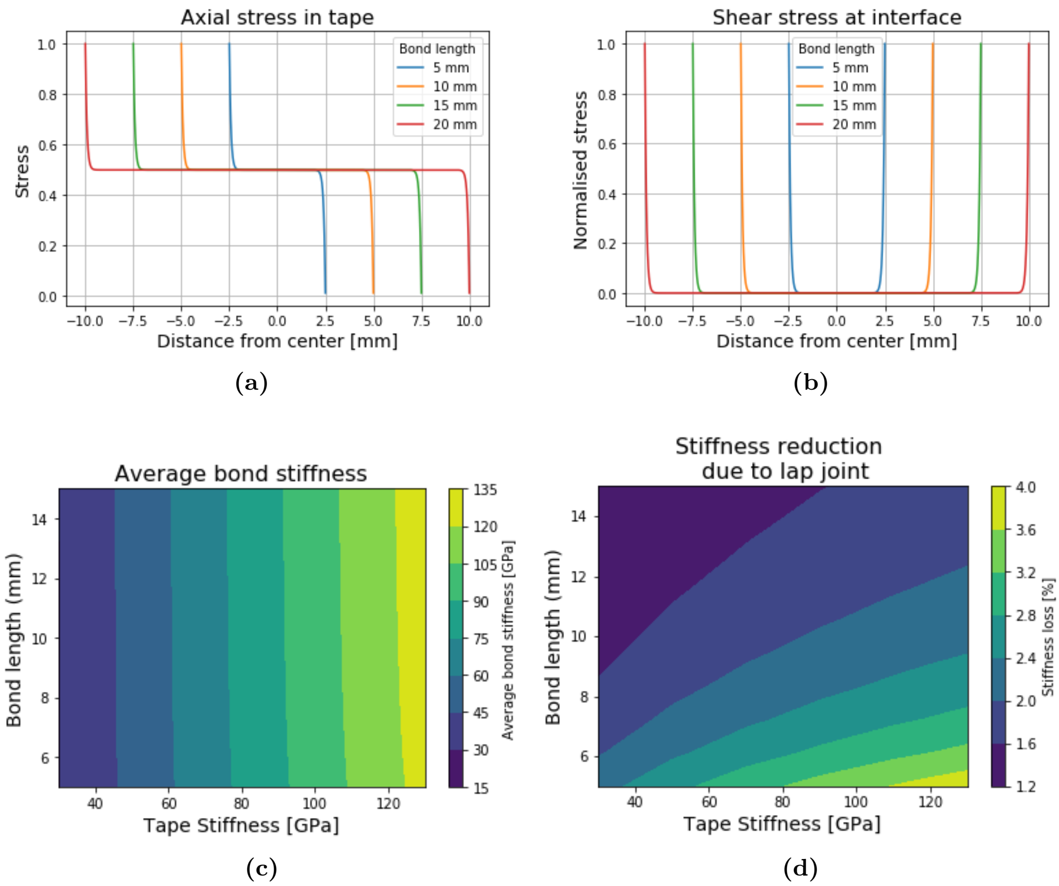

Figure 6.21: Results of shear lag calculations for an arbitrary load, a) Axial stress in tape over bond for different lengths, b) Shear stress at interface over bond for different lengths, c) Effective stiffness in the loading direction of the bond, d) Stiffness reduction in loading direction of the bond compared to tape stiffness

6.8.4 Results and conclusion

With the method for determining the strains in the lap joint, the average stiffness of the joint can be determined. It has been found that that the introduction and extraction of loads at the ends of the tapes cause local strains that are larger than the average in the joint. This indicates that long contact areas between the tapes would result in less reduction in tape stiffness. The other parameter that has been of interest, is the effect of tape stiffness in the loading direction. Due to different tape orientations, the effective stiffness will differ. Based on the used model it is concluded that stiffer tapes lose relatively more stiffness due to the difference in stiffness between the tape and film. When different tape sizes are combined, it is expected that the effective stiffness will also be reduced more. This is caused by a larger thickness of the film between the tapes because the fibers of the tapes can not merge together during the manufacturing process.

The averages of the stiffness reduction will be taken for multiple lap joints with a contact length between 5 and 15 mm. This has resulted in a stiffness reduction of 2.4% for the 0°

aligned tapes, 1.5 % for the ±45° orientations, and 1.6% for the random orientation distribution. Because the ±45° centered samples with PEEK film have a higher percentage of the matrix material, it can be assumed that the average boundary layer between tapes becomes thicker. Based on the same models, this results in a higher stiffness reduction. The average bond thickness has not been measured. As an example, an increase in bond thickness to five microns results in a stiffness reduction of 6.4%.

In order to see the reduction in stiffness in other loading conditions (such as the shear loading of the ±45° orientation distribution), different models have to be made that take shear into account. Although this has not been done, it is expected that the stiffness reduction will be less because of the lower difference in shear stiffness between the tapes and the polymer film.

What can also be noted is that the stresses at the interface show peaks at the edges of the tapes where loads are being introduced. This is one of the explanations why the material failure is more influenced by the matrix than continuous fiber composites.

Chapter 7

Applicability of alignment methods from lab scale to industrial scale

In chapters 5, the selected alignment method has been described and used on a lab scale. In this chapter, the methods will be described for use on an industrial scale. In order to do this, not only the size of the alignment tool but also a suitable manufacturing process will be described.

The manufacturing process of DFC lends itself very well to applications that demand an automated manufacturing process. With the use of thermoplastics and the use of molding as a shaping process, very few steps can't be automated with the use of robotics and programmed presses. With an increase in automation, the uncertainties about the quality of a part will be less due to the reduction in manual labor. It is expected that due to the reduction in manual labor, the properties of the produced parts will become more consistent. A process for the manufacturing of DFC parts consists out of many different steps which will be described separately in this chapter. This description will be based on the literature review and the gained experience from the manufacturing of plates with the use of the alignment tool. In this chapter, the manufacturing process will be divided into multiple segments which will be described separately. After this, the required research will be mentioned to apply the described process.

7.1 Breakdown of the manufacturing process

The manufacturing process can be divided into multiple steps that can be executed in chronological order. These actions are DFC tape manufacturing, mold preparation, material dosing, material deposition, tape alignment, pressure-temperature cycle, part removal, and mold cleaning. In this section, these steps will be described, and if applicable a design will be presented which can be applied in real-life manufacturing. Despite that this process is different from the other composite processing techniques, it has many resemblances with injection molding whereby a part is also produced under high pressures in a closed mold. Parts of the knowledge about this process will be used to describe the manufacturing process of DC. Although this chapter aims to describe a fully functioning manufacturing line, only the aspects that are considered as “novel” will be described in detail.

7.1.1 Tape manufacturing

The manufacturing of the tapes that are used for the plates has not been part of the current thesis work. The material that has been used during the thesis is made from continuous CF/PEEK tows. For an automated process, large quantities of this material need to be ordered or manufactured locally. Hereby, both options can be based on cost comparisons. The tows can be made by splitting a sheet of CFC prepreg in the fiber direction followed by cutting the strands to the desired length. The dimensional requirements for this cutting are low compared to normal part tolerances. With the current use of a composite that contains thermoplastic material, the storage is simple, as long as the material is stored in a dry place and not in direct sunlight. The handling of the material should be done with care because the tapes can split easily in the length direction.

7.1.2 Mold preparation

The mold preparation involves the cleaning and application of the release agent onto the working surfaces. During the current thesis, this is done by hand but can also be done with the use of robot-arms with a spray head [60, 61]. Dependent on the shape of the mold and process parameters, different specifications are required for the robot and robot head.

7.1.3 Tape dosing before deposition

DC has a high viscosity while molten, there is no option to make use of an overflow area in the mold. This results in the need for high accuracy material deposition. Within the industry, many gravimetric systems can create batches with the desired weight. Most of these systems are designed for granular material deposition which uses a screw-drive feeding mechanism. In order not to damage the tapes, a vibrational feeder dosing system can be used, such as is developed by Orbetron [62].

7.1.4 Material deposition into alignment tool

The deposition of tapes into the mold is done with the use of the alignment tool as described in chapter 3. This tool has is used by depositing batches into it followed by shaking and removal of the tool. By doing this several times, a layer-wise deposition can be created. Based on practical experience that has been gained by working with the alignment tool, it was found that the distribution of the tapes during deposition is of importance for the reduction of material flow during the molding cycle. As an exploration of this topic, a single working mechanism has been designed and tested, and described in the next section. Although a fully operational system for this has not been developed, an experiment has been done for a tape-dispersion system. Hereby the DFC tapes are firstly placed in a setup that pushes air in between the tapes which disperses the tapes over a surface. Although the initial working principle was that the bulk of the material would fluidize, this did not occur due to the properties of the tapes. The airflow did scatter the tapes within the bounds of the system, which is the main objective.

After the tapes have been dispersed, they can be transferred with a pick-and-place system to the mold. If a whole batch will be deposited simultaneously into the alignment tool, the size of the dispersion system must be equal to or larger than the mold. For larger parts, it can be chosen to deposit a single tape layer in smaller batches with a tool that covers a smaller area. This would reduce the size and requirements of the dispersion- as well as the pick-and-place system. A smaller dispersion and alignment system can also be used for molds of different sizes which makes the process more flexible.

The pick-and-place system can be a robotic arm in combination with a vacuum suction head. Hereby, the specification regarding location precision and carrying load is not critical. To lift the tapes, the suction head has to be able to create high airflow over a surface. Due to the limited batch size, it is expected that the majority of the tapes lay with the flat side upwards. Because of this, the suction head can most likely exist out of an array of small suction pads that are suitable for the size of a single tape. During the depositing of the tapes, the amount of material can be measured as well.

7.1.5 Material alignment by means of the selected tool

This process of alignment can be automated with the control of material deposition and the relative movements of the alignment tool to the mold. The practical experience with hand deposition with the alignment tool has shown that the "shaking" and handling do not require precise movements to create an aligned distribution. The use of a system comparable to an additive manufacturing machine could be a good starting point to prove these concepts. Hereby only the movement in sideways and upwards directions are needed. Figure 7.1 shows how this can happen. Besides this option, the alignment tool does not weigh more than the average printing head and can thus easily be replaced without restrictions in movement speed.

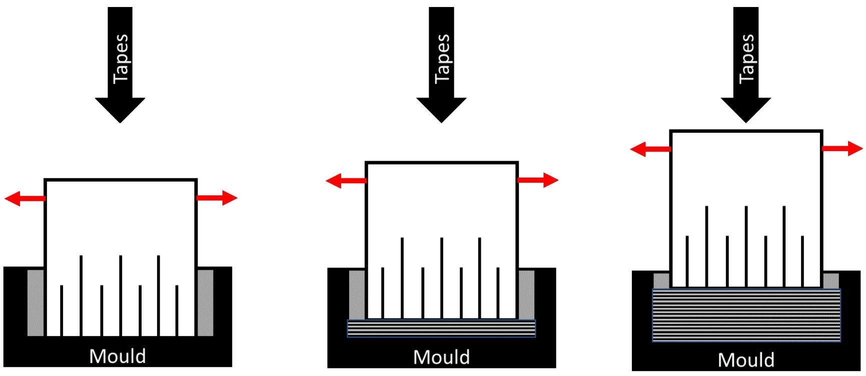

Figure 7.1: Alignment tool movement during tape deposition

When different orientations are used the tool can be placed in a fixture which allows for changing of the tool. This change can be done with the use of a revolver or manually. Because the shape of the tool is dependent on the mold, the design of this system has to be such to allow different tool sizes.

7.1.6 Pressure-temperature cycle

The process cycle will be as described in chapter 5. For each part, the manufacturing settings such as pressure, temperature, and dwell times can be defined per design. Because the heating and cooling of the material will affect its properties, the heat up and cool down ramp should not be inclined too much. By separately pre-heating the mold and tapes the processing time can be reduced. Hereby it should be noted that the effect of temperature on the working of the alignment tool is unknown. Although it is expected this won't be affected much below the Tg of the matrix material.

7.1.7 Part removal

During the manufacturing, the removal of the plates was found to be a labor-intensive action. The automation of parts is not as straightforward as with ejection molding due to the stiffness of the material.

To remove a part, large forces are needed when a part is clamped by the mold due to a difference in thermal shrinkage. By designing the mold such that the part inside can not be clamped when the mold is opened this action can be done within minutes. This can be done with the use of release angles as is done with metal molding. If a large force is still needed, a jig and pressing tools are needed to remove a plate with the help of hydraulics. The design of a mold like this will require large investments (money and time-wise) to make a suitable mold for a specific part.

7.1.8 Mold cleaning

The cleaning of the mold (removal of flashing and remaining material) can be done automated by a robotic arm. Because the requirements for cleaning the mold surface for TP-based composite parts are not as strict as with TS composites, this cleaning can be done quickly. The technology for automated mold cleaning is known within the working field of infusion molding and RTM processing.

7.2 Experimentation with tape dispersion

One of the challenges for automating the chosen tape alignment method is that the tapes have to be deposited equally onto the surface of the mold. A method that will be examined is the fluidized bed method. By using a gas (compressed air preferably) a bulk of loose particles can behave like a liquid and disperse evenly over a surface. In combination with a pick-and-place system, this can be used to deposit the tapes evenly into the alignment tool. This process is suitable for automation because it does not need any human labor. Before it can be assumed that this method is suitable, an assessment will be done to understand the dynamics of the tapes and determine if the method is feasible. In this section, firstly the necessity for a tape dispersion system is proven by measuring the effect of dropping tapes from a height. Afterward, the working principle of the system will be explained. The dynamic forces will be calculated followed by the description of simple experiments that have been executed to gain more practical knowledge about the method. Finally, a conclusion will be made on the feasibility of the system and the implementation of the system into an automated production line.

7.2.1 Necessity of tape dispersion system

During the manufacturing of the plates, the dispersion of the tapes was done by hand. Based on the observed tape distribution over the surface of the mold, new tapes were deposited on areas that seemed to have less material. When automating this process this can not be done during the deposition. Because of this, a system has to be used that disperses the tapes sufficiently throughout the mold. Because the most simple method of deposition is dropping the tapes from a height, it has been decided to see how effective this is with dispersing of tapes. Hereby it is expected that the aerodynamic forces will disperse the tapes although it is unclear to what extend.

Methodology

To quantify the dispersion of tapes in free fall, the measurement setup for measuring the tape distribution has been changed. By dropping small batches of DFC tapes from different heights and observing the locations at which the tapes lay afterward a characteristic can be made on the dispersion. Because of the limitations due to the height of the frame that has been used, the test has been executed with 105, 150, 200, 250, and 340 mm as heights. By overlapping images of multiple tests, an intensity image can be made for each drop height which indicates the chance of a tape falling at a certain location. After this has been done, the image has been reduced to a one-dimensional representation by changing the pixel indices to the distance of the pixel to the center of the view (from which the tapes have been dropped). Because of the size of the image and the size of the mold that is in use, only the pixels that have been 120mm or less from the center have been used for this process. With the measurements, a curve-fit of the probability (p) that a tape is dropped at a certain distance (r) from the center has been done based on an exponential behavior as expressed in equation 7.1 whereby C_1 and C_2 are the unknown parameters.

$$p = C_1 e^{C_2 r} \tag{7.1}$$

Results and conclusion

In figure 7.3 the measurements for each of the heights have been shown. In figure 7.2 the curve fits are plotted in one graph. Here it can be seen that with an increase of height, the dispersion of the tape also increases. Although the curves flatten, it is not enough for the application. Besides this it has been observed that the tapes disperse the most due to the bouncing of the tapes, this effect is most likely less when the surface on which the tapes land are also tapes. With this, it has been concluded that the simple method of dropping the tapes from a single location is not suitable as a tape-dispersing method. Because of this, another system has to be designed to improve the dispersion. Because there are many methods suitable for this, the remainder of this chapter will be devoted to the showcase of an air-based dispersion system.

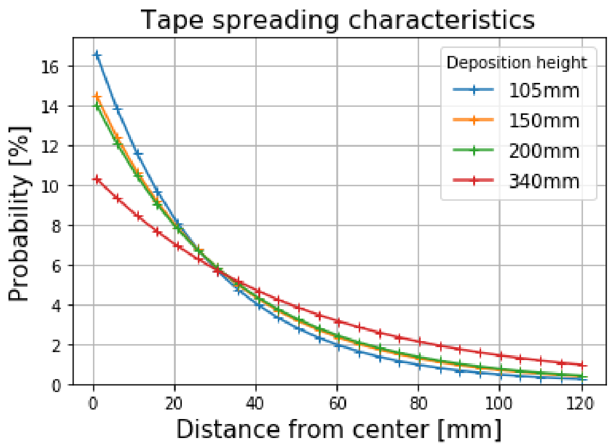

Figure 7.2: Tape dispersion for different drop heights

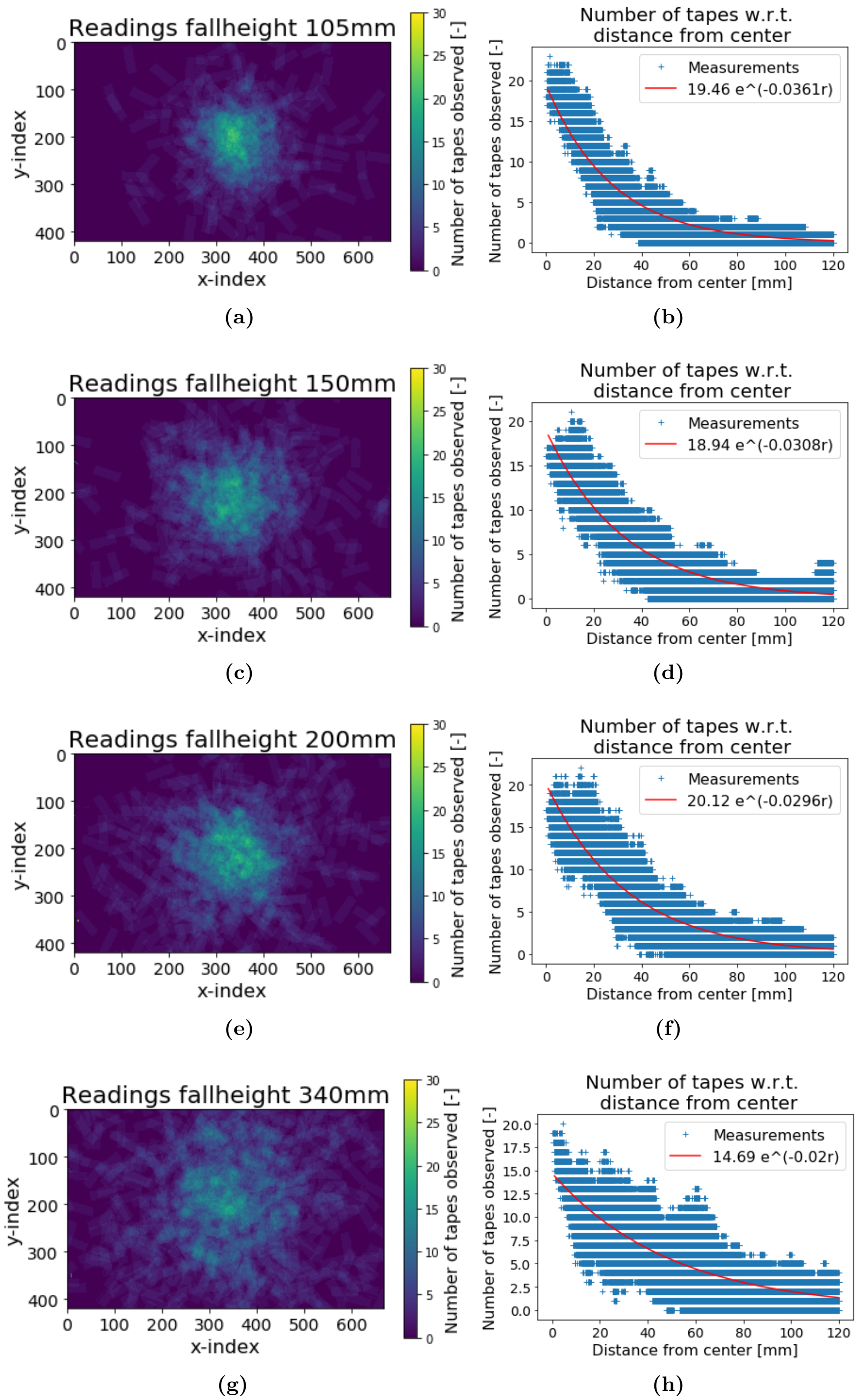

Figure 7.3: Tape dispersion distribution due to free falling from different heights (top to bottom, 105, 150, 200, 340 mm) left side images are intensity, right side images are the simplified measurements with an exponential curve fit

7.2.2 Working principles of fluidization

Fluidization means that a solid (in this case composite tapes) behaves like a fluid. This is normally done by letting a gas or liquid flow upwards through the particles. When the drag forces that act on the particles are equal or greater than the gravitational forces, the particles start to fluidize. Because the aerodynamic drag has to be in the opposite direction of the gravitational forces, the gas or liquid has to be injected from underneath the particles and move upwards. For the current application, the most interesting behavior of fluidization is that the top surface of particles will become horizontal independent of the bottom surface. This means that if tapes are deposited in a certain location, the fluidization will cause the tapes to be dispersed over the surface within the boundaries.

To fluidize particles, the drag forces that act on them must be greater than the gravitational forces. These drag forces are dependent on the shape and orientation of the particles, the fluid or gas that is used, and the speed at which these are injected. In the known case of using round grains (such as sand) as particles, the orientation of the particles will not influence the drag forces. Because of the scale of these particles, the area over volume ratio is large which makes them suitable for fluidization. Another advantage of the use of grains is that the round shapes will make the stacking of the particles on top of each other less likely. Because of this particles can not locate themselves easily in the wake of another particle and combine their gravitational forces to overcome the drag forces. Once the drag forces overcome gravity, the grains start moving upwards, during the start of the movement the grains can rotate to come loose from their neighboring particles.

In the case of composite tapes, these advantages are not present. Because of their rectangular shape, they have large aspect ratios, which causes the aerodynamic forces on a tape to change significantly during the rotation of a tape. This could cause one tape to be lifted when its biggest surface is perpendicular to the airflow and another to fall when the tape is orientated sideways. This is caused by the differences in drag-coefficient and aerodynamic area of the tape. Tapes can also stack upon each other and behave as a single particle. This increases the gravitational force while the drag force is almost the same as for one tape.

7.2.3 Modeling of tapes during fluidization

To know if tapes can be fluidized the forces that can act on a tape should be quantified. Hereby different cases (based on tape orientations) are taken into consideration to judge if tapes can be fluidized and to know what is needed for this. The cases that will be examined are listed below. Hereby the needed flow for air will be used to see how feasible the application can be. For all the cases, the gravitational and drag forces will be taken into account. To simplify the model all tapes are assumed to be the same size (22.5 x 7.5 x 0.2 mm) and only the up and down-ward forces will be taken into account.

- Flat side up (one tape)
- Flat side up (two tapes stacked)
- Flat side up (five tapes stacked)
- Long edge up (one tape)
- Short edge up (one tape)

Gravitation

The gravitational force that acts on a tape is dependent on its mass and the gravitational acceleration of -9.8 $\frac{m}{s^2}$. With a density of 1600 kgm^{-3}, the gravitational force is estimated at 0.53 mN per tape.

Aerodynamic drag

The drag forces of a tape are dependent on the medium (as or liquid), the speed of the medium, and the shape and orientation of the tape. The relationship between the properties of the medium and the drag force is relatively straightforward and is shown in equation 7.2.

$$F_{drag} = C_{drag}\frac{1}{2}\rho v^2 A \tag{7.2}$$

The calculation of the drag coefficient is mainly dependent on the geometry and orientation of the tape. To determine the drag forces, the drag coefficient of the tapes has been estimated based on SolidWorks Flow simulations. These have been executed for three different tape orientations (each of the sides of a tape). Hereby it is assumed that these orientations are will create the highest drag forces. In figure 7.4 the pressure profile around the tape is shown for different tape orientations. Based on these pressures, the resultant forces and drag coefficients can be calculated.

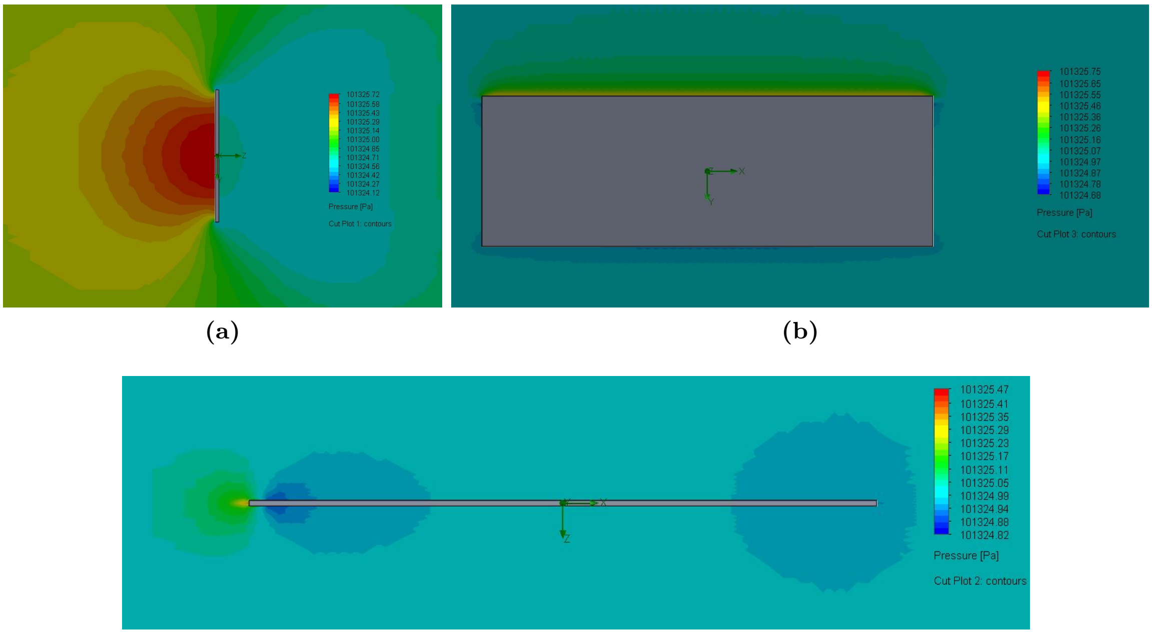

(a) (b) (c)

Figure 7.4: Pressure fields around tapes for different air-flow directions obtained with SolidWorks CFD simulations. a) Airflow parallel to normal of flat side (left), b) Airflow parallel to normal of long side (top), c) Airflow parallel to normal of short side (left)

Although it is not expected that the results of these simulations are accurate, they will yield values for the drag coefficient that are assumed to be accurate enough for the current exercise. For these simulations, a wind speed of 1 $\frac{m}{s}$ is used in combination with the properties of air. Based on the results from the simulation, the drag coefficients and the needed velocity for the air to overcome gravity have been determined and shown in table 7.1. Here it can be seen that there is a significant difference in air velocity that is needed to lift the same tape in different orientations. This is mainly caused by the difference in the frontal area of the configurations, although the drag coefficient also contributes to this.
In practice, this will result in a situation where tapes that are orientated with the flat side downward will be lifted long before other orientations can be lifted. This will most likely result in that tapes will make a "jump" when the drag forces are high but will fall quickly because of their rotation. With more tapes stacked on top of each other, the needed air velocity increases. When the difference in drag forces needs to be decreased, the ratio's between the different dimensions should be closer to a value of one. The shape of the tapes could be altered to increase the coefficient of drag by making the edges concave although this will most likely not be enough to close the gap.

When comparing these differences to grain bases particles (such as sand), there are no big differences in drag forces due to orientation. Because this is not the case for tapes, it is expected that tape can not be used for a fluidized bed in the same manner as sand can be used. What should be noted is that with high air velocities it is expected that the tapes can still be scattered over a surface when the airflow is stopped. This will be discussed in the remainder of this section.

Table 7.1: Drag coefficients based on CFD and needed air velocities to overcome gravity

Orientation	C_D [-]	v_{air} $[ms^{-1}]$
Flat side (1 tape)	1.55	1.84
Flat side (2 tapes)	1.55	2.60
Flat side (5 tapes)	1.55	4.11
Long side	1.34	12.12
Short side	0.83	26.51

7.2.4 Experimentation

To obtain practical knowledge about the workings of a fluidized bed it has been decided to create a showcase prototype that is suitable for the dispersion of tapes for the alignment tool that is currently in use. Although the calculation made use of constant airflow, the prototype will have local air introduction utilizing small holes. In figure 7.5 the design of the fluidized bed consists out of a hollow box. On the top surface, the holes are located while at the bottom there is a connection piece threaded inside a hole. With this connection, the prototype can be connected to a regulated source of pressurized air. To make the box suitable for FDM without any support material, ribs with cutouts have been designed inside the cavity. These ribs allow bridging of the material during printing but also distribute the airflow from the inlet to the holes more evenly.

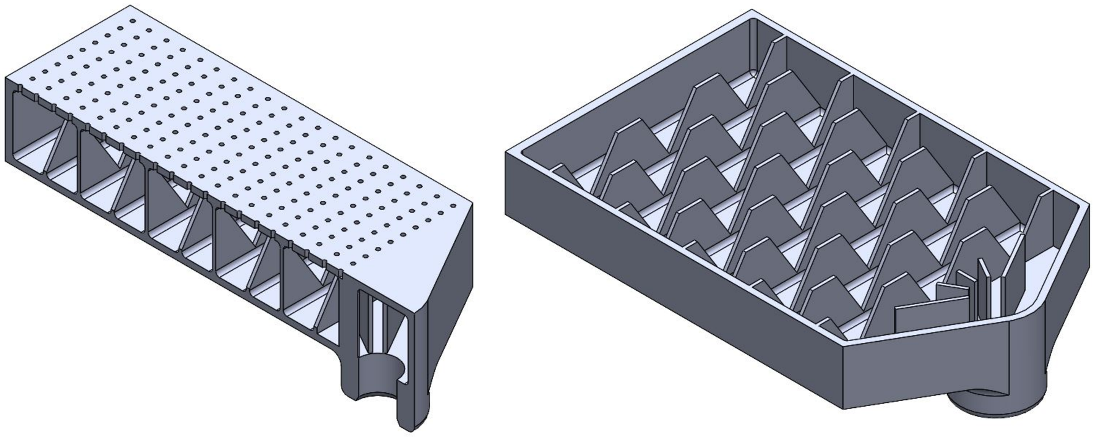

(a) (b)

Figure 7.5: Isometric cross-sections of fluidized bed prototype design. a) side-view, b) top-view

During the testing of the prototype, a box has been placed on the surface. the top side of the box contained holes to ensure the air has to travel through the particles. Before opening the air valve, the tapes have been deposited into the box. The amount of tapes is equal to the amount that is needed to manufacture one plate as described in chapter 5. At the start of the experiment, the regulator was set at 1 bar which was enough to feel a constant airflow above the surface. The pressure of the regulator has been increased to a maximum of around 5 bars whereby the tapes were fully affected by the airflow. The state of the tapes is not fluidized, but they are moving randomly throughout the space in the box. This effect is also visible when fewer tapes are used although hereby the dispersion of the tapes is not effective due to the low number of tapes. When more tapes are added the tapes start acting differently. Instead of flying around, the tapes stack and press upon each other which prevents movement. The air is still flowing but only in areas where tapes are not stacked. Because the airflow is not controlled for each hole but just in general it will flow through the path of least resistance.

During the iteration process that has to lead to the design of the prototype, it was found that some features are of importance to make the system work. During the first iterations, it was found that the box on top of the surface that contains the tapes has to be smooth on the inside and should have good contact with the surface. This contact is needed to avoid alternative air flows that cause tapes to cluster at a corner. For the same reason, holes should be designed as close to the edges of the box as possible to ensure that tapes can't stay at those locations. In order to explain the design more clearly, a technical drawing of the design has been shown in appendix B.3. In this drawing, the overall dimensions and features of the design are shown.

In figure 7.6 observations of the tapes are shown before, during, and after the introduction of airflow. At the start, tapes are all placed in the center of the container. After the airflow is turned off, the tapes are dispersed over the surface. During the randomization of tapes, the tapes move quickly through the available volume which makes them dispersed.

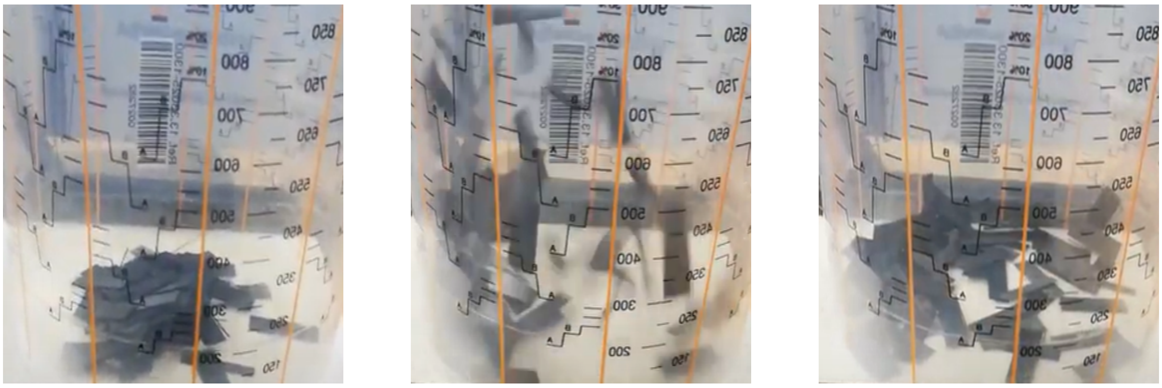

(a) (b) (c)

Figure 7.6: Observations during testing of fluidized bed design. a) Before randomisation, b) During randomisation, c) After randomisation

7.2.5 Conclusion

Due to the significant differences in velocities that are needed to lift tapes, it is concluded that the application of a fluidized bed can not be used to get the same particle dynamics as with grain-like particles. Nevertheless, the method can be used to scatter the tapes over a surface by letting the tapes move and collide in the air. By controlling the local airflow better, it can be avoided that tapes will cluster in one area and don't disperse at all. The described method is suited to disperse tapes over a surface.

7.3 Needed research for implementation of tape alignment tool

To create a manufacturing line, research has to be done on multiple aspects of the production process. For this, a part will have to be defined that determines the specifications of all the manufacturing equipment. Below, all the research is listed that has to be done to create a working manufacturing line:

- Part design
  By designing a manufacturing line, the specifications of the part should be determined, This means that the needed material and possible layer orientations should be chosen which also leads to the design of the alignment tool(s).
- Mold design
  A mold needs to be designed and manufactured for each specific part. Based on the weight and size of the part, the mold should have certain features that enable efficient handling of the mold.
- Deposition system
  The deposition system should distribute the material over the full surface of the mold. When this is not disperse evenly, more material flow is needed which can cause changes in alignment. The results from this chapter should be developed further for successful implementation.

- Integration into process
  After a mold is designed, a test can be done to see if all (or some) the manufacturing steps (mold preparation, deposition, part removal, and mold cleaning) can be executed inside the press. After this, the alignment tool (for each of the required tape orientations) can be designed followed by the design of the deposition system

Chapter 8

Conclusion and recommendations

In chapter 2 the objectives and research questions of the thesis have been formulated. The current chapter will summarise the conclusions that have been found concerning these questions. Afterward, recommendations have been formulated that can be used for further research and improvements on the current findings. These recommendations have been based on the obtained experience during the thesis and can be suggestions for new research directions or improvements on the current research.

8.1 Conclusions

The alignment methods have been examined to tailor the orientation distribution of DFC tapes are described in chapter 3. From these, the methods that have been studied most extensively are based on the dynamic behavior of the CF/PEEK tapes and have been upgraded to proofs-of-concept. Moreover, the four selected proofs-of-concept are suitable for high production rates which is of importance for mass production.

The performance of the *vibrational box* and *morphing surface* proofs-of-concept is not only investigated experimentally but also numerically with the use of Rhino 6®. It was found that the simulation software was only suitable for simple dynamics such as sliding of tapes. The obtained results from these tests are discussed in appendix C.

By means of the OpenCV [40] library, digital image recognition has been used to measure the tape orientation distribution. This distribution is synthesised into the orientation tensor described in chapter 4. The orientation tensor from each proof-of-concept has been assessed using OpenCV and the measurement setup as described in chapter 4. Based on these results and a rating of the proofs-of-concept, the *vibrational box* concept has been proposed for the manufacturing process of the specimens.

The proposed concept is applied by positioning the alignment tool in the mold cavity and depositing tapes into it. The alignment of the tapes is achieved by applying vibrations onto the tool. After the tapes have deposited, the tool is removed. This process can be repeated for multiple batches with the same or different tape orientations as described in chapter 5. As introduction to the usage of this alignment tool for mass production, an outlook for a suitable manufacturing process has been described in chapter 7.

After manufacturing, the samples have been tested in tensile and shear loading. The mechanical properties have been determined by a load cell and DIC strain measurements as described in chapter 6. It was found that the benchmark samples with randomly orientated tapes have an average tensile modulus of 32.5 GPa and a UTS of 202 MPa. The samples with tapes aligned in the loading direction showed a higher tensile modulus of 79.7 GPa with a UTS of 396 MPa. This represents an increase of 145% in stiffness and 96% in strength. These results show that with the used manufacturing process, the UTS and tensile modulus of the material increase. Based on the results extracted from the ±45° samples, the average USS and shear modulus of the material have been determined. These are 104.9 MPa and 7.9 GPa respectively. Through the analysis of the ±45° samples with and without PEEK film, it was found that the addition of the PEEK film did not improve the mechanical properties.

When comparing the measured stiffness to an homogenized CLT model, it was found that CLT overestimated the tensile modulus by up to 50%. For the shear modulus this difference is less, which can be an indication that the shear properties are matrix-dominated for both DFC and CFC. With this, it has been concluded that CLT does not capture the material properties with enough accuracy for the combination of sample geometry and tape orientation distribution used during this thesis.

8.2 Recommendations

This thesis has been an experimental investigation on the manufacturing and characterization of DFC. Based on this, recommendations have been formulated on the topics that could not be answered within the time frame and scope of the thesis. This section will give advice into the future research that can be done based on the experience build throughout the project. The recommendations are split up into different sections based on the subject.

8.2.1 Image recognition

The measurement setup and software have been developed to be able to estimate the tape distribution of the aligned tapes for a flow-based deposition system. As stated in chapter 4 the current measurement system can measure orientations of tapes with a maximum standard deviation of 2.8°. With this, approximately 70% of the measurements are within a ±3° margin of error. If this accuracy needs to be improved, the first step would be to use more precise hardware to capture images.

While the current system is only able to recognize single tapes and small clusters of tapes, the software can be developed to process a larger number of overlapping tapes. To do this, more research needs to be done into topics such as orientation invariant image recognition with the use of neural networks. When doing this, higher resolution images should be used to recognize features on the surface of the tapes. When this is applied, the setup may be used to create digital twins of the tape layups within a mold before molding. With this method, a second camera or dynamic lighting could be added to create a 3D image of the tapes, this can help with recognizing separate tapes.

Finally, the drivers of the cameras should be researched to turn off the white balance and reduce the effect of noise from outside of the system. This noise makes it difficult to set threshold values in the code. If the drivers can be turned off, the readings are expected to be more constant and less sensitive to light from outside the measurement system. Currently, this is not possible with the OpenCV library but can be done by altering the drivers of the camera itself.

8.2.2 Alignment methods

The thesis project has ended with the description of the final working principle that has been used for the manufacturing of test samples. The efficiency and applications of these methods can be further explored to optimize for different tape sizes and orientations. The current design has been made for rectangular tapes with a length and width of 22.5 by 7.5 mm respectively and is thus less efficient for smaller and larger widths. For different sizes, parametric studies can be executed to find a suited wall spacing (estimated at 1 mm wider than the width is expected).

The alignment method can also be designed to be used as a form of local fiber steering. This could be done by making the walls of the alignment tools curved. Although a random orientation is notch-insensitive, this is expected not to be the case for aligned orientations. This effect has not been examined and should be done at a later stage. The steering of tapes is most likely useful for parts with notches such as holes.

To create a suitable alignment method, simulation can be used. The exploration of this tool has not led to realistic results, but can still give insight into particle behavior. To be able to predict the efficiency of the alignment tool, a simulation method has to be found or developed which can create realistic results. Hereby the aerodynamics and tape interactions are of importance for the reliability of the simulation. Because of aerodynamics, it is expected that these simulations require high computational effort.

The current methods have been developed to align rectangular tapes. When different shapes are being used (such as shredded composites, the used method will most likely be useless. New methods should be developed and tested for different particle sizes and shapes for this application. Hereby the knowledge and findings of chopped tapes can help determine the efficiency of these methods.

8.2.3 Material characterisation

The size of the samples that have been tested during the thesis is limited by the mold that was available for manufacturing. In the future, it would be an improvement to be able to create larger samples with a larger gauge length during testing. During the testing, the clamping length should be long enough in order not to cause too high stresses at the ends of the samples where the mechanical properties are low. This can be done by using long paper tabs, or with the use of GFRP or aluminum tabs.

Other research that can be done, is to go further into the effect of alignment on manufacturing and mechanical properties such as dwell time, molding pressure, and shrinkage. The latter introduces also another topic, which is the effect of thermal residual stresses on the overall properties of DC. This research can be done with numerical methods and experiments involving Raman spectroscopy to determine polymer properties such as crystallization. Examples of mechanical properties that could be further explored are the compression properties, strength in single-axis and bi-axial load cases, and notch sensitivity.

Chapter 6 stated that the Poisson ratios that have been found during the mechanical testing, do not seem to be correct for the 0° centered specimen. To prove if these findings are correct or not, more experiments have to be executed employing mechanical testing but also with the creation of numerical models. This can also be used to predict the elastic properties of the material with higher accuracy.

8.2.4 Manufacturing and sustainability

The choice of material for DFC tapes is possibly not the best because most of the mechanisms are matrix-driven. Aspects such as processing temperature and viscosity of the matrix should be taken into account as well. Another aspect such as the cooling rate of the mold could also be further examined to gain knowledge about the influence of the crystallinity of the matrix in the mechanical properties and manufacturing cycle. This research could probably be based on empirical data for specific molds.

During the manufacturing of the plates, the process was dependent on the readings of the thermocouples. This would result in a long time at elevated temperatures. Chapter 6 has shown that this can cause problems regarding the degradation of the matrix. If plates in the future will be manufactured, the maximum time at an elevated temperature should be taken into account. This will also limit production time and thus increase production costs.

Because the manufacturing cycle of a plate can take a long time, lots of energy will be lost to the environment. With a flexible isolation barrier around the mold, this loss can be reduced.

Chapter 6 has described the use of PEEK films as a separation layer between different tape orientations which was found to be infeasible. Although the results show that the use of the 0.25 mm thick films decreased the material properties, this could be caused by the concentration of the polymer due to the thickness of the film. To see if the use of these films might show positive effects, the same experiments have to be done with thinner films where the benefits of layer separation could be more visible in the material properties.

References

[1] Marina Selezneva, Steven Roy, Sean Meldrum, Larry Lessard, and Ali Yousefpour. Modelling of mechanical properties of randomly oriented strand thermoplastic composites. *Journal of Composite Materials*, 51(6):831–845, 2017.

[2] Ike Y Chang and James F Pratte. Ldf™ thermoplastic composites technology. *Journal of Thermoplastic Composite Materials*, 4(3):227–252, 1991.

[3] Dominic LeBlanc, Benoit Landry, Arthur Levy, Pascal Hubert, Steven Roy, and Ali Yousefpour. Compression moulding of complex parts using randomly-oriented strands thermoplastic composites. In *Proceedings of the SAMPE technical conference. Seattle, USA*, 2014.

[4] Mohammed Iqbal Abdul Rasheed. Compression molding of chopped woven thermoplastic composite flakes. 2016.

[5] Maxime Roux, Nicolas Eguémann, Clemens Dransfeld, Frédéric Thiébaud, and Dominique Perreux. Thermoplastic carbon fibre-reinforced polymer recycling with electrodynamical fragmentation: From cradle to cradle. *Journal of Thermoplastic Composite Materials*, 30(3):381–403, 2017.

[6] SR Naqvi, H Mysore Prabhakara, EA Bramer, W Dierkes, R Akkerman, and G Brem. A critical review on recycling of end-of-life carbon fibre/glass fibre reinforced composites waste using pyrolysis towards a circular economy. *Resources, conservation and recycling*, 136:118–129, 2018.

[7] Hugues Lessard, Gilbert Lebrun, Abdelhaq Benkaddour, and Xuan-Tan Pham. Influence of process parameters on the thermostamping of a [0/90] 12 carbon/polyether ether ketone laminate. *Composites Part A: Applied Science and Manufacturing*, 70:59–68, 2015.

[8] Marina Selezneva. *Experimental and theoretical investigations of mechanical properties of randomly-oriented strand (ROS) composites.* McGill University (Canada), 2015.

[9] T Osswald, L Turng, and P Gramann. Injection molding handbook. hanser, 2001.

[10] H Yu, Kevin D Potter, and Michael R Wisnom. A novel manufacturing method of aligned short fibre composite. In *Proceedings of ECCM15-15th European conference on composite materials. Venice, Italy*, 2012.

[11] Khong Wui Gan, You Wei Ho, Zheng Yang Ow, Haris Ahmad Israr, and King Jye Wong. Aligned discontinuous carbon fibre tows in hybrid composites and their tensile behaviour: An experimental study. *Journal of Composite Materials*, 53(26-27):3893–3907, 2019.

[12] D DeWayne Howell and Scott Fukumoto. Compression molding of long chopped fiber thermoplastic composites. In *CAMX Conference*, 2014.

[13] Rajni Chahal, Ashfaq Adnan, Kenneth Reifsnider, Rassel Raihan, Yuan Ting Wu, Vamsee Vadlamudi, and Muthu Ram Prabhu Elenchezhian. Molecular dynamics for the prediction of the interfacial shear stress and interface dielectric properties of carbon fiber epoxy composites. Proceedings of the American Society for Composites—Thirty-third Technical . . . , 2018.

[14] MP Todor, C Bulei, T Heput, and I Kiss. Researches on the development of new composite materials complete/partially biodegradable using natural textile fibers of new vegetable origin and those recovered from textile waste. In *IOP Conference Series: Materials Science and Engineering*, volume 294, page 012021. IOP Publishing, 2018.

[15] Soraia Pimenta and Paul Robinson. An analytical shear-lag model for composites with 'brick-and-mortar'architecture considering non-linear matrix response and failure. *Composites science and technology*, 104:111–124, 2014.

[16] Marina Selezneva and Larry Lessard. Characterization of mechanical properties of randomly oriented strand thermoplastic composites. *Journal of composite materials*, 50(20):2833–2851, 2016.

[17] Paolo Feraboli, Elof Peitso, Tyler Cleveland, and Patrick Stickler. Characterization of discontinuous carbon fiber/epoxy systems for aerospace applications: Part ii. In *49th AIAA/ASME/ASCE/AHS/ASC Structures, Structural Dynamics, and Materials Conference, 16th AIAA/ASME/AHS Adaptive Structures Conference, 10th AIAA Non-Deterministic Approaches Conference, 9th AIAA Gossamer Spacecraft Forum, 4th AIAA Multidisciplinary Design Optimization Specialists Conference*, page 1939, 2008.

[18] C. Kassapoglou. Modeling the effect of damage in composite structures. 2015.

[19] Christos Kassapoglou. *Design and analysis of composite structures: with applications to aerospace structures*. John Wiley & Sons, 2013.

[20] Marco Alves and Soraia Pimenta. Analysing the effect of fibre waviness on the stiffness of tow-based discontinuous composites. 2018.

[21] Marco Alves and Soraia Pimenta. The influence of 3d microstructural features on the elastic behaviour of tow-based discontinuous composites. *Composite Structures*, page 112484, 2020.

[22] Hong Gun Kim. Prediction of elastic properties in discontinuous composite materials. In *Key Engineering Materials*, volume 297, pages 1265–1269. Trans Tech Publ, 2005.

[23] Gergely Czél, Soraia Pimenta, Michael R Wisnom, and Paul Robinson. Demonstration of pseudo-ductility in unidirectional discontinuous carbon fibre/epoxy prepreg composites. *Composites Science and Technology*, 106:110–119, 2015.

[24] LT Harper, TA Turner, JRB Martin, and NA Warrior. Fiber alignment in directed carbon fiber preforms—a feasibility study. *Journal of Composite Materials*, 43(1):57–74, 2009.

[25] Yizhuo Li, Soraia Pimenta, Jordan Singgih, Stefan Nothdurfter, and Karsten Schuffenhauer. Experimental investigation of randomly-oriented tow-based discontinuous composites and their equivalent laminates. *Composites Part A: Applied Science and Manufacturing*, 102:64–75, 2017.

[26] Paolo Feraboli, Elof Peitso, Tyler Cleveland, Patrick B Stickler, and John C Halpin. Notched behavior of prepreg-based discontinuous carbon fiber/epoxy systems. *Composites Part A: Applied Science and Manufacturing*, 40(3):289–299, 2009.

[27] NM Neves, G Isdell, AS Pouzada, and PC Powell. On the effect of the fiber orientation on the flexural stiffness of injection molded short fiber reinforced polycarbonate plates. *Polymer composites*, 19(5):640–651, 1998.

[28] Shinichiro Yamashita, Koji Hashimoto, Hirofumi Suganuma, and Jun Takahashi. Experimental characterization of the tensile failure mode of ultra-thin chopped carbon fiber tape-reinforced thermoplastics. *Journal of Reinforced Plastics and Composites*, 35(18):1342–1352, 2016.

[29] Luca M Martulli, Leen Muyshondt, Martin Kerschbaum, Soraia Pimenta, Stepan V Lomov, and Yentl Swolfs. Carbon fibre sheet moulding compounds with high in-mould flow: Linking morphology to tensile and compressive properties. *Composites Part A: Applied Science and Manufacturing*, 126:105600, 2019.

[30] Lee Thomas. Harper. *Discontinuous carbon fibre composites for automotive applications.* University of Nottingham, 2016.

[31] H Yu, Kevin D Potter, and Michael R Wisnom. A novel manufacturing method for aligned discontinuous fibre composites (high performance-discontinuous fibre method). *Composites Part A: Applied Science and Manufacturing*, 65:175–185, 2014.

[32] Samantha Huntley, Thomas Rendall, Marco Longana, Thomas Pozegic, Juhyeong Lee, Kevin Potter, Ian Hamerton, et al. Modelling of the hiperdif method for manufacturing recycled composites using smoothed particle hydrodynamics. *ICCM22 2019*, page 4141, 2019.

[33] S Huntley, T Rendall, M Longana, T Pozegic, J Lee, K Potter, and I Hamerton. Sph for design of an industrial scale composites recycling process.

[34] Marco L Longana, Natalie Ong, HaNa Yu, and Kevin D Potter. Multiple closed loop recycling of carbon fibre composites with the hiperdif (high performance discontinuous fibre) method. *Composite Structures*, 153:271–277, 2016.

[35] M-S Scholz, BW Drinkwater, and RS Trask. Ultrasonic assembly of anisotropic short fibre reinforced composites. *Ultrasonics*, 54(4):1015–1019, 2014.

[36] Sergii G Kravchenko and R Byron Pipes. Progressive failure analysis in discontinuous composite system of prepreg platelets with stochastic meso-morphology. In *Proceedings of the Science in the Age of Experience (SIMULIA Global User Meeting), Boston, MA, USA*, pages 18–21, 2018.

[37] Sridhar Ranganathan and Suresh G Advani. Characterization of orientation clustering in short-fiber composites. *Journal of Polymer Science Part B: Polymer Physics*, 28(13):2651–2672, 1990.

[38] Yi Wan and Jun Takahashi. Tensile and compressive properties of chopped carbon fiber tapes reinforced thermoplastics with different fiber lengths and molding pressures. *Composites Part A: Applied Science and Manufacturing*, 87:271–281, 2016.

[39] Chen Yuan Chung, Shia Chung Chen, and Kuan Ju Lin. The influence of magnetic fiber orientation on the electric properties of conductive polymer composite material by using magnetic-assisted injection molding. In *Key Engineering Materials*, volume 825, pages 114–122. Trans Tech Publ, 2019.

[40] Gary Bradski and Adrian Kaehler. *Learning OpenCV: Computer vision with the OpenCV library.* " O'Reilly Media, Inc.",, 2008.

[41] Freedom Munitions. How ammo is made - ammoload machines loading ammo at shot show 2015. https://www.youtube.com/watch?app=desktop&v=hVV__K9RwdU&ab_channel=FreedomMunitions, Februari 2015.

[42] Dina R Berkowitz and John Canny. Designing parts feeders using dynamic simulation. In *Proceedings of IEEE International Conference on Robotics and Automation*, volume 2, pages 1127–1132. IEEE, 1996.

[43] Anil R Ravindran, Raj B Ladani, Shuying Wu, Anthony J Kinloch, Chun H Wang, and Adrian P Mouritz. The electric field alignment of short carbon fibres to enhance the toughness of epoxy composites. *Composites Part A: Applied Science and Manufacturing*, 106:11–23, 2018.

[44] Justin Daniel, Licheng Ju, Jinshan Yang, Xiangzhen Sun, Nikhil Gupta, Amanda Schrand, and Chengying Xu. Pearl-chain formation of discontinuous carbon fiber under an electrical field. *Journal of Manufacturing and Materials Processing*, 1(2):22, 2017.

[45] Shengqiang Jiang, Yixuan Ye, Yuanqiang Tan, Sisi Liu, Jingang Liu, Hao Zhang, and Dongmin Yang. Discrete element simulation of particle motion in ball mills based on similarity. *Powder Technology*, 335:91–102, 2018.

[46] Suresh G Advani and Charles L Tucker III. The use of tensors to describe and predict fiber orientation in short fiber composites. *Journal of rheology*, 31(8):751–784, 1987.

[47] G. Bradski. The OpenCV Library. *Dr. Dobb's Journal of Software Tools*, 2000.

[48] M Day, T Suprunchuk, JD Cooney, and DM Wiles. Thermal degradation of poly (aryl-ether–ether-ketone)(peek): A differential scanning calorimetry study. *Journal of applied polymer science*, 36(5):1097–1106, 1988.

[49] M Day, D Sally, and DM Wiles. Thermal degradation of poly (aryl-ether-ether-ketone): Experimental evaluation of crosslinking reactions. *Journal of Applied Polymer Science*, 40(9-10):1615–1625, 1990.

[50] Olivier De Almeida, Emeline Bessard, and Gérard Bernhart. Influence of processing parameters and semi-finished product on consolidation of carbon/peek laminates. In *Proc. 15th European Conference on Composite Materials ECCM15*, 2012.

[51] Paolo Feraboli, Elof Peitso, Francesco Deleo, Tyler Cleveland, and Patrick B Stickler. Characterization of prepreg-based discontinuous carbon fiber/epoxy systems. *Journal of reinforced plastics and composites*, 28(10):1191–1214, 2009.

[52] M Zeeshan Siddiqui, Fawad Tariq, Nausheen Naz, and M Fahad Ahmed. Determination of young's modulus of metallic and composite materials by digital image correlation. *Journal of Space Technology*, 1(1):32–37, 2012.

[53] Victor Munoz Cuartas, Marianne Perrin, Marie-Laetitia Pastor, Hélène Welemane, Arthur Cantarel, and Moussa Karama. Determination of the elastic properties in cfrp composites: comparison of different approaches based on tensile tests and ultrasonic characterization. *Advances in aircraft and spacecraft science*, 2(3):pp–249, 2015.

[54] Pedro Ponces Camanho, C G Davila, and MF De Moura. Numerical simulation of mixed-mode progressive delamination in composite materials. *Journal of composite materials*, 37(16):1415–1438, 2003.

[55] Fiberforge GmbH. *Fiberforge Carbon/PEEK Unidirectional Blank*, 4 2012.

[56] TJ Vogler and S Kyriakides. Inelastic behavior of an as4/peek composite under combined transverse compression and shear. part i: experiments. *International Journal of Plasticity*, 15(8):783–806, 1999.

[57] TenCate. *TenCate Cetex® TC1200 PEEK Resin System*, 5 2014.

[58] Properties: Supplier data - polyetheretherketone (peek) (goodfellow). https://www.azom.com/properties.aspx?ArticleID=1882, Feb 2014.

[59] JL Troutman. Variational calculus and optimal control, undergraduate texts in mathematics, 1996.

[60] Concrete Industry. Hood with manifold sprayer. http://www.automacad.com/ConcreteIndustry/ConcreteIndustry-5/ReleaseAgentApplication-10/HoodwithManifoldSprayer-20.html, Januari 2020.

[61] Autecautomation. Robot for releasing agent application. https://www.autecautomation.com/en/robot-releasing-agent-application/, December 2019.

[62] Ovf220 series feeder. https://www.orbetron.com/product/orbetron/ovf220-series-feeder, author = orbetron, month = Januari, year = 2021 journal=Orbetron.

Appendix A

Reflection analysis for determination of digital image recognition threshold

During the beginning development of the image recognition, the color filter and background have been chosen based on trial and error for the background surface, lighting color, and filter selection. Initially, a white wooden plate has been used as a background of the tapes. This was combined by illuminating red light and using a red filter. Because it has been decided that the tapes will be transported with conveyor belts, it is not possible to have the wood as a background surface and a more flexible surface needs to be used. Because of the design of the conveyor belts, it is preferred to use paper or material that can be used as thin flexible film.

Based on the color of the wood, it was first assumed that the same settings would suffice with regular white paper. When only the background was changed from white wood to white paper, the code was not able to recognize any tape. Further research had to be executed to ensure optimal settings of the image recognition code.

For a better understanding of the reflection of light from the background surface and the tapes, multiple parameters were tested within the measuring setup. These parameters are the background (white paper, blue paper, red paper, green paper, and white painted wood as reference) and the lighting color coming or from the LEDs (white, red, green, and blue). With the use of the camera, an image was captured whereby every pixel returns an intensity value for red, green, and blue (RGB) light. In table A.1, the average of the RGB values is shown for the different configurations. It can be noted that the red value for white wood and white paper differ significantly. These measurements explain why the current code settings did not work with the white paper as they did for the white painted wood. For the other colors of paper, it was observed that the color that is the most captured by the camera is the color of the paper and the color of the lighting. The red light seems to be reflected by all the surfaces.

		White wood			White paper			Red paper			Blue paper			Green paper		
		B	G	R	B	G	R	B	G	R	B	G	R	B	G	R
light	White	255	255	144	255	190	34	176	86	181	255	179	0	150	170	39
	Red	98	48	255	99	48	255	101	44	255	54	18	191	7	1	253
	Green	196	106	0	193	203	0	118	142	0	191	189	0	100	197	0
	Blue	255	173	0	255	177	0	255	110	0	255	168	0	255	146	0

Table A.1: First background reading

When looking at the images of the separate RGB values of only the tapes, it was noted that the surfaces of the tape have a large scatter in red value which seems to differ from tape to tape. Why this is the case, will not be examined. Figure A.1 shows the RGB values under red light with the respective histograms to show the distribution in scatter.

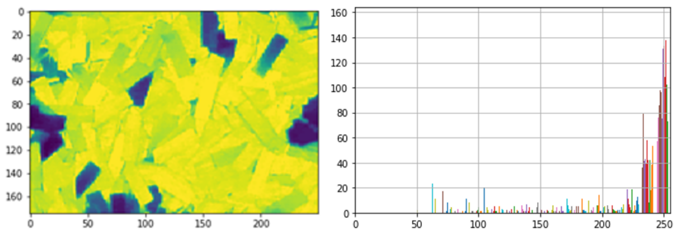

(a)

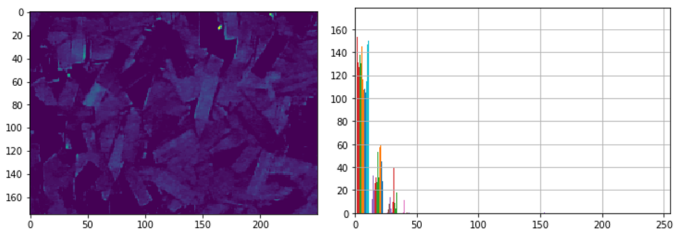

(b)

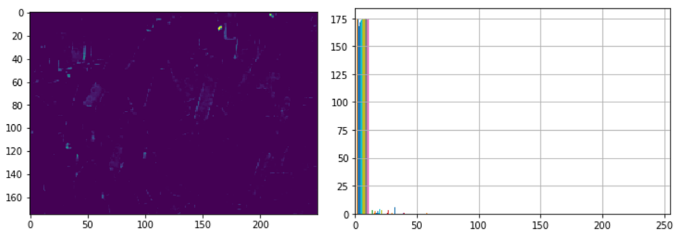

(c)

Figure A.1: Scatter in RGB values of reflective reading of CF/PEEK DC tapes under red light. On the left, a high contrast images are shown and on the left histograms of the occurrence of light intensity values are given, a) Red values, b) Green values, c) Blue values

This scatter in values is a concern because it will affect what percentage of the tapes can be recognized as tape. The larger this scatter is, the less certainty there will be. To get more insight into this scatter and to make a better choice in settings, the measurements were done again. This time, the scatter was expressed by the average and normal distribution (this is not completely valid because the range of values is not infinite and other distribution functions can be more suited). The measurements of the different backgrounds and lights are shown in table A.2.

In table A.2 it can be seen that the scatter in value is significantly larger for the CF/PEEK tapes than for the paper types. It can also be noted that the RGB values from the second reading are different than from the first readings, especially when looking at the red values of the white wood and white paper. The difference between the two readings is expected to be caused by the moment of the measurements and the light coming from outside of the measurement system. The first reading was done in the afternoon and the second was done hours after sunset. Although the measurements were done in a darkened room, there was no possibility to completely work in full darkness. To confirm this hypothesis, a daytime reading was done the next day (still in the darkened room) and shown in table A.3. Hereby it can be seen that the values changed again although the large differences from the first readings were not found again. This could be caused by the changing white balance of the camera. This can not be changed because the OpenCV library does not support this feature.

		White wood			White paper			Red paper			Blue paper			Green paper			CF/PEEK tapes		
		B	G	R	B	G	R	B	G	R	B	G	R	B	G	R	B	G	R
light	White	233	192	141	230	188	137	119	76	255	255	185	0	250	188	0	141	103	64
		4.1	3.8	4.2	4.8	4	4.5	5.2	4.5	0	0	4	0	5.1	4.1	0	53.3	46.5	38.3
	Red	42	31	255	43	32	255	42	25	255	8	0	253	59	19	240	2	1	224
		3.8	3.2	0	4.1	3.4	0	4.1	3.1	0	3.3	0.7	1.7	4.1	2.4	6.4	9	3.2	45.4
	Green	130	226	0	131	228	0	60	154	0	199	194	0	188	199	0	51	132	1
		4.2	4	0.2	4.2	4	0	4.8	6.3	0	3.9	3.7	0	3.7	3.4	0	36	49,3	5.5
	Blue	255	187	0	255	182	0	255	125	0	255	171	0	255	154	0	238	90	0
		0	3.2	0	0	3.5	0	0	5.8	0	0	2.4	0	0	3.8	0	36	38.8	2.1

Table A.2: Second background reading

		White wood			White paper			Red paper			Blue paper			Green paper			CF/PEEK tapes 1		
		B	G	R	B	G	R	B	G	R	B	G	R	B	G	R	B	G	R
light	White	255	189	146	255	195	109	144	72	255	255	188	0	168	184	49	164	124	88
		0.1	3.7	4.1	0	3.9	4.3	5.1	4.3	0	0	4.1	0	5.1	4.1	4	46	44	38.7
	Red	66	26	255	83	41	255	66	18	255	35	1	254	9	2	255	4	2	239
		3.8	3.2	0	4.8	3.3	0	4	3.2	0	4.5	1.6	1.8	3.6	2	0.6	7.5	5.3	31
	Green	152	255	0	175	222	0	142	155	0	169	202	0	106	205	0	61	150	1
		4.5	4.4	0.2	4	3.7	0	6.6	5.9	0	4.3	3.5	0	4	4.5	0	33.1	45.1	5.5
	Blue	255	183	0	255	182	0	255	125	0	255	177	0	255	168	0	247	111	0
		0	4.2	0.1	0	3.6	0	0	5.8	0	0	2.9	0	0	4	0	26.6	37.3	2

Table A.3: Third background reading

With these readings, a choice has been made for the light, background filter, and threshold value within the code. This choice is based on the wish to create the largest certainty when separating the tapes from the background. Because the CF/PEEK tapes show such a large scatter for most of the settings, the feasible options are:

- Red light with Blue filter
- Red light with Green filter
- Green light with Red filter
- Blue light with Red filter

It was chosen to use white paper in combination with red light and the blue filter. This was done because of the separation between the means and the low standard distribution of the blue values. The white paper was also preferred because of the availability of the material. Based on the mean values and normal distributions that were found, the threshold value was set at 20. Every pixel with a blue value above this is identified as tape and everything above will be identified as background. When implementing these changes, the code was able to recognize the tapes successfully again. Because the blue values seem to affect the reflection of the tapes less and the difference between the two values (tapes and background) is large, it has been decided that the indirect lighting will not be avoided more and the white balance will not be controlled. When problems arise around the choice of filter this might be done at a later point in the project.

Appendix B

Technical drawings

In this appendix the technical drawings are presented for the topics that are stated below:

1. The drawings of the proofs-of-concepts that have been described in chapter 3.

2. The drawings of the alignment tools that have been used for the manufacturing of DC plates, as described in chapter 5.

3. The drawing that is made of the concept of the fluidized bed as described in chapter 7.

B.1 Proofs-of-concept

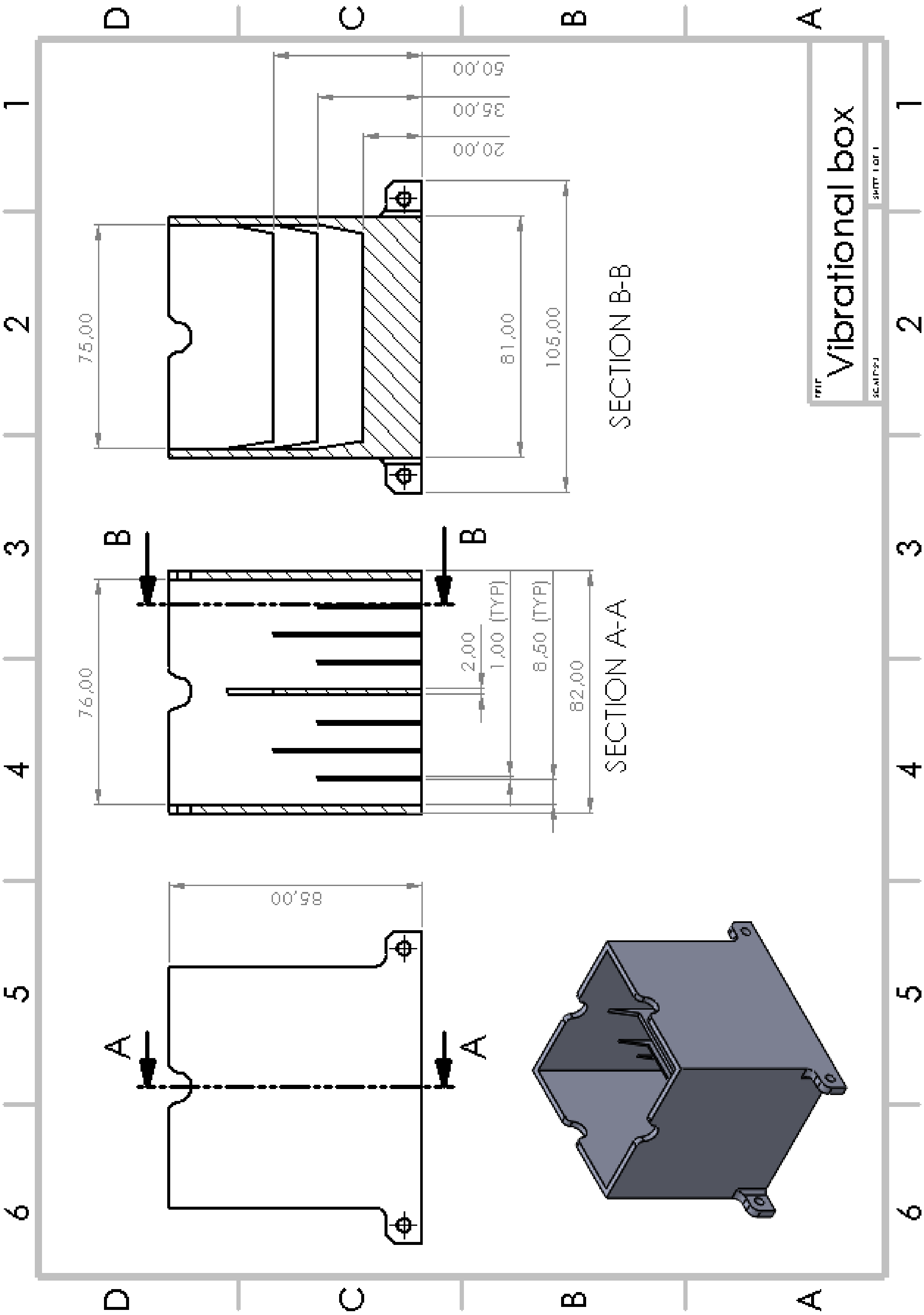

Figure B.1: Technical drawing vibrational box

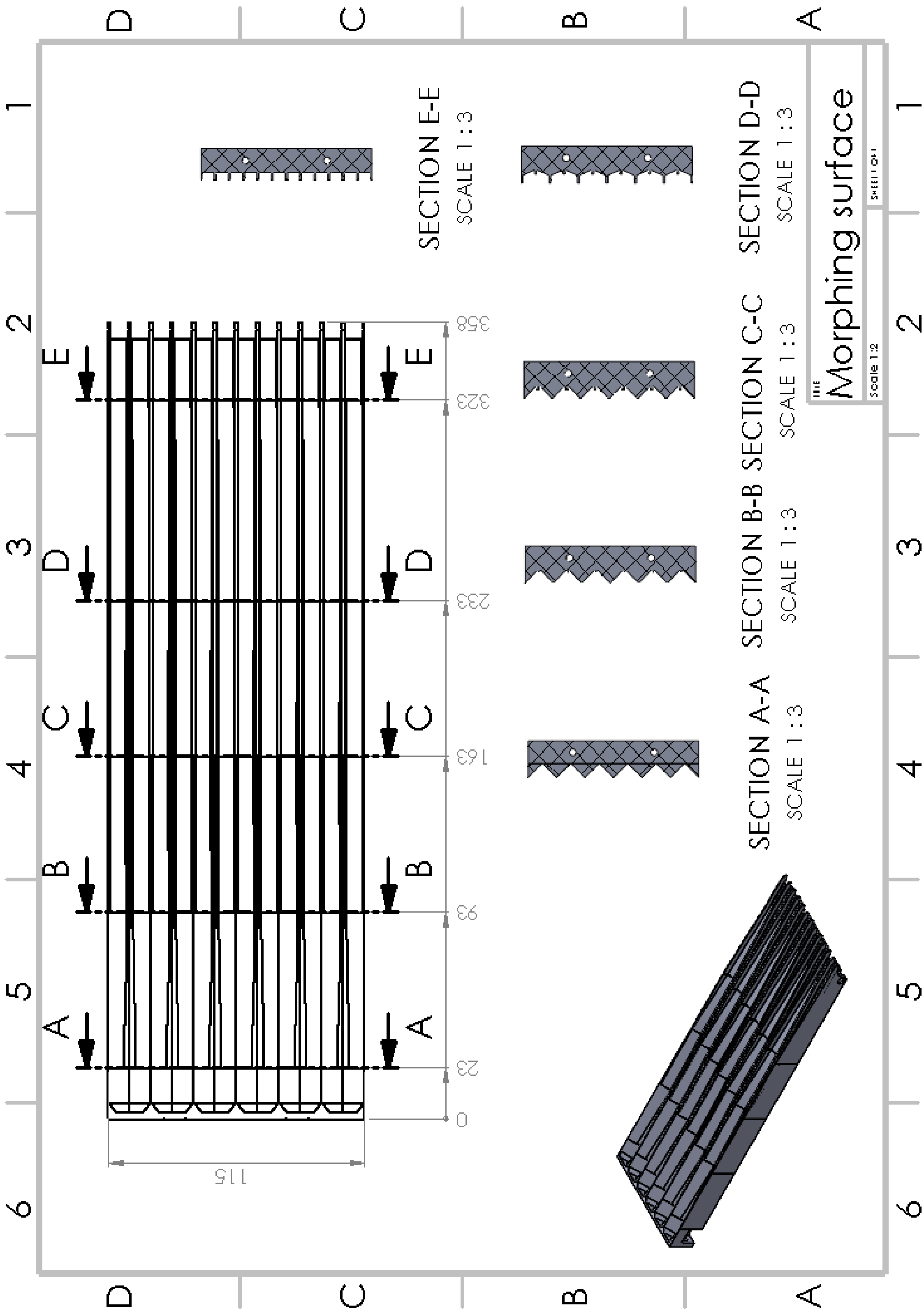

Figure B.2: Technical drawing morphing surface

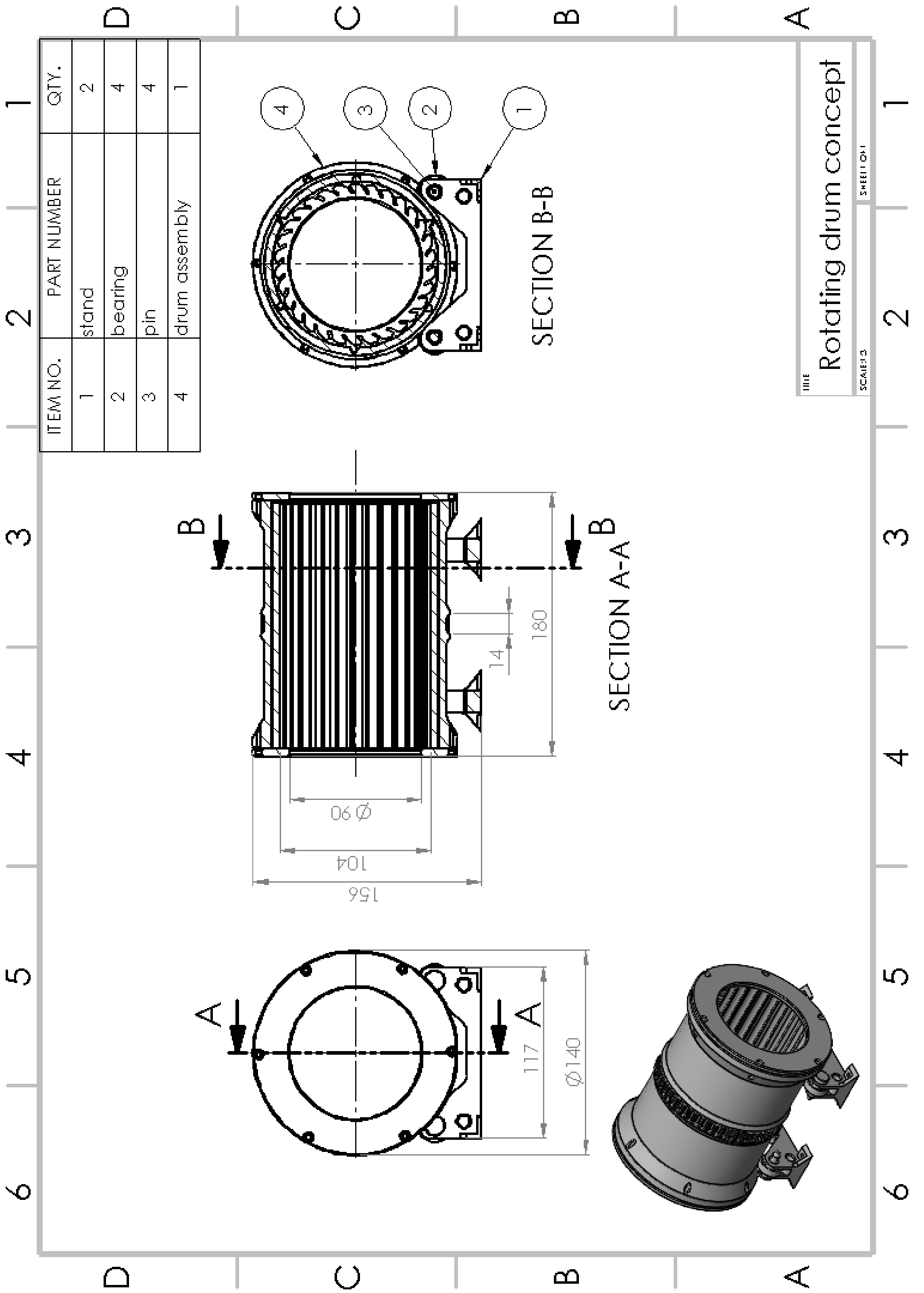

Figure B.3: Technical drawing rotating drum

B.2 Alignment tools for manufacturing

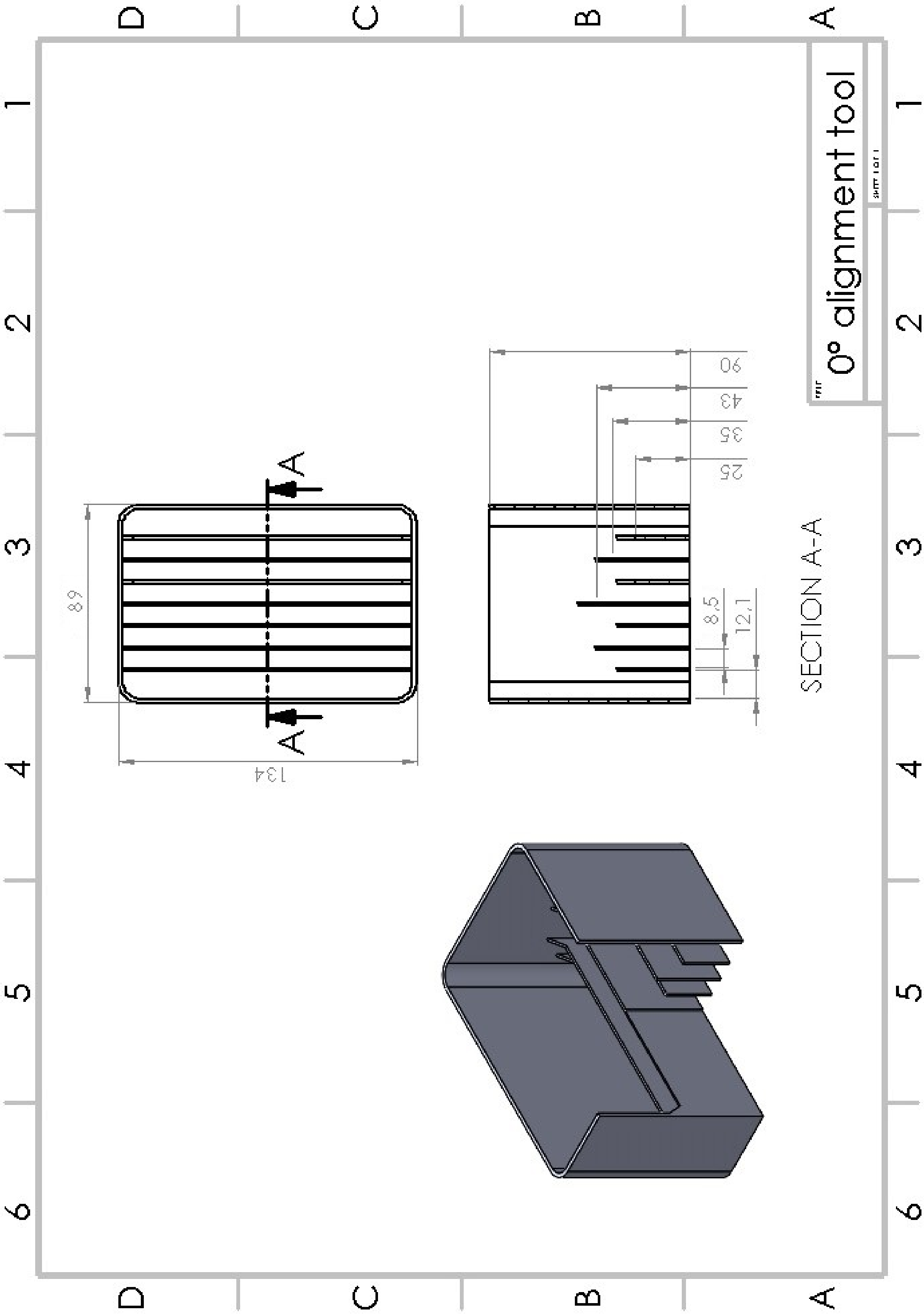

Figure B.4: 0° alignment tool for manufacturing

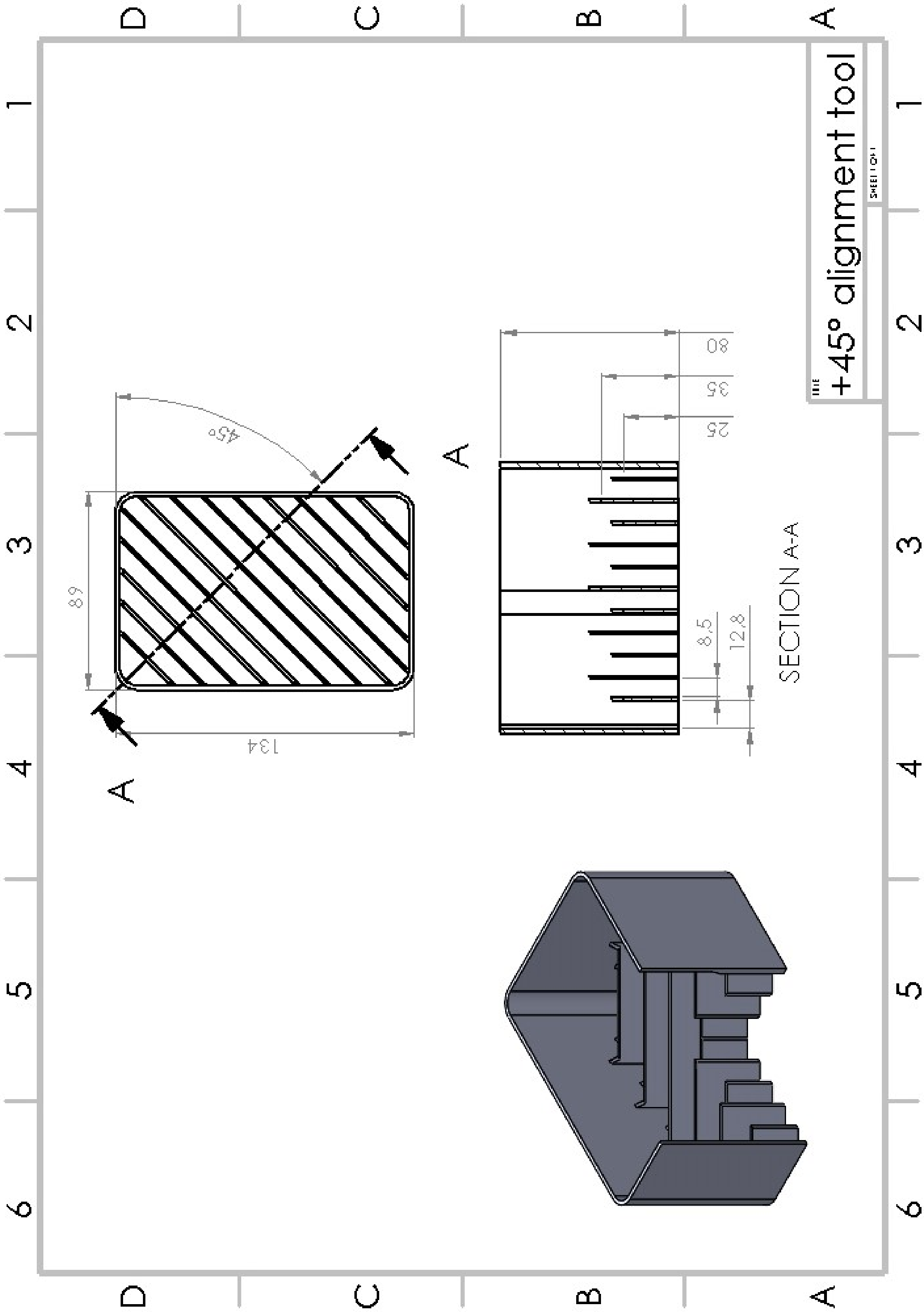

Figure B.5: +45° alignment tool for manufacturing

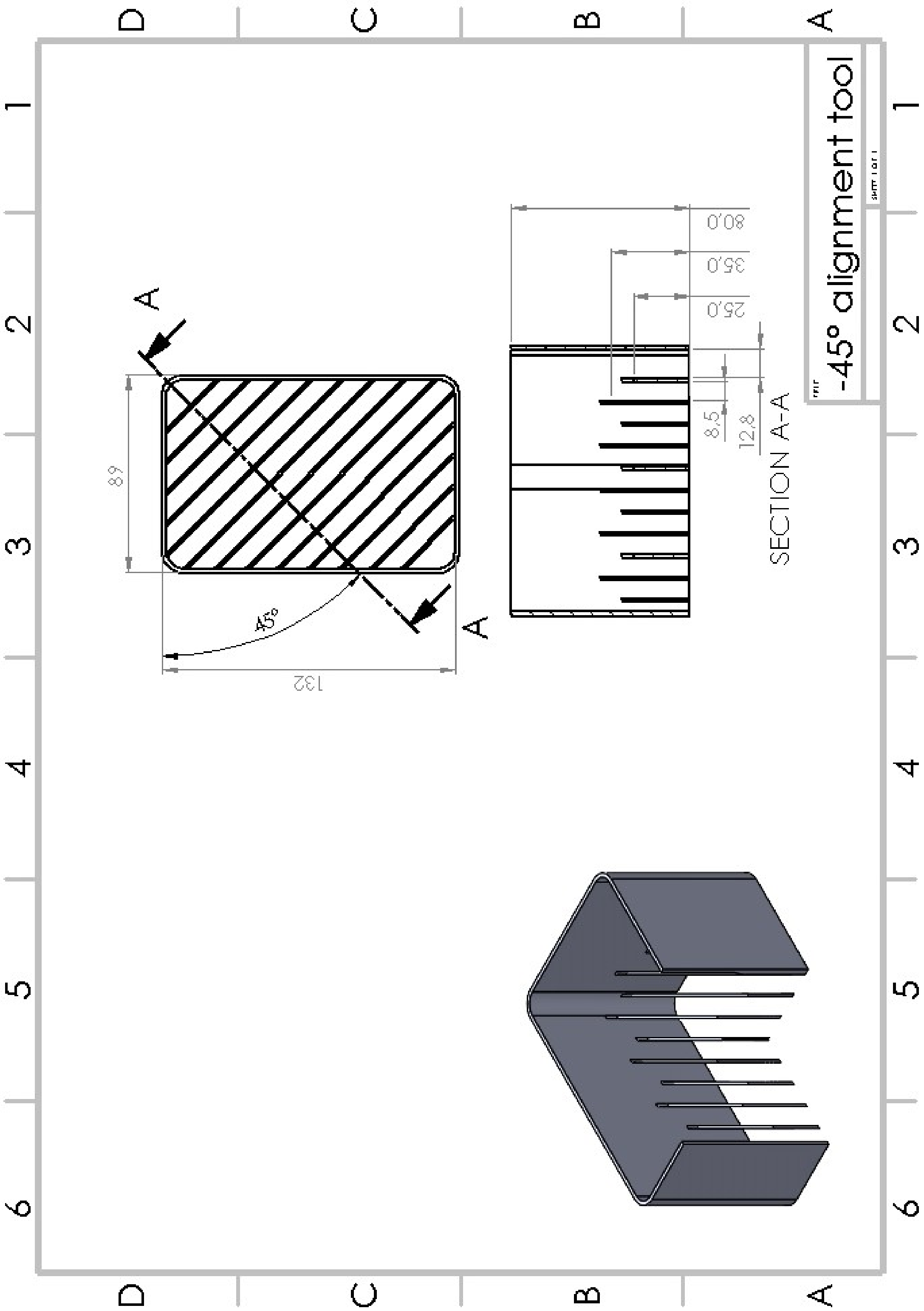

Figure B.6: -45° alignment tool for manufacturing

B.3 Fluidized bed design

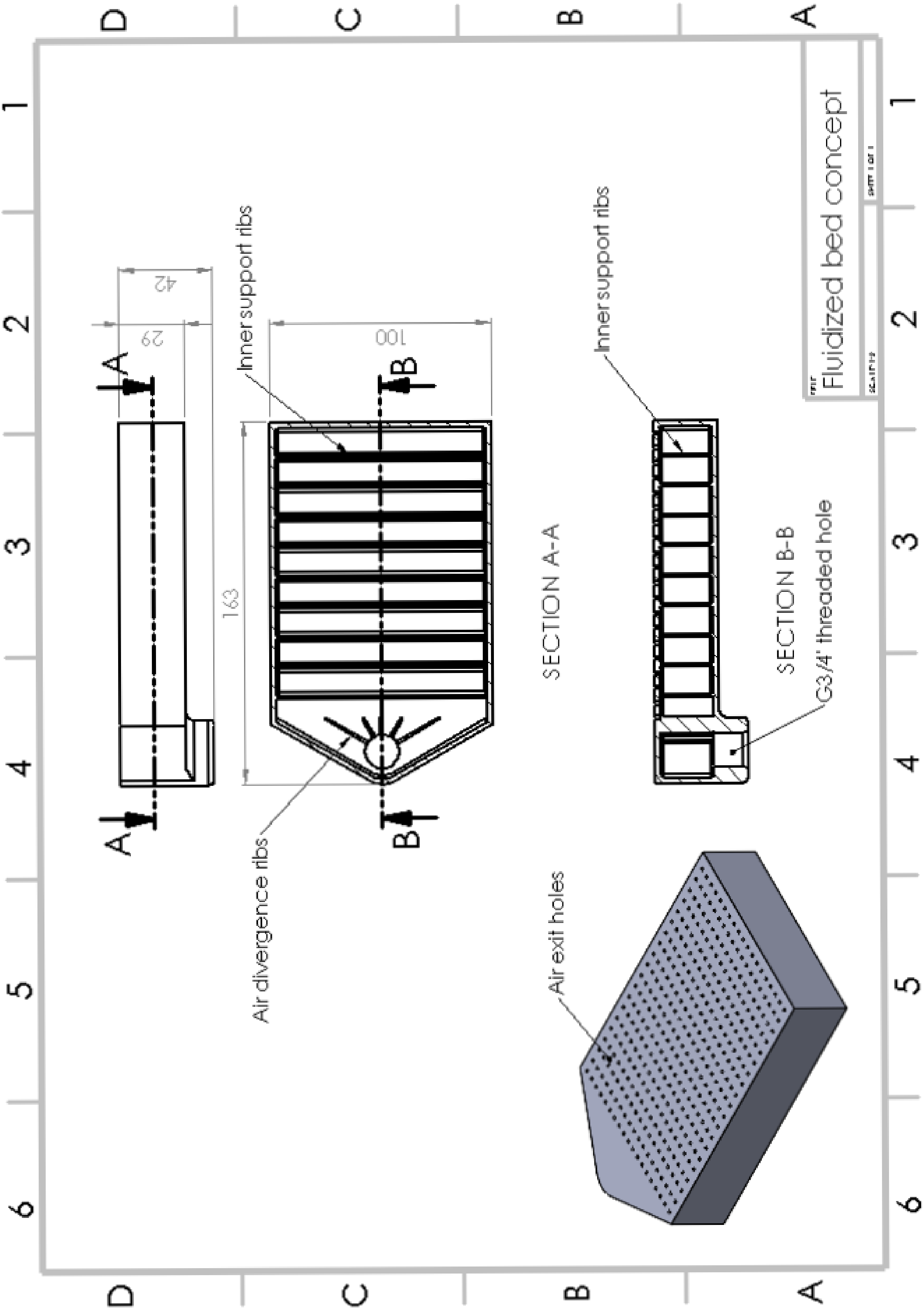

Figure B.7: Design tape spreading surface

Appendix C

Understanding of the alignment mechanism with numerical simulation

C.1 Objective

During the development of the proofs-of-concept, the possibility to simulate the concepts was researched to be able to validate, verificate and to improve the current concepts. The use of simulation is preferred over prototyping because the testing with simulations requires no physical labor and uncertainties with the setup and measurements. Simulations are also able to run a large number of tests in a short period.

At the beginning of this investigation, it was decided to use the Grasshopper add-in of Rhino 6® as the preferred software. Grasshopper contains a pseudo physics engine. The parts and environment can be built within a visual block-based environment. This means that a solver tries to mimic physical behavior instead of calculating it.

C.2 Simulation of vibrational box concept

The "vibrational box" concept was modeled because of the idea that the concept was promising and it seemed that the design parameters (such as wall height, wall spacing, and tape size) could easily be changed to create an improved design.

During the first simulation trails, the same wall heights were used as the initial design. After completing the previous steps, the results were read and are shown in figure C.1 for different randomization seeds. In the histograms in figure C.1, the orientation histograms from the simulated tapes before and after falling on the walls are shown. Hereby the x-axis represents the orientation in degrees and the y axis the probability of a tape to be within one of the groups of orientations. It can be seen in these histograms that the orientation centers around 0° because of the walls.

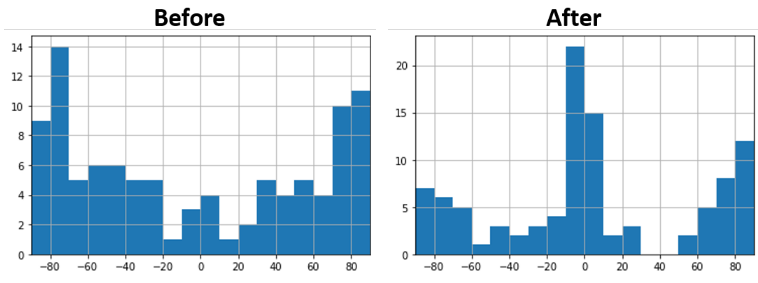

(a)

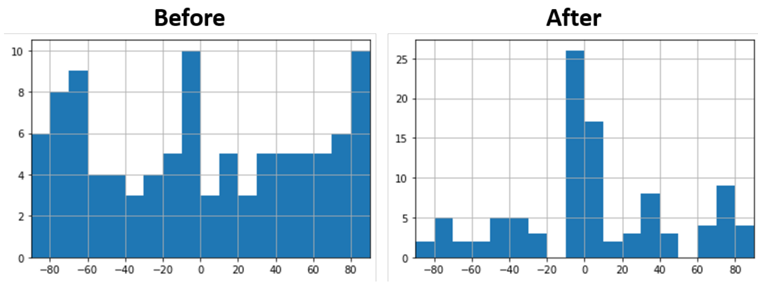

(b)

Figure C.1: Simulated orientation histograms of tapes before and after deposition, a) Randomization seed 1-2, b) Randomization seed 2-3

During the simulation, unwanted behavior of the tapes was observed. While some of these can be explained by the parameters that are used (mainly friction), others do not have an explanation. These flaws are stated below. Because of these flaws, it was questioned if this method can be used for validation and verification of the concepts.

- Tapes were not affected by the gravity and moved upwards
- Tapes "stuck" to the walls
- Tapes moved through the walls
- Tapes moved after being stationary on the floor-plane

To make the simulation as real as possible some parameters should be understood more and determined with experiments or literature research. These parameters are stated below. The experiments to determine these values will be discussed in the next sections.

- Dynamic friction is the friction between the tapes and the walls when the surfaces are moving relatively from each other. This parameter can be determined by sliding a tape on a slope and measuring the reaction forces.

- Static friction is the friction between the tapes and the walls when the surfaces are not moving relatively from each other. This parameter can be determined by placing a tape that is located on a slope with a variable angle and increasing the slope until the tape starts moving.

- Restitution is the velocity loss due to impact. This parameter is tricky because it also depends on the orientation due to the aerodynamic effects that happen when the objects are close to each other. One approach is to separate these two effects into a general restitution factor and an aerodynamic force based on the orientation of the tape.

C.3 Static friction measurements

For the determination of the static friction coefficients a single setup is designed. This design consists out of a plate that can be rotated around a hinge. The material of this plate can be any material as long as it is available as a plate. To change the angle of the plate, a single block with a fixed height (15 mm) is used. This is done by moving the block close to the side of the hinge. After the objects that are placed on the plate have started moving, the position of the block is measured to calculate the coefficient of friction. This test will be done with PLA, stainless steel, and aluminum as one surface and the CF/PEEK tapes as the other. For the PLA, two surfaces were tested. The first one is the surface that is in contact with the print bed during manufacturing which has a very smooth finish. The other one is the top surface of the print which is a bit rougher than the previous one.

At first, the composite tapes were placed flat on the surface. The angle of the plate got increased, but the tapes did not move at the expected angles. It is suspected that electrostatic forces between the surfaces are high compared to the gravitational forces. To minimize this effect, the tapes will have to be tested on their sides. To do this a clamp has been designed and printed, this clamp holds 4 tapes where only the long side of the tapes can make contact with the counter surface. When the test was executed again, the friction values were in the expected range which are shown in figure C.2.

It can be seen that on average the metals show a lower friction coefficient than the PLA which could be caused by the surface roughness although other parameters will not be rejected at this point. Because all the concepts make use of PLA parts, the simulation will use friction values of 0.3 based on these measurements.

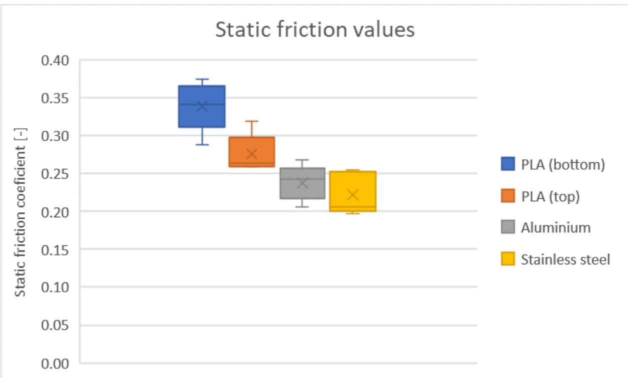

Figure C.2: Experimental friction values

C.4 Restitution measurements

The restitution value is the ratio between the speed at which a particle collides and bounces of another particle. A value of 1 means that the speeds are the same, and a value of 0 means that the particle will not bounce off the other. To determine these values, experiments have been carried out. Hereby the CF/PEEK tapes will be dropped on a surface made out of a chosen material. The tapes are dropped onto the surface. The surfaces that have been chosen are; AL 6082, Stainless steel, and PLA. During the moment of impact, a high-speed camera captures the movement of the tapes. These images will be processed with the help of image recognition. Using this method, the coordinates of the center of a tape are determined per frame from which the velocities before and after impact can be determined. In figure C.1 two of the readings of the high-speed camera test are shown.

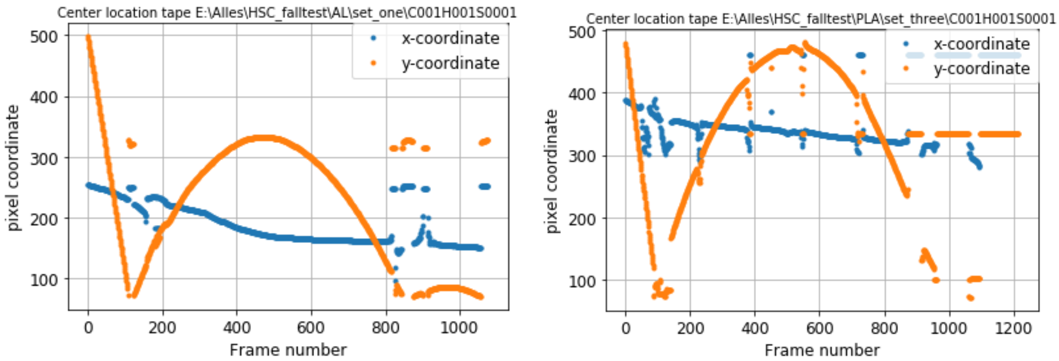

(a) (b)

Figure C.3: Tape center coordinate readings, a) Tape falling on flat AL surface, b) Tape falling on PLA surface

Because there is a high level of noise around the moment of contact between the tape and surface (due to reflection and shadow) the velocity of the tape when bouncing off has been determined by measuring the height of the first bounce. Converting the potential energy to kinetic energy would result in an estimation of the velocity right after impact. It was found that the restitution values are low. Where a value in the order of 0.6 was expected, none of the values reached above 0.05.

It is expected that the tapes slow down due to their low mass (due to drag) and thus this method cannot be used. The speed after impact can be estimated with a 3rd order curve fit of the data points before impact. These results, shown in tables C.1, C.2 and C.3, gave higher restitution values between 0.17 and 0.46. This is a relatively large scatter but more realistic than the previous ones. The scatter can be caused by the orientation of impact, hereby the aerodynamics should be taken into account and the orientation of the fiber.

Table C.1: Al flat surface bounce

	fps $[m^{-1}]$	pixel size [m]	v_0 $[ms^{-1}]$	v_1 $[ms^{-1}]$	restitution [-]
set_one	10E3	1.02E-04	-19.632	8.196	0.417
set_two	10E3	1.02E-04	-19.930	8.591	0.431
set_three	10E3	1.02E-04	-24.165	4.201	0.174
set_four	10E3	1.02E-04	-22.261	10.230	0.460
set_five	10E3	1.02E-04	-23.653	6.753	0.285
Average			-21.928		0.353

Table C.2: PLA flat surface bounce

	fps $[m^{-1}]$	pixel size [m]	v_0 $[ms^{-1}]$	v_1 $[ms^{-1}]$	restitution [-]
set_one	10E3	1.02E-04	-18.582	6.823	0.367
set_two	10E3	1.02E-04	-20.400	5.493	0.269
set_three	10E3	1.02E-04	-20.906	7.500	0.359
set_four	10E3	1.02E-04	-19.200	7.196	0.375
Average			-19.772		0.342

Table C.3: Stainless steel flat surface bounce

	fps $[s^{-1}]$	pixel size [m]	v_0 $[ms^{-1}]$	v_1 $[ms^{-1}]$	restitution [-]
set_one	10K	1.02E-04	-21.958	11.182	0.509
set_two	10K	1.02E-04	-19.195	3.954	0.206
set_three	10K	1.02E-04	-20.071	9.372	0.467
set_four	10K	1.02E-04	-19.875	8.709	0.438
set_five	10K	1.02E-04	N.A.	N.A.	N.A.
Average			-20.275		0.405

Based on the values that were measured, a restitution value of 0.35 has been chosen for the simulation. If a different material is used, this value might have to be changed.

During the running of the simulation, it was found that the implementation of the measured values did not improve the behavior compared to the measurements. Besides this, it is not possible (with the current software) to implement aerodynamic forces or custom forces based on location, orientation, and speed of particular tapes. The restitution was also not implemented successfully because the value of restitution did not seem to change the behavior of the tapes during the simulation. Because of these findings, it was decided to leave the vibrational box simulation as it is and try the morphing surface concept.

C.5 Simulation of morphing surface concept

To showcase the potential of simulation and also use the build op knowledge about the software. It was decided to simulate a simplified version of the morphing surface. Because the tapes are not falling or bouncing, this concept is expected to be realistically simulated. During the simulation, the tapes will be dropped onto the model of the morphing surface. The only forces the tapes are affected by are the contact forces between all the particles, the frictional forces due to the contacts, and the gravitational forces. The gravity has been set in a 25° direction to simulate the slope of the surface during the working. To make the simulation more simplified, the vibrations that are used in the real model will not be implemented. While running the simulation, a clear change in orientation can be seen during the movement of the tapes. At first, all the tapes are random but quickly align with the groves on the surface. This behavior is also observed during experimental testing. The screen captures in figure C.4, show the transition from random to aligned tapes during the simulation.

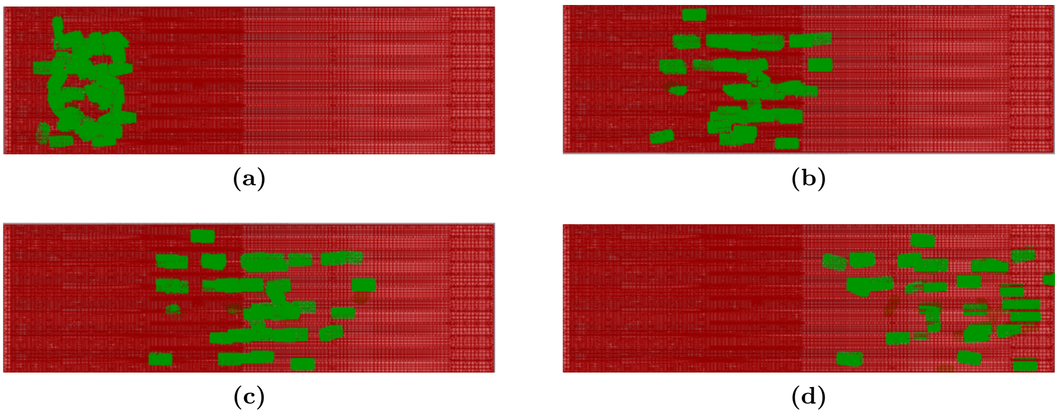

Figure C.4: Simulation observation of tapes (green) moving over morphing surface (red) , a) Start of simulation, b) Alignment phase, c) Transportation phase, d) End of simulation

During the simulation, the coordinates of each node of the tapes were saved in a .txt file and read by a python code. When the center of gravity of a tape passed a certain y-value, the tape was assumed to existing the concept, the in-plane angle was calculated and measured. Because the tapes sometimes showed weird behavior by falling through the geometry of the concept, also the z-coordinate was checked to avoid false readings. The simulation was run 3 times for two different tape sizes each. The first tape size is the one that is used in the other concepts but showed a bit too big for the channels at the end of the surface (width = 7.5 mm). During simulation, this was not the case and the orientation distribution was very good as is shown in the histogram of figure C.5.

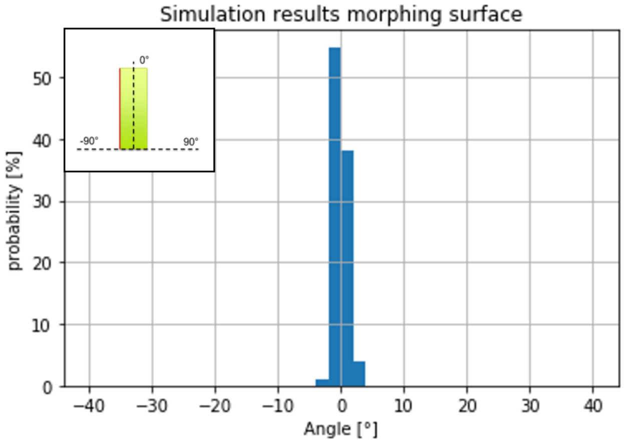

Figure C.5: Simulation result morphing surface tape width = 7.5mm

When the smaller tape size was simulated there seemed to be more spread (although not a lot) in the orientation. This distribution is shown in figure C.6a. It should be noted that these results have a much higher level of alignment than the real version of the surface as shown in figure C.6b. This could be caused by the vibrations, conveyor belt, and measurement accuracy although it is not expected that this would cause this big of a difference. Based on these findings it can be concluded that if these simulations are used, they can only tell if a concept can work, but it will not results in information about the alignment distribution. Besides this, the simulation can be used to compare different configurations with each other although this should be done with caution.

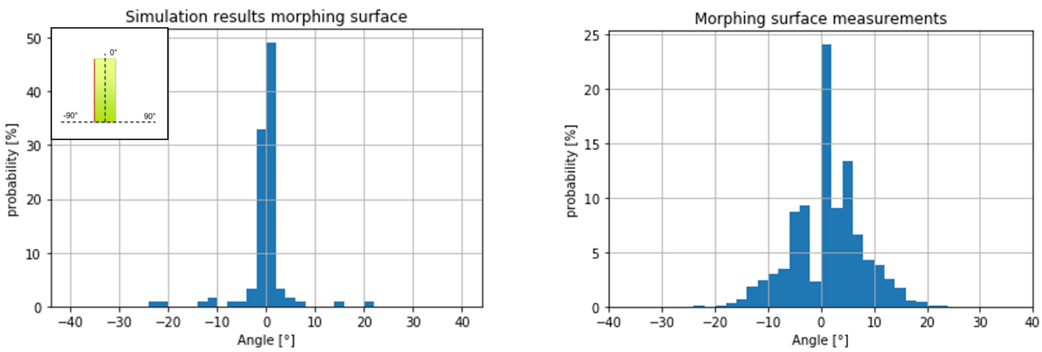

(a) **(b)**

Figure C.6

To check if the results make sense, the same simulations have been executed with rectangular tapes. Hereby it is expected that two equal peaks of probability will be measured because the 0° and 90° rotations are equally stable. In figure C.7a, the histogram of 3 simulations is shown. The distribution. Because of the difficulty to define the edge of a tape, it has been decided to calculate the angle of a different line. This line starts at the first node of a tape (which is always in the corner) and stops at the center of gravity. Because of this, it is expected that the peeks will be at ±45°. In the histogram, these peaks are not well defined although the directions of 0° and 90° show a lower probability. This can be caused by the size of the tapes (6 x 6 mm) which is smaller than the width of the channels of the concept.

To confirm this suspicion, the same simulation was performed with larger tapes (7.5 x 7.5 mm). This simulation was performed for 3 different random orientation seeds of the tapes are resulted in the results as shown in figure C.7b. Hereby it can be seen that the peaks around ±45° are more distinguishable than with the previous tape size.

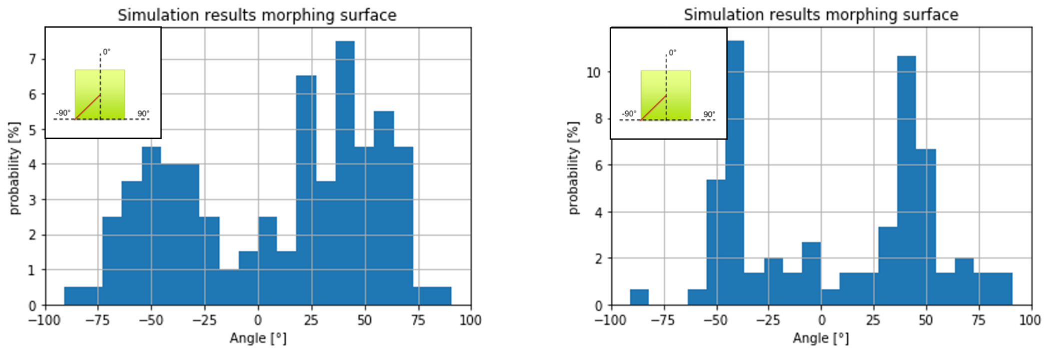

(a) **(b)**

Figure C.7: Simulation result morphing surface tape. a) tapesize = 6 x 6 mm, b) tapesize = 7.5 x 7.5 mm

C.6 Conclusions on simulation

Based on the findings of the vibrational box concept it was found that the current method of simulation can be used to determine if simple alignment methods work (validation). Based on the comparison with real measurements, it was found that the current work is not suited for the verification and improvement of designs. Especially with the vibrational box concept, it was shown that aspects such as aerodynamics can have a significant effect on the dynamic behavior of the tapes while passing through the alignment tool. With the morphing surface concept, it was found that these simulations are more suited for alignment methods that are only concerned with the "sliding" of the tapes. Although the simulations seem to agree with the observations during testing, it was found that the simulations seem to give an optimistic characterization of the methods and can thus also not be used for the improvement of the current designs.

If simulations are needed, it should be considered that the creation of these will require a lot of experiments and modeling time before realistic results can be achieved. The computational cost of each simulation will be orders of magnitude higher than with the current simulations. In some cases, it might be easier to manufacture and test different design configurations than to simulate them.

Appendix D

Python code: Shear lag

The code that is presented in this chapter has been used in order to compare the stiffness of bonds with different configurations with the calculations as described in chapter 6. Hereby the effective stiffness of a bond is compared to the stiffness of the tapes. As result, the average in stiffness reduction of all the calculated configurations.

```
import numpy as np
import matplotlib.pyplot as plt

#different tape stiffnesses (as to imitate different tape orientations)
E_tapes = np.array([30E3,50E3,70E3,90E3,110E3,120E3,130E3])

#polymer properties
G_bond = 1.4E3 #MPa https://www.azom.com/properties.aspx?ArticleID=1882

#bond dimentions
t_tape = 0.145/2 #mm
t_bond = 0.001/2 #mm
L_bonds = np.linspace(5, 15, 10) #mm

#integration step
dx = 0.001 #mm

#tape width (does not influence stresses)
w = 7.5 #mm

#arrays for storing data for plotting
results_strain = np.zeros((len(L_bonds),len(E_tapes)))
results_stiffness = np.zeros((len(L_bonds),len(E_tapes)))
results_stiffness_red = np.zeros((len(L_bonds),len(E_tapes)))

#loop for calculation of stiffnesses of bonds
for a, L_bond in enumerate(L_bonds):
    # for b, t_bond in enumerate(t_bonds):
```

```
    for b, E_tape in enumerate(E_tapes):
        E_tape = E_tape
        #cross-section area of tape
        A_tape = w*t_tape

        #linspace over length of half the bond
        x = np.linspace(-L_bond/2,0,int(1+L_bond/(2*dx)))

        #differential equation part
        A = (t_bond*t_tape*E_tape/(2*G_bond))**0.5
        #stress in bond
        tau = np.sinh(x/A)*np.sinh(L_bond/A)

        sigma_0 = 1
        P = sigma_0*A_tape

        #integration of shear stress
        tau_total = np.sum(abs(tau))*dx #MPa
        #compensation for use of half the width
        tau = (P/tau_total)*tau/2 #MPa

        #array for calculation of stress in tape
        sigma = np.zeros_like(tau)

        for i, t in enumerate(tau):
            #sum of all the shear forces intil location
            sum_tau = np.sum(abs(tau[:i]))*dx
            #calculation of stress based on shear forces
            sigma[i] = sigma_0-sum_tau/A_tape

        #strain in tape
        epsilon_x = sigma/E_tape
        #effective stiffness of bond
        E_bond = (sigma_0*t_tape/(2*t_tape+2*t_bond))/np.average(
            epsilon_x)

        results_strain[a,b] = np.average(epsilon_x)
        results_stiffness[a,b] = E_bond
        results_stiffness_red[a,b] = 100*(1-(E_bond/E_tape))
```

Appendix E

Digital image recognition code flow

During the thesis, multiple codes have been written to measure the tape orientation distribution for different concepts and calculate the effect of this on mechanical properties. To clarify the cooperation between these codes, a diagram has been made as shown in figure E.1. At the top of this diagram are codes that are used to facilitate the code that reads the orientation of the tape. The settings that are found with these programs are used in the remaining codes. After this, the programs that read the tape orientations and filter the readings are shown. With the found tape orientations analytical codes have been made. These are shown at the bottom of the diagram. The codes that are in a white box will be presented in the appendices afterward.

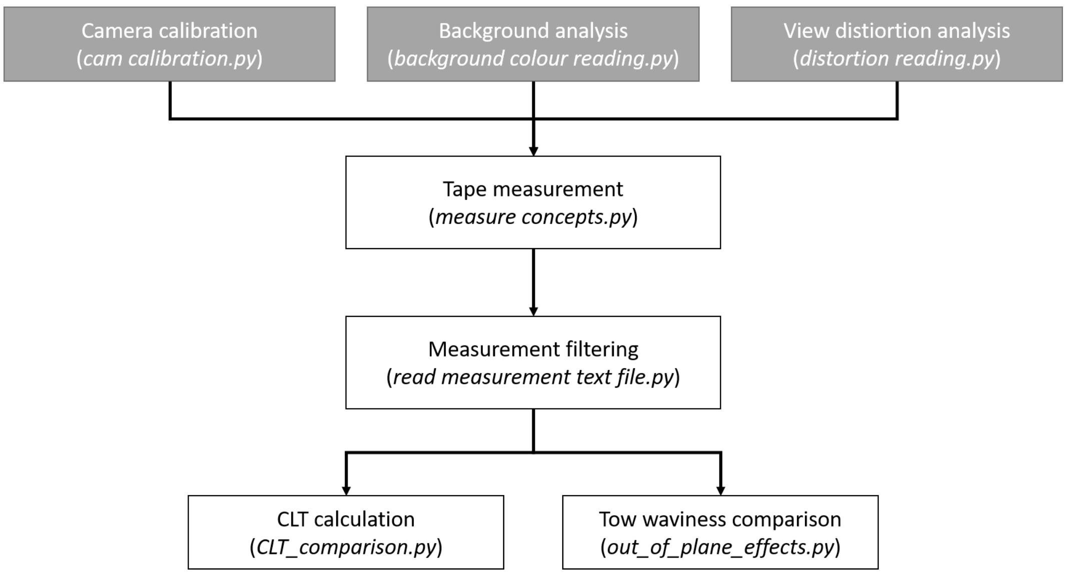

Figure E.1: Code flow diagram

Appendix F

Python code: Tape orientation measurement

The measurement of the tape orientations on a large scale has been done by using a USB cable that has been connected to a computer. The images that have been captured have been processed by a code that uses the OpenCV library [47] in python. Firstly the images are read and simplified using blurring, eroding, and threshold values. After this, the contours of tapes can be recognized. By using logic, tapes have been recognized in the contours which enables the calculation of the tape orientation of tapes. The code that is described below is used in combination with the measurement frame. This makes the accuracy of the code dependent on the situation in which is used (type of camera, lighting, indirect light, background, etc...). For the choice of background, lighting, and settings such values for thresholds, blurring, and eroding, tests have been performed which are not described in this thesis.

```
import numpy as np
import cv2
import os
import time
import matplotlib.pyplot as plt
import pygame as pg
import array
import datetime


def last_node(node_1, node_2, node_3):
    "creates a 4th node (based on 3 others) and make a rectangle fit
        based on all 4"
    delta = np.subtract(node_3, node_2)
    node_4 = node_1 + delta
    contour = np.array([node_1, node_2, node_3, node_4])
    bbox = cv2.minAreaRect(contour)
    box = cv2.boxPoints(bbox, contour)
```

```
    box = np.int0(box)
    return(box)

def line_angle(node_1, node_2):
    "calculates the angle of a line defined by two pixels"
    x1, y1 = pixel_coord(node_1)
    x2, y2 = pixel_coord(node_2)

    dx = x2-x1
    dy = y2-y1

    if dx==0:
        hoek = np.pi/2
    else:
        hoek = np.arctan(dy/dx)

    return(np.rad2deg(hoek))

def box_fit(nodes):

    "Fits a rectangle (with parallel sides) over 4 given points"
    bbox = cv2.minAreaRect(nodes)
    box = cv2.boxPoints(bbox, nodes)
    box = np.int0(box)

    return(box)

def box_correction(rect):
    "creates a box-fit om drie nodes"
    node_1 = rect[0]
    node_2 = rect[1]
    node_3 = rect[2]

    return(last_node(node_1, node_2,node_3))

def pixel_coord(node):
    "Convertes pixel coordinates to real coordinate based on array"
    # global x
    # global y

    x1 = node[1]
    y1 = node[0]

    x_coord = x1
    y_coord = y1

    return(x_coord, y_coord)

def box_orientation(rect, soort):
    "Calculates the angle of the longest side of the first four sides of
       a a contour"
    "Should be used with a box-fit rectangle"
```

```
    "This definition calculates all the angles of all tapes that are
       measured"

    x0 , y0 = pixel_coord(rect[0,:])
    x1 , y1 = pixel_coord(rect[1,:])
    x2 , y2 = pixel_coord(rect[2,:])
    x3 , y3 = pixel_coord(rect[3,:])

    x_center = (x0 + x1 + x2 + x3)/4
    y_center = (y0 + y1 + y2 + y3)/4

    #lengths of sides
    l1 = (((x1-x0)**2)+((y1-y0)**2))**0.5
    l2 = (((x2-x1)**2)+((y2-y1)**2))**0.5
    l3 = (((x3-x2)**2)+((y3-y2)**2))**0.5
    l4 = (((x0-x3)**2)+((y0-y3)**2))**0.5

    #angle of all sides
    if y1-y0 == 0:
        d1 = 0
    else:
        d1 = np.arctan((-(x1-x0)/(y1-y0)))

    if y2-y1 == 0:
        d2 =0
    else:
        d2 = np.arctan(-((x2-x1)/(y2-y1)))

    if y3-y2 ==0:
        d3 = 0
    else:
        d3 = np.arctan(-((x3-x2)/(y3-y2)))

    if y0-y3 ==0:
        d4 = 0
    else:
        d4 = np.arctan(-((x0-x3)/(y0-y3)))

    #convert angles to degrees
    [d1,d2,d3,d4] = np.rad2deg([d1,d2,d3,d4])

    #the angle of the longest side is used
    if l1 == max(l1,l2,l3,l4):
        deg = d1

    elif  l2 == max(l1,l2,l3,l4):

    elif  l3 == max(l1,l2,l3,l4):
        deg = d3
    else:
        deg = d4

    #Draws the regognized contour in the image
```

```
    cv2.drawContours(image,[rect],0,(255,0,0),2)

    #returns, coordinate of the center and the angle of the tape
    return(np.round(x_center,1), np.round(y_center,1), np.round(deg,1))

def plot_distribution(data):
    "makes a picture of the rectangles that are recognized and saved in data"
    "seems to stop after a certain time"
    pg.init()
    black = (0,0,0)
    white = (255,255,255)

    xmax =550
    ymax = 550
    screen=pg.display.set_mode((xmax,ymax))

    screen.fill(white)
    for contour in contours[1:]:
        for i in range(len(contour)):
            x1 = contour[i,0,0]
            y1 = contour[i,0,1]
            x2 = contour[i-1,0,0]
            y2 = contour[i-1,0,1]

            pg.draw.line(screen,black,(x1,y1),(x2,y2))

    pg.display.flip()

    return("done")

def read_image(img):

    "use some or all recognition strategies"
    chck_1 = False #Single tapes
    chck_2 = True #Clusters
    chck_3 = True #Long sides
    chck_4 = True #Short sides

    #chooses the filters that are used on the image
    # this can be Blue, Green, Red or grayscale
    imgGrey = img[:,:,0]
    # imgGrey = cv2.cvtColor(img, cv2.COLOR_BGR2GRAY)


    #the erode and dilate function smoothen the features in the material
    #to make smoother transitions after the threshold is applied
    #the more it, the smoother it will be, but it also removes features
    it = 5
    imgGrey = cv2.erode(imgGrey,None, iterations = it)
    imgGrey = cv2.dilate(imgGrey,None, iterations = it)

```

```
    #blur does kind of the same as the previous step, the combiation is based on trail-and-error
    imgGrey = cv2.blur(imgGrey,(3,3))

    #by setting a threshold value, all the intensity values within the pixels of the image
    # the value range is reduced from 0-255 to 0 0-1. This is needed for the contour function
    # _, thrash = cv2.threshold(imgGrey, 40 , 255, cv2.THRESH_BINARY)
    _, thrash = cv2.threshold(imgGrey, 20 , 255, cv2.THRESH_BINARY)

    #find contours
    contours, _ = cv2.findContours(thrash, cv2.RETR_TREE, cv2.CHAIN_APPROX_SIMPLE)



    #to make the code more efficient the code only focusus on contours that can resemble a tape
    # the values are based on readings
    tape_width = 22
    tape_length = 60
    d_dim = 5

    A_tape_max = 4875000.0

    #empty list for the saving of orientations
    orientations = np.array([])

    #each image results in a list of contours
    #for each contour (which can be as many points as it needs to be degned (100+))
    #the following steps can be taken
    for contour in contours[:]:
        #for visual validation, all the detected contours are drawn on the image
        cv2.drawContours(img,contour,0,(0,250,0),2)

        #the contour will be simplified a bit such that arcs with a small h/R ratio will be seen as lines
        approx = cv2.approxPolyDP(contour, 0.02* cv2.arcLength(contour, True), True)

        #First it will be checked if a contour can be from a single tape (based on the length and area of it)
        "Single tapes"
        if 150 > cv2.arcLength(approx, True) > 90 and chck_1 == True:

        # if 120 > cv2.arcLength(approx, True) > 70:

            #if it can be a single tape a box fit will be done and the orientation is found
            if cv2.contourArea(approx) < A_tape_max:
```

```
                box = box_fit(approx)
                # cv2.drawContours(img,[box],0,(0,0,255),2)
                x_center, y_center, deg = box_orientation(box, "st")
                orientations = np.append(orientations, deg)


            "clusters"
        #if the cluster is too large, it can be a cluster of tapes.
        # based on the contour coordinates, posible tapes are tried to be found
        elif 400 >  cv2.arcLength(contour, True) > 50 and len(approx) > 4 and chck_2 == True:
            cv2.drawContours(img,[approx],0,(0,250,0),2)

            #make arrays for the saving of the properties of the line between nodes
            degs = np.zeros((len(approx),1))
            angles = np.zeros((len(approx),1))
            vectors = np.zeros((len(approx),2))

            "calculate angles"
            for i, j in enumerate(approx):

                #reconstruct coordinate of contour corners from contour array
                vector_1 = (np.subtract(approx[i], approx[i-1]))[0]
                vector_2 = (np.subtract(approx[i-1], approx[i-2]))[0 ]

                vectors[i,:] = vector_1

                #create unitvector of two lines that share a node in order
                # to calculate the angle between them
                unit_vector_1 = vector_1 / np.linalg.norm(vector_1)
                unit_vector_2 = vector_2 / np.linalg.norm(vector_2)

                dot_product = np.dot(unit_vector_1, unit_vector_2)
                angle = np.arccos(dot_product)

                degs[i] = np.rad2deg(angle)

                dot_product = np.dot(unit_vector_1, np.array([1,0]))
                angle = np.arccos(dot_product)

                angles[i] = np.rad2deg(angle)



            "calculate line lenghts & clasify lines"

            #when trying to see if two lines are perpendicular, and are probably  corner of a tape
```

```
# an error in angle is used to allow for missing corners
d_angle = 10

lines = np.zeros((len(approx),1))
lengths = np.zeros((len(approx),1))

"regognize sides of tapes"
#for all lines that are defined by two points in the contour
for i, j in enumerate(vectors):
    #Calculate length
    lengths[i] = np.linalg.norm(vectors[i])
    #check if the line can be the long side of a tape
    if tape_length-d_dim < np.linalg.norm(vectors[i]) < tape_length+d_dim:
        line = np.array([approx[i-1], approx[i]])
        # cv2.drawContours(img,[line],0,(255,0,0),3)
        lines[i] = 2
    #check if the line can be the short side of a tape
    if tape_width-d_dim < np.linalg.norm(vectors[i]) < tape_width+d_dim:
        line = np.array([approx[i-1], approx[i]])
        # cv2.drawContours(img,[line],0,(0,0,255),3)
        lines[i] = 1

"long sides"
#at this point all the corners have an angle of the lines that come together at that node
# and a list of if all the lines can be seen as long or short sides of a tape
#with this some paterns that defines a tape are tried to be found
for i in range(len(lines)):
    if lines [i-2] == 2 and chck_3 == True:
        #if two angles next to eachother are roughly 90   it can be a tape where one short side is missing
        if 90-d_angle < degs[i-2] < 90+d_angle and 90-d_angle < degs[i-1] < 90+d_angle:

            lines[i-3], degs[i-3] = -1 ,-1
            lines[i-2], degs[i-2] = -1 ,-1
            lines[i-1], degs[i-1] = -1 ,-1
            line = np.array([approx[i-4],approx[i-3], approx[i-2], approx[i-1]])
            # cv2.drawContours(img,[line],0,(0,0,255),3)

            if 90-d_angle < degs[i-4] < 90+d_angle:
                lines[i-4], degs[i-4] = -1 ,-1

            if 90-d_angle < degs[i] < 90+d_angle:
                lines[i], degs[i] = -1 ,-1

            #a box shape will be created and the angle will be saved
```

```
                        box = box_correction(line)
                        x_center, y_center, deg = box_orientation(box, "lt")
                        orientations = np.append(orientations, deg)

            "short sides"
            for i in range(len(lines)):
                if lines[i-2] ==1 and chck_4 == True:
                    #if two angles next to eachother are roughly 90  it can be a tape where one long side is missing
                    if 90-d_angle < degs[i-2] < 90+d_angle and 90-d_angle < degs[i-1] < 90+d_angle:

                        lines[i-3], degs[i-3] = -1 ,-1
                        lines[i-2], degs[i-2] = -1 ,-1
                        lines[i-1], degs[i-1] = -1 ,-1
                        line = np.array([approx[i-4],approx[i-3], approx[i-2], approx[i-1]])
                        # cv2.drawContours(img,[line],0,(0,0,255),3)

                        if 90-d_angle < degs[i-4] < 90+d_angle:
                            lines[i-4], degs[i-4] = -1 ,-1

                        if 90-d_angle < degs[i] < 90+d_angle:
                            lines[i], degs[i] = -1 ,-1

                        #a box shape will be created and the angle will be saved
                        box = box_correction(line)
                        x_center, y_center, deg = box_orientation(box, "ss")
                        orientations = np.append(orientations, deg)

    #returns the given image with the found contours and recognized tapes drawn on them
    # besides this the last found contour and orientations of the tapes are returned
    return(img,contour, contours, orientations)


rectangles = np.zeros((1,4,2))


"Coordinate system of pixels"
#calculates the array that is used to determine the real coordinate of each pixel
# this is done by interpolating a cone onto a flat surface. heareby eachpixel
# has two angles and results in and x and y value
if False:
    #shape the image has
    N = 720
    M = 1280
```

```

    #experimentaly found value that defines the curvature of the cone of view
    R1 = 1350
    R2 = 850

    #actual length and width at the center of the image
    l =531
    w = 275

    #angle of view
    alpha = np.arctan(l/(2*R1))
    beta = np.arctan(w/(2*R2))

    #arrays of which angle each pixel has
    alphas = np.linspace(-alpha,alpha,M)
    betas = np.linspace(-beta,beta,N)

    #initial calculation
    xs = R1*np.tan(alphas)
    ys = R2*np.tan(betas)

    global x
    global y

    #list of coordinates which a given line lenght can reach from the center of the camera
    x = np.zeros((M,N))
    y = np.zeros((M,N))
    z = np.zeros((M,N))

    #multiplying the line by the z-coordinate
    # calulating interpolated coordinates
    for n in range(N):
        for m in range(M):
            z[m,n] = R1 - np.sqrt((np.square(R1))-(np.square(xs[m]))-(np.square(ys[n])))
            x[m,n] = xs[m]*(R1/(R1-z[m,n]))
            y[m,n] = ys[n]*(R2/(R2-z[m,n]))


# capture image from webcam
cam = cv2.VideoCapture(0)

#create folder where readings are saved
# os.mkdir("Readings")
#creation of names of folders to save data and images
picpath1 = time.strftime("Readings\%Y-%m-%d_%H%M")
picpath2 = time.strftime("Readings\%Y-%m-%d_%H%M\pics")
#creation of path
os.mkdir(picpath1)
os.mkdir(picpath2)

```

```
#creation of text file for data with folder path that has just been created
filename = time.strftime("Readings\%Y-%m-%d_%H%M\data.txt")

#open or create file that is used to write the measurements too
f = open(filename, "w")
readings = np.array([])

#start counter for file name when saving images
img_counter = 0
t0 = time.time()
t = []
while True:

    #image name
    img_counter = img_counter + 1
    picname = time.strftime("Readings\%Y-%m-%d_%H%M\pics") + str("/") + str(img_counter) + str(".jpg")
    # picname = picname.replace("\\", "\")

    #get image from webcam
    ret, image = cam.read()

    #saving of image
    cv2.imwrite(picname, image)

    #choose area of interest
    image = image[180:300, 275:385]

    if not ret:
        print("failed to grab frame")
        break

    #get results from image recognition
    result, contour, contours , orientation = read_image(image)

    #if there is a tape recognized, the orientations are saved in an array
    if len(orientation) > 0:
        for i in orientation:
            readings = np.append(readings,i)

        f.write((str(orientation).replace("[", " ")).replace("]", " "))
        f.write(str("\n"))

    #wait to lower sample frequency to maximal 20 fps
    # time.sleep(0.05)

    #show live measurements with recognized tapes and contours drawn in image
    cv2.namedWindow("result", cv2.WINDOW_NORMAL)
    cv2.resizeWindow("output", 450, 600)
    cv2.imshow("result", result)
```

```
    cv2.resizeWindow("result", 600, 450)
    t = np.append(t,(time.time()-t0))

    # ESC pressed
    k = cv2.waitKey(1)
    if k%256 == 27:
        print("Escape hit, closing...")

        break



#close camera
cam.release()

#close writing of measurement
f.close()

#end program
cv2.destroyAllWindows()

#comfirmation of closing of program
print("program succesfully closed")
print(filename)
```

Appendix G

Python code: Tape measurement filter

After a *.txt*-file has been created by the code in appendix 4 the raw data is processed by the code below. By comparing the values of readings, strings of values can be linked together and are saved as a single measurement. Because of the noise in the readings, a value is added to a string if it is within a certain range from the average of the string of measurements. Although this method is not flawless, it can create reduce up to 20 readings to a single value that has higher accuracy than a single reading due to the averaging. Below the code is shown.

```
import numpy as np
import matplotlib.pyplot as plt

def first_value(reading):
    "Check where and what the first (next) value is"
    check1 = False
    r1 = 0
    c1 = 0
    v1 = 0
    while check1 == False and np.min(reading) != 100:

        for i in range(len(reading)):
            for j in range(20):

                if reading[i,j] != 100 and check1 == False:
                    r1 = i
                    c1 = j
                    v1 = reading[i,j]
                    check1 = True
                    break

    if np.min(reading) == 100:
        check1 = False

    return(r1, c1, v1, check1)
```

```python


def next_value(r1,c1,vals,reading):
    "find (if posible) the next measurement that is comparable to the first found value"
    val_ref = np.average(vals)
    d = 3
    check2 = False
    i = int(r1+1)
    r2 = c2 = v2 = 0
    if i >= len(reading)-1:
        check2 = True

    if check2 == False:
        for j in range(20):
            vn = reading[i,j]
            if vn != 100 and check2 == False and vn < val_ref + d and vn > val_ref - d:
                r2 = i
                c2 = j
                v2 = vn
                check2 = True
                break

    return(r2, c2 ,v2,check2)

def clean_reading(row,col,read):
    "remove the values that are found and saved as one single tape reading"
    for i in row:
        for j in col:
            read[int(i),int(j)] = 100

    return(read)


"txt files of the measurements of the concepts"
files = np.array(["Readings/2020-12-15_1530\data.txt",
                  "Readings/2020-12-21_1343\data.txt",
                  "Readings/2020-12-21_1611\data.txt",
                  "Readings/2020-12-21_1631\data.txt",
                  "Readings/2020-12-21_1732\data.txt",
                  "Readings/2020-12-22_1443\data.txt",
                  "Readings/2020-12-22_1506\data.txt",
                  "Readings/2020-12-22_1524\data.txt",
                  "Readings/2020-12-22_1533\data.txt",
                  "Readings/2020-12-22_1539\data.txt",
                  "Readings/2020-12-23_1512\data.txt",
                  "Readings/2020-12-23_1623\data.txt",
                  "Readings/2020-12-23_1632\data.txt",
                  "Readings/2020-12-23_1640\data.txt",
                  "Readings/2020-12-23_1652\data.txt"])

```

```

values = []

"Read text file(s)"
for file in files[:5]:
    #open file
    f = open(file,"r")

    readings = 100*np.ones((20,1))

    #read lines
    lines = f.readlines()

    reading = 100*np.ones((len(lines),20))

    for i, line in enumerate(lines):
        while line.startswith((' ', '\t')):
            line = line[1:]

        while line.endswith((' ', '\t')):
            line = line[:-1]

        words = (((line.replace("    ", " ")).replace("  "," ")).replace("\n","")).split(" ")

        #convert string values to float values
        words = np.asfarray(words[:-1],float)

        word = 100*np.ones((20,1))
        for j , k in enumerate(words):
            word[j,0] = k


        readings[:len(word),0] = word[:,0]

        reading[i,:] = readings[:,0]

    #close text file
    f.close()

    "destill values"
    # difference the next value is allowed to have compared to the average of the string of found values
    d = 2.5
    check = True
    check1 = True


    while check == True:
        row = []
        col = []
        vals= []

```

```
        r, c, v, check1 = first_value(reading)

        if check1 == True and np.min(reading) != 100:
            row = np.append(row,r)
            col = np.append(col,c)
            vals = np.append(vals,v)

            check2 = True

            while check2 == True:
                r, c, v, check2 = next_value(row[-1], col[-1], vals, reading)
                if check2 == True and np.max(col) != 100:
                    row = np.append(row,r)
                    col = np.append(col,c)
                    vals = np.append(vals,v)


            val_avg = np.average(vals)
            values = np.append(values,val_avg)
            reading = clean_reading(row,col,reading)


        if np.min(reading) == 100:
            check = False
            break



#add 90  tapes (knockdown) for compensation batchwise tape deposition
# n = np.round(len(values)*((1/0.92)-1),0)
# knockdown = 90*np.ones((int(n),1))
# values = np.append(values, knockdown)

#the material properties that are used to define H-value
E_x     = 122.5E3
E_y     = 8.48E3
nu_xy   = 0.29
nu_yx   = 0.29
G_xy    = 5.171E3

#creation of the local stiffness matrix
Q_11 = E_x/(1-nu_xy*nu_yx)
Q_22 = E_y/(1-nu_xy*nu_yx)
Q_12 = E_y*nu_xy/(1-nu_xy*nu_yx)
Q_66 = G_xy

Q = np.array([[Q_11 , Q_12 , 0     ],  #MPa
              [Q_12 , Q_22 , 0     ],
              [0    , 0    , Q_66  ]])

# the be able to compare the measurements with a conventional layup the readings can be overwriten
```

```
# values = np.zeros((1,1))
# values = 90*np.ones((1,1))
# values = np.arange(-90,90)
# values = np.array([45, -45])

#array of all the tapes
H = np.zeros((3,3))
a11 = 0
a12 = 0
a22 = 0

#calculate the values of the in-plane orientation tensor and H values
N = len(values)
for i in values:
    #convert measurements from degrees to radians
    i = np.deg2rad(i)

    #create array for values of individual tapes
    h = np.zeros((3,3))

    #simplification of formulas to come
    m = np.cos(i)
    n = np.sin(i)


    h[0,0] = (m**4)        *Q[0,0] + (n**4)        *Q[1,1] + 2*(m**2)*(n
        **2)    *Q[0,1] + 4*(m**2)*(n**2)      *Q[2,2] #MPa
    h[1,1] = (n**4)        *Q[0,0] + (m**4)        *Q[1,1] + 2*(m**2)*(n
        **2)    *Q[0,1] + 4*(m**2)*(n**2)      *Q[2,2] #MPa
    h[0,1] = (m**2)*(n**2)*Q[0,0] + (m**2)*(n**2) *Q[1,1] +  ((m**4)+(n
        **4))   *Q[0,1] - 4*(m**2)*(n**2)      *Q[2,2] #MPa
    h[0,1] = h[1,0]
    h[2,2] = (m**2)*(n**2)*Q[0,0] + (m**2)*(n**2) *Q[1,1] - 2*(m**2)*(n
        **2)    *Q[0,1] + ((m**2)-(n**2))**2   *Q[2,2] #MPa
    h[0,2] = (m**3)*n     *Q[0,0] - (n**3)*m      *Q[1,1] + (m*(n**3)-(m
        **3)*n)*Q[0,1] + 2*(m*(n**3)-(m**3)*n)*Q[2,2] #MPa
    h[0,2] = h[2,0]
    h[1,2] = (n**3)*m     *Q[0,0] - (m**3)*n      *Q[1,1] + (n*(m**3)-(n
        **3)*m)*Q[0,1] + 2*(n*(m**3)-(n**3)*m)*Q[2,2] #MPa
    h[1,2] = h[2,1]

    #make average of all the values
    a11 = a11 + (np.cos(i)**2)/len(values)
    a12 = a12 + (np.cos(i)*np.sin(i))/len(values)
    a22 = a22 + (np.sin(i)**2)/len(values)
    H = H + h/len(values)

#compose in-plane orientation tensor
a = np.array([[a11, a12],
              [a12, a22]])
```

Appendix H

Python code: CLT and orientation comparison

The code below will use the filtered data and make a virtual layup with it. With this layup in combination with the material properties, homogenized elastic properties can be calculated through classical laminate theory. This has to be done for the orientation distribution as has been measured and for distributions where the angles have been moved with 3° to obtain the scatter as described in chapter 6. Below the lines of code are stated.

```
import matplotlib.pyplot as plt
import numpy as np
import numpy.linalg as la

def ABD_matrix (layup):
    layup = np.deg2rad(layup)

    ttotal = tply*np.shape(layup)[0]
    "define material"
    z = np.zeros(((np.shape(layup)[0]+1)))



    #laminate interface thickness coordinates
    z = np.linspace(-ttotal/2, ttotal/2, np.shape(layup)[0]+1)    #mm


    q = 1-vxy**2   #-

    #local stiffness matrix
    Q = np.array([[E_L/(1-v_LT*v_TL)       , v_LT*E_T/(1-v_LT*v_TL) , 0 ],  #MPa
                  [E_T*v_LT/(1-v_LT*v_TL) , E_T/(1-v_LT*v_TL)      , 0 ],
```

```
                  [0          , 0          , G_LT    ]])


    "calculate ABD matrix"
    Qi = np.zeros((3,3))
    a_tensor = 0

    for i in range(np.shape(layup)[0]):

        m = np.cos(layup[i])
        n = np.sin(layup[i])

        T = np.array([[m**2 , n**2,  2*m*n      ],
                      [n**2 , m**2, -2*n*m      ],
                      [-n*m , m*n  ,(m**2)-(n**2)]])

        Q_ij = T @ Q @ T.T

        #ply-stiffness matrix
        Qi = Qi + Q_ij*tply


    a = la.inv(Qi)

    E11 = Qi[0,0]/ttotal
    E22 = 1/(a[1,1])/ttotal
    v12 = Q[0,1]/Q[1,1]
    G12 = 1/(a[2,2]) /ttotal

    return ()

"define layups"
#chosen ply layup

reading = np.load("Filtered readings vibrational box.npy")

perp = 90*np.ones(int(0.08*len(reading)/0.92))

orientations = np.concatenate((reading, perp))

orientations_0 = orientations[:]

orientations_plus_45 = orientations +45*np.ones(len(orientations))

orientations_min_45 = orientations - 45*np.ones(len(orientations))

orientations_45 = np.concatenate((orientations_plus_45,
    orientations_min_45))

orientations_random = np.arange(-90,91,1)

"Layups with noise"
orientations_0_high = np.zeros(np.shape(orientations_0))
```

```
orientations_0_low = np.zeros(np.shape(orientations_0))
orientations_45_high = np.zeros(np.shape(orientations_45))
orientations_45_low = np.zeros(np.shape(orientations_45))
orientations_random_high = np.zeros(np.shape(orientations_random))
orientations_random_low = np.zeros(np.shape(orientations_random))

sigma = 1.01*3
for i,j in enumerate(orientations_0):
    if j < -sigma:
        orientations_0_high[i] = orientations_0[i] + sigma
        orientations_0_low[i] = orientations_0[i] - sigma
    elif j > sigma:
        orientations_0_high[i] = orientations_0[i] - sigma
        orientations_0_low[i] = orientations_0[i] + sigma
    else:
        orientations_0_high[i] = 0
        orientations_0_low[i] = orientations_0[i] + sigma

for i,j in enumerate(orientations_45):
    if j < -sigma:
        orientations_45_high[i] = orientations_45[i] + sigma
        orientations_45_low[i] = orientations_45[i] - sigma
    elif j > sigma:
        orientations_45_high[i] = orientations_45[i] - sigma
        orientations_45_low[i] = orientations_45[i] + sigma

for i,j in enumerate(orientations_random):
    if j < -sigma:
        orientations_random_high[i] = orientations_random[i] + sigma
        orientations_random_low[i] = orientations_random[i] - sigma

    elif j > sigma:
        orientations_random_high[i] = orientations_random[i] - sigma
        orientations_random_low[i] = orientations_random[i] + sigma

layup = orientations_random

#the material properties that are used to define the A-values of the ABD
    matrix
tply = 1     #mm

"Material Properites"
E11 = 121.6E3
E22 = 10.2E3
E33 = 10.2E3
G12 = 6.3E3
G13 = 6.3E3
G23 = 3.6E3
v12 = 0.29
v13 = 0.29
v23 = 0.47

"Local compliance matrix"
```

```
S_local = np.array([[1/E11      , -v12/E11   , -v13/E11   , 0      , 0      ,
     0      ],
                    [-v12/E11   , 1/E22      , -v23/E22   , 0      , 0      ,
     0      ],
                    [-v13/E11   , -v23/E22   , 1/E33      , 0      , 0      ,
     0      ],
                    [0          , 0          , 0          , 1/G23  ,0       ,
     0      ],
                    [0          , 0          , 0          ,0       , 1/G13  ,
     0      ],
                    [0          , 0          , 0          ,0       ,0       ,
     1/G12  ]])

C_local = la.inv(S_local)

"Check values"
E11 = C_local[0,0]
E22 = C_local[1,1]
E33 = C_local[2,2]
E12 = C_local[0,1]
E13 = C_local[0,2]
E23 = C_local[1,2]
E66 = C_local[5,5]

"Stiffnesses with plain stress assumtion"
Qxx = E11-(E13**2)/E33
Qxy = E12-(E13*E23)/E33
Qyy = E22-(E23**2)/E33
Qss = E66

E_L = Qxx-(Qxy**2)/Qyy
E_T = Qyy-(Qxy**2)/Qxx
v_TL = Qxy/Qxx
v_LT = v_TL*Qxx/Qyy
G_LT = Qss

"Calculate ABD matrix values"

ABD_matrix(orientations_45)
```

Appendix I

Python code: Effect of tow waviness

The code below will use the filtered data and make a virtual layup with it. By using the measured out-of-plane tow angles that have been obtained with optical microscopy (as described in chapter 6 the elastic properties have been rotated in-plan as well as out-of-plane. By doing this an estimation has been made on the stiffness reduction due to the out-of-plane angle. Because the relation between the in-plane and out-of-plane angle is unknown, all the combinations have been calculated and an average has been taken from these results. Below the code is states.

```
"When all out-of-plane angles are used"
oop_random = np.sort(np.load("oop angels random.npy"))
# oop_0 = np.sort(np.load("oop angels random.npy"))
# oop_45 = np.sort(np.load("oop angels random.npy"))

"When average of out-of-plane angles is used"
# oop_random = [0, 4.2]
# oop_0 = [0, 2.8]
# oop_45 = [0, 3.2]

"in-plane orientation distributions"
distribution = np.load("Filtered readings vibrational box (copy).npy")  # reading of file
N = int(np.shape(distribution)[0]*(0.08/(1-0.08)))
add = 90*np.ones((N))
distribution = np.concatenate((distribution,add))  # add till 8% is perpenidicular

ip_0 = np.sort(distribution)
ip_45 = np.sort(np.concatenate((distribution+45,distribution-45)))
ip_random = np.arange(-90,91,1)

"Material properties"
E11 = 121.6E3
```

```
E22 = 10.2E3
E33 = 10.2E3
G12 = 6.3E3
G13 = 6.3E3
G23 = 3.6E3
v12 = 0.29
v13 = 0.29
v23 = 0.47

"Compliance matrix"
S_local = np.array([[1/E11      , -v12/E11   , -v13/E11   , 0       , 0       , 0      ],
                    [-v12/E11   , 1/E22      , -v23/E22   , 0       , 0       , 0      ],
                    [-v13/E11   , -v23/E22   , 1/E33      , 0       , 0       , 0      ],
                    [0          , 0          , 0          , 1/G23   ,0        , 0      ],
                    [0          , 0          , 0          ,0        , 1/G13   , 0      ],
                    [0          , 0          , 0          ,0        ,0        , 1/G12  ]])


gammas = ip_random
betas = oop_random

K = np.shape(gammas)[0]
J = np.shape(betas)[0]

vals_E11 = np.zeros((J,K))
vals_S11 = np.zeros((J,K))
vals_E22 = np.zeros((J,K))
vals_G12 = np.zeros((J,K))
vals_v12 = np.zeros((J,K))

for i, alpha in enumerate([0]):
    alpha = np.deg2rad(alpha)

    s = np.sin(alpha)
    c = np.cos(alpha)

    T_alpha = np.array([[1      ,0      ,0      ,0              ,0      ,0],
                        [0      ,c**2   ,s**2   ,2*c*s          ,0      ,0],
                        [0      ,s**2   ,c**2   ,-2*c*s         ,0      ,0],
                        [0      ,-c*s   ,c*s    ,(c**2)-(s**2)  ,0      ,0],
                        [0      ,0      ,0      ,0              ,c      ,-s],
```

```
                        [0        ,0        ,0        ,0              ,s        ,
                            c]])
    for k, gamma in enumerate(gammas):

        gamma = np.deg2rad(gamma)
        s = np.sin(gamma)
        c = np.cos(gamma)

        T_gamma = np.array([[c**2  ,s**2 ,0  ,0  ,0  ,2*c*s          ],
                            [s**2  ,c**2 ,0  ,0  ,0  ,-2*c*s         ],
                            [0     ,0    ,1  ,0  ,0  ,0              ],
                            [0     ,0    ,0  ,c  ,s  ,0              ],
                            [0     ,0    ,0  ,-s ,c  ,0              ],
                            [-c*s  ,c*s  ,0  ,0  ,0  ,(c**2)-(s**2)  ]])

        for j, beta in enumerate(betas):

            beta = np.deg2rad(beta)

            beta = np.arctan(np.tan(beta)*np.cos(gamma))

            s = np.sin(beta)
            c = np.cos(beta)

            T_beta = np.array([[c**2 ,0  ,s**2 ,0  ,2*c*s          ,0],
                               [0    ,1  ,0    ,0  ,0              ,0],
                               [s**2 ,0  ,c**2 ,0  ,-2*c*s         ,0],
                               [0    ,0  ,0    ,c  ,0              ,-s],
                               [-c*s ,0  ,c*s  ,0  ,(c**2)-(s**2)  ,0],
                               [0    ,0  ,0    ,s  ,0              ,c]])



            S_global = S_local
            S_global =  T_beta  @ S_global @ T_beta.T
            S_global =  T_gamma @ S_global @ T_gamma.T

            C_global = la.inv(S_global)

            E11_global = C_global[0,0]
            S11_global = S_global[0,0]
            E22_global = C_global[1,1]
            G12_global = C_global[5,5]
            v12 = -S_global[0,1]*S_global[0,0]

            vals_E11[j,k] = E11_global
            vals_S11[j,k] = S11_global
            vals_E22[j,k] = E22_global
            vals_G12[j,k] = G12_global
            vals_v12[j,k] = -S_global[0,1]/S_global[0,0]

vals_rel = np.zeros_like(vals_E11)
E11 = np.average(vals_E11[0,:])
S11 = np.average(vals_S11[0,:])
```

```
E22 = np.average(vals_E22[0,:])
G12 = np.average(vals_G12[0,:])

for k in range(K):
    vals_rel[:,k] = 100*vals_E11[:,k]/np.max(vals_E11[:,k])
```